MICRO-SCALE INSTRUMENTS APPLIED TO A BOVINE NUCLEAR TRANSFER SYSTEM

by A. L. Clow

A thesis submitted in partial fulfilment of the requirements for the Degree of Doctor of Philosophy

University of Canterbury

2010

Abstract

Manual handling of biological cells is routine in most laboratories. This is gradually changing with the development of robotic cell handling systems, and micro-scale lab-on-chip devices. Attempts were made to develop devices that automate or assist cell handling in the context of a bovine nuclear transfer (NT) system. The system, a zona-free bovine NT cloning system, formed a baseline reference for tool design and performance evaluation.

Bovine NT can, as other cell handling procedures, be improved by rapid and precise cell positioning. Improvements in cell handling can increase the quantity of cells processed, and the uniformity of conditions the cells are subject to during processing.

Tools were developed for two areas of cell handling: cell fusion and cell transportation. Designs suitable for implementation in microscale lab-on-chip systems were evaluated. Tool development was predominantly experimental, assisted by numerical modelling. The experimental investigation concerned device fabrication and operational performance.

A number of cell handling tool designs were built and tested. Coplanar electrodes are not commonly used in bovine NT and reports on their efficacy were not available. These electrodes, which are simple to fabricate, were tested to determine fusion rates achievable in comparison with those of the baseline procedure. A novel fusion device, the micropit, was designed to assist bovine cell pairing and electrofusion. It was initially uncertain whether this device was capable of achieving cell fusion. Tests were conducted; and cell fusion and micro-positioning were demonstrated, as was an increase in biological cell processing throughput.

Many miniaturised lab-on-chip systems rely on cell transportation. One illustration in the baseline procedure is the on-chip transport of cells to the cell fusion device. Potential cell transport mechanisms for a miniature cloning system were evaluated by prototype construction and testing. These mechanisms included travelling wave dielectrophoresis and capillary fluid actuation. To facilitate automation of on-chip cell transportation, a low cost electrically isolated cell detection system was developed based on a DVD pick-up unit. Various obstacles that were encountered during the course of device construction are noted, as are the fabrication methods employed.

Preface

This document discusses research undertaken between June 2005 and November 2009 at: the Electrical & Computer Engineering Department of the University of Canterbury, the Reproductive Technologies division of AgResearch in Hamilton, and at the University of Waikato.

The investigation focussed on the development of tools for handling small quantities of biological cells. The variety of aspects to the development of NT tools provided a source of interest, but also some consternation at the range of experimental obstacles that should be overcome within a short time frame to obtain practical laboratory tools. The challenge meant that not all aspects could be conducted single handedly.

I would like to thank my supervisors Dr. Paul Gaynor and Dr. Björn Oback in particular: for their proposal of research ideas, collaboration with research experiments, and assistance with the preparation of publications. Assoc. Prof. Maan Alkaisi assisted with project planning and his support during the thesis is appreciated. Thanks are also to Ms. Helen Deveraux and Mr. Gary Turner (for microfabrication assistance and maintaining chemical supplies and laboratory equipment in working order) and to Mr. David Healy for mechanical engineering support. Dr. Mathieu Sellier assisted with providing imaging equipment and useful discussions concerning capillary transport, and Dr. David Leung kindly made time to discuss cell preparation.

Optical cell detection work was conducted at the University of Waikato for ~ 7 months. Discussions with Assoc. Prof. Rainer Künnemeyer (University of Waikato) and Dr. John Sharpe (HortResearch) provided rapid identification of a suitable experimental design for cell detection. I am grateful for support provided by the staff of the Physics and Engineering Department at the University of Waikato and the staff at the Reproductive Technology Division of AgResearch for assistance during visits to their laboratory. Last I would to thank friends and family who have helped , by way of various discussions, to keep a clear focus on research objectives and disregard the inevitable distractions.

List of Publications

Aspects of this research are described in the following articles:

Peer reviewed Journal articles:

- A. Clow, P. Gaynor, and B. Oback, "Coplanar film electrodes facilitate bovine nuclear transfer cloning," *Biomed Microdevices,* vol. 11, pp. 851-9, Aug 2009.
- A. Clow, P. Gaynor, and B. Oback, "A novel micropit device that integrates automated cell positioning by dielectrophoresis and nuclear transfer by electrofusion," Biomed Microdevices, Under Review 2009.

Peer reviewed conference papers

- A. Clow, R. Künnemeyer, P. Gaynor, and J. C. Sharpe, "Low cost optical particle detection for Lab on Chip systems based on DVD technology," *Biomems and Nanotechnology III,* vol. 6799, pp. U189-U197, 210, 2008.
- A. Clow, P. Gaynor, and B. Oback, "A micropit for biological cell positioning," presented at the 7th IEEE International Conference on Control and Automation Christchurch, 2009 (In Press).

Peer reviewed conference abstract

- A. Clow and P. Gaynor, "Electrofusion of Asymmetrical sized biological cells" presented at the Advanced Materials and Nanotechnology III Conference, Wellington, 2007. Abstr. O128

Table of Contents

Abbreviations

AC	alternating current
AESF	adult ear skin fibroblasts
ATP	adenosine triphosphate
AZ1518	a positive photoresist polymer
DC	direct current
DEP	dielectrophoresis
DMAP	dimethylaminopurine
DNA	deoxyribonucleic acid
DVD	Digital Versatile Disk
EDM	Electro Discharge Machining
EFC	Elizabeth Follicular Cells (named after the donor animal)
FACS	Fluoresence Activated Cell Sorter
FCS	Fetal Calf Serum
H199	Hepes-buffered M199 with 15 mM Hepes, 5 mM NaHCO3 and 0.086 mM kanamycin monosulfate [28]
HEPES	4-(2-Hydroxyethyl)-1-piperazine-ethane-sulfonic acid [19]
HMC	Hand-Made-Cloning
HSOF	HEPES buffered Synthetic Oviduct Fluid
LOC	lab-on-chip
MEMS	Micro Electro Mechanical System
NT	Nuclear Transfer
PB	Polar Body
PDMS	poly-dimethyl-siloxane
PHA-P	phytohemagglutinin-P
PMMA	poly-methyl-meth-acrylate

PVA	polyvinyl alcohol oxidase
RF	Radio Frequency
RIE	Reactive Ion Etch
rms	root mean square
SCNT	Somatic Cell Nuclear Transfer
SNR	Signal to Noise Ratio
SU-8	a negative photoresist polymer (MicroChem Corp.)
twDEP	travelling wave DEP
UV	ultra-violet
V	voltage

List of Figures

Index of Tables

1 Introduction

Specialised laboratory equipment is becoming commonly available due to improvements in fabrication technology and device design. Systems for handling micro-scale and nano-scale biological specimens such as blood cell counters, fluorescence based cell sorters and DNA sequencers offer improvement in speed, throughput, repeatability, precision and yield, which facilitate preparation of inexpensive high-quality samples. This is to such an extent that it is not practical to conduct many scientific experiments without them.

The topic of this study was the development of tools for handling micro-scale quantities of cells. A tool is defined [29] by the task or problem which it solves: "*Tool*. (n) A device or implement ... used to carry out a particular function".

Nuclear Transfer (NT) cloning is an important method for creating genetic libraries of animals, improving livestock quality, creating cost effective pharmaceutical products and conducting research into embryo development [30, 31]. A NT application was selected to provide motivation for tool development and to clearly define a set of problems. The selection of a particular cell handling procedure facilitated identification of criteria against which tool performance could be evaluated. The cell handling procedure selected was the zona-free NT of genetic information from bovine cells. Other NT procedures such as the common zona-intact cell fusion process [32], direct donor nucleus injection into a cytoplast [33-36], karyoplast injection [37] and the automation friendly Hand-Made-Cloning (HMC) technique [31, 38-41] were not considered as a basis for tool development. This exclusion was mainly due to the proximity of the research lab[1] and the desire to test devices in an operating cloning laboratory.

Cell handling devices were built and tested. The tools developed fall into two categories: cell fusion devices and cell (or fluid) transport devices. Background material is provided to cater for readers unfamiliar with bovine NT (chapter 2), electro-manipulation of cells (chapter 3) and microfabrication (chapter 4), and may be overlooked by those readers familiar with these subjects. Chapter 5 reviews microtools applicable to the bovine NT process. Contributions to current research are presented in the experimental chapters 6 and 7 and are described in the conclusion (chapter 9). Not all experimental work directly contributed to existing knowledge on microtool development. However description of this

[1]Reproductive technologies section, Applied biotechnologies group, AgResearch Ruakura campus, Hamilton, NZ

work (section 6.4 HourGlass Fuser & 6.5 'T' junction Fuser) has been retained. This is to provide continuity in the account of the tools developed for NT and to illustrate common obstacles involved in the design of microfluidic devices. Chapter 8 summarises the work conducted, and discusses direction for future research.

Research emphasis was placed upon: using electric fields to actuate movement, simplicity of device design and speed of fabrication. Initial interest was in improving laboratory handling of small quantities of cells (1-100). The approach to the task of microtool development was from the bottom up, developing solutions to small problems in the zona-free NT system.

Microtool design differed from many lab-on-chip devices because the operation of these other devices concern fluids rather than particulates or cells. The selected NT application further constrained tool development as handling bovine cells is unique in two respects: one of the cells (an oocyte) is costly to obtain, and the diameters of the cells handled in the procedure vary by an order of magnitude.

The zona-free NT procedure is presented in the following chapters beginning with an overview of bovine reproduction and the history of NT. The baseline (or reference) NT procedure is introduced in more concrete terms, and then discussion proceeds to the basic principles for cell handling and manipulation using electric fields.

Microtools previously applied to bovine NT are reviewed and an overview of equipment and methods that were employed are presented before commencing discussion of experimental work and results. Cell fusion is discussed first and then cell transportation. Various obstacles to successful tool fabrication are noted.

The importance of tool fabrication to the development of suitable cell handling tools was made evident during the course of research, and as a result the design of tools for fabrication was considered. The thesis is concluded by summary remarks and recommendations for future research.

2 Cloning

The majority of the instructions for the growth of a living organism are stored in DNA. In animals, identical copies of these instructions are contained within the nucleus of every living cell. In general there are two similar sets of data within each cell consisting of a number of homologous chromosome pairs. Each homologue is stored as two strands in a helical structure, each strand being exactly complementary in every quaternary data element [42]. Proteins (mainly histones) surround the helix, protecting it, and controlling the transcription of the data to messenger RNA for fabrication. The DNA is further, during interphase (see Appendix A), surrounded by a nuclear membrane that controls the transport of elements into and out of the nucleus. The control centre of the cell is thus contained within the nucleus, and building instructions are in general sent outside for fabrication. These instructions are essential to the existence of any living animal, and therefore must be transferred to progeny.

Cattle have a male and female sex. They are monotocous, bearing a single offspring. As is commonly known, genetic information is inherited from part of the paternal and part of the maternal diploid chromosomal material. One of the outcomes of sexual reproduction is evidently that the diversity of offspring that is created exceeds that of asexual (clonal[2]) reproduction. Because each offspring is unique, each individual will have different environments to which it is optimally suited. This will have the tendency to scatter the progeny to grow in slightly differing circumstances, and provide less competition between progeny for scarce resources [43].

2.1 Bovine Reproduction

The bovine cloning processes is a modification of a naturally occurring biological process. Consideration of this natural process, bovine reproduction, facilitates understanding and appreciation of factors that are involved in the laboratory reconstruction of an embryo by NT. It also provides background necessary for tool selection and design.

Historically, the investigation of cellular processes have concerned chronological changes in cellular and sub-cellular morphology, attributable with little doubt to the development of microscale optical sensing equipment during the 18th and 19th centuries. This chronological,

[2]e.g. tapeworms and budding plants can reproduce by mitosis, cattle can not reproduce by mitosis or parthenogenesis [1]. Clonal cattle offspring do however occur (e.g. monozygotic twins).

morphological viewpoint provides both an account of the transfer of genetic information during the reproduction process, and insight into the development of tools and systems related to NT cloning. A brief overview of the formation of the gametes, their fusion and subsequent embryo development is now given.

Spermatogenesis

The male gametes are formed from precursor cells that have a full (diploid) DNA complement. The gonacytes are the "first" of the precursor cells and are formed before birth. At birth the gonacytes differentiate into spermatogonia. Spermatocytogenesis is the process where these diploid precursor cells multiply and subsequently (and finally) divide by meiosis[3]. The precursor cells differ in morphology according to their generations and are classified as: type A spermatogonia, intermediate spermatogonia, type B spermatogonia and finally the primary spermatocyte. The primary spermatocyte divides by meiosis first to form secondary spermatocytes and then haploid spermatids. The spherical spermatids finally transform (spermiogenesis) without cytokinesis into spermatazoa.

Bovine Oogenesis

The female equivalent to the primary spermatocytes, the primary oocytes, are formed prior to birth, and are not replicated [44] . These primary oocytes are arrested at the dictyate (a resting) substage of meiosis prophase I, with duplicate (4N) chromosomal material. A diagram of the oocyte and surrounding cells is shown in Fig. 1.

Each oestrus cycle, one of the oocyte follicles is induced by hormones to develop. The oocyte divides (Meiosis I) asymmetrically, unlike spermatocytogenesis. The smaller of the two cells thus formed, the first polar body (PB1), is retained in the periviteline space (Fig. 2) and does not not undergo division (written correspondence B.J. Oback).

After the completion of Meiosis I, the cell enters Meiosis II and is at Metaphase II with diploid (2N) chromosome number when the follicle in which the oocyte is contained ruptures. The cumulus cells disintegrate between 3 and 6 hours post ovulation and are probably not present at fertilisation [45]. The oocyte is released into the 25cm long bovine oviduct, and subsequently traverses the oviduct in 40 - 80 hours.

[3]Some precursor cells remain as stem cells [2]. Summaries of the Mitotic and Meiotic cell division processes may be found in Appendix A: Cell Growth and Division.

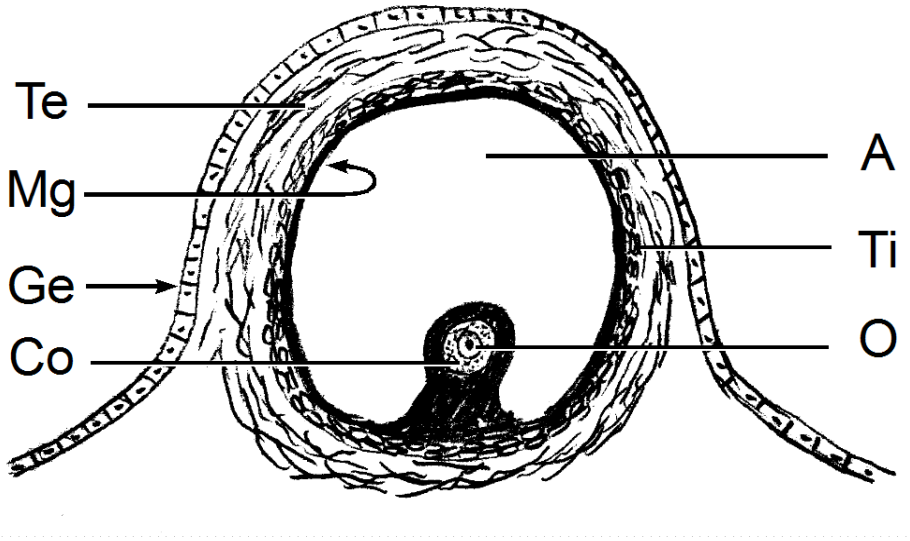

Fig. 1 Grafian follicle (adapted from [21]**)**

(A) Antrum (filled with liquor folliculi). (**Co)** Cumulus Oophorus. These cells differentiate from growing follicle granulosa cells, and remain in contact with the oocyte during ovulation. (**Ge)** Germinal Epithelium at the surface of the ovary wall. (**Mg)** Membrana granulosa. (**O)** Oocyte. (**Te)** Theta externa (myoid-type) cells and fibrocytes . (**Ti)** Theca interna - ovarian fibrocytes and stromal cells (these differentiate to epitheliod cells late in follicle maturation). The basal membrane separates the interior of the follicle from the Ti cells and vasculature.

Bovine Fertilisation

In nature fertilization of the oocyte occurs by the fusion of the spermatazoa with the oocyte. Fertilisation normally occurs in the upper and middle regions of the ampula in the oviduct. The haploid DNA of the spermatazoa is transferred to the oocyte, and the membrane surrounding the spermatocyte nuclei dissolves. Calcium release causes cortical granules (vesicles) located at the periphery of the oocyte to fuse with the plasma membrane. The release of cortisol from the cell hardens the zona pellucida, preventing subsequent fertilization events. After fertilisation, the corona radiata cells if present detach and the cell once more divides asymmetrically forming the second polar body (PB2) [46]. The two membrane bound pronuclei then fuse within the cytoplasm to form a zygote [47]. This cell is genetically distinct from both parents, and multiplies clonally via mitosis to form an entire individual animal. In general, cells of this animal will contain genetic (DNA) copies identical to that of the zygote[4].

[4] Except B and T-cells where the genome is rearranged to permit the immune system to detect a vast variety of pathogens. Myoid (muscle) cells may be multi-nucleated but still contain identical copies.

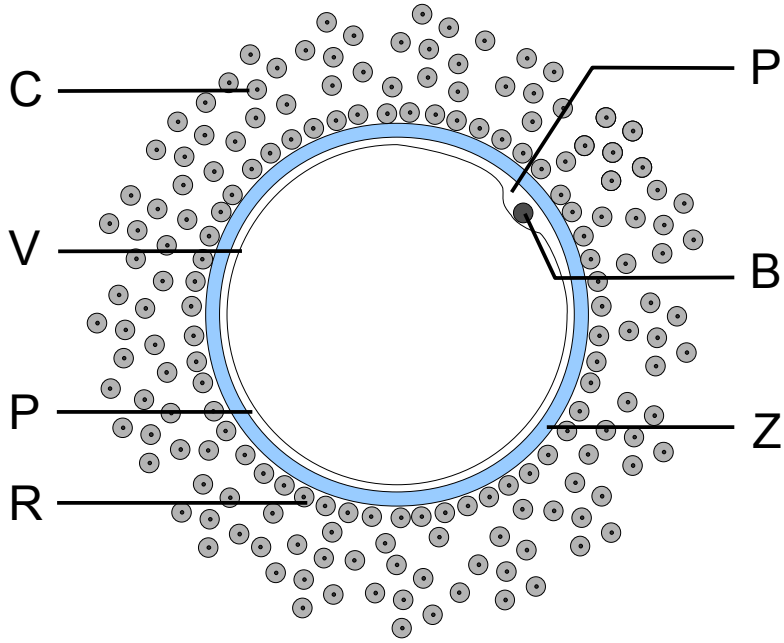

Fig. 2 Cumulus Oophorus Complex (COC) after metaphase I cytokinesis and ovulation.

Note that the germinal vesicle has disintegrated. (**C)** Cumulus Oophorus, (**R)** Corona radiata (innermost layer of cumulus cells in contact with the zona pellucida. **(Z)** Zona-pellucida. **(P)** perivitelline space **(V)** vitelline membrane (or oolema) **(B)** 1st polar body

Embryo Development

The embryo moves down the uterine tube and during this time it develops. The early stages the embryo proceeds to divide without increasing in mass[5]. The cells initially divide synchronously, the first few stages of division form a blastomere consisting of 2, 4 and then 8 cells. It enters the uteris (day 4-6 post insemination [48]) at the 8 or 16 cell stage. At the 32 cell stage, the embryo undergoes compaction. At the 64-128 cell stage fluid accumulates within the embryo forming the blastocyst (day 6-8 post ovulation [49]). The blastocyst consists of an outer layer of cells, the trophectoderm (which later becomes part of the placenta), an inner cellular mass and a fluid filled cavity. During this time, intra-uterine fluid weakens the zona surrounding the embryo in preparation for hatching. The blastocyst hatches from the zona pellucida (Fig. 2) at approximately day 9. The blastocyst remains in the uterine lumen until at approximately day 35 a weak attachment is formed with the uterine wall [50]. The time to develop to term is about nine months.

[5] This may reduce the time for DNA replication by omitting G1 and G2 phases, and improve intercellular communication.

2.2 Embryo Reconstruction (History)

While there has been much work on cloning over the last 25 years, it would be an omission not to briefly outline two key events in the history of somatic nuclear transfer. Hans Spemann[6], while not primarily interested in genetic transfer, did related experiments with newt's eggs and first proposed the idea of taking the nucleus of one cell and inserting it into an enucleated oocyte (p.211 [51]; and next section 2.3). Unfortunately, he reported that he was unable to find a method for completing two stages of the procedure, the enucleation and injection of the nucleus into the cytoplasm. The execution of the experiment, was left until 1952 when Briggs and King succeeded in accomplishing the procedure using a glass micro-pipette [52], the embryo successfully developing to a tadpole stage.

Initially cells of different species were selected for large cell size to simplify cell handling e.g. Rana Pipiens & Xenopus laevis (frogs) have been used due to the large size of the embryos (~1mm diameter [53]).

Early attempts (1970-1990) to clone mammals used embryonic donor cells (for example live offspring were produced from nuclear transfer: rabbits (1975, [54]), sheep (1986,[55]) and cattle (1987, [56, 57]). The first successful live offspring from nuclear transfer from adult somatic cells to enucleated oocytes resulted in the now well known "Dolly the Sheep" [32]. A large number of mammals have now been cloned including: cattle, gaur, goats, horses, deer, pigs, mice, rats, cats and dogs [58, 59] and many donor cell types have been used, however the developmental success rate to weaning of cloning remains low: in cattle it ranges from 4-16% depending on the method [28]. Impaired development of the reconstructed embryo is attributed to epigenetic changes in the nuclei of adult cells [60, 61]. Other factors that influence development are the stage of the donor cell cycle [62, 63], donor cell type [64] and in vitro cell handling. In vitro cell handling is not the main cause of low developmental rates in cattle. This is illustrated by comparison of somatic cell NT cloning with a very similar laboratory procedure, IVF, where the development rate is ~30% [65].

The physiological causes of failure to develop to term (including: foetal overgrowth and an enlarged heart) are often related to the placentome [66]. High losses occur early and late in pregnancy [31]. The majority of losses occur in the first trimester. Losses late in pregnancy (usually due to hydroallantois) may require surgical intervention. Of the pregnancies that

[6] Nobel Prize 1935, for work in developmental embryo biology.

complete gestation, the metabolism of the calves born are not considered normal until 6 months after birth (two thirds of calves delivered survive until weaning [28]). Although abnormal foetal development often occurs, it is not inheritable by offspring of cloned cattle [67, 68].

2.3 Zona-free NT cloning

Currently the most common method [69] of cloning is the zona-intact method used by Wilmut et al. for cloning dolly the sheep [32]. Here a zona-free NT system (Oback et al [28]) is presented as a standard reference NT system for tool development. The following description of the process considers the mechanical cell handling aspects of the process, but retains a general description of the entire process for completeness. This method was developed at AgResearch, and was at the time research began (2005) their standard operating procedure. It is the process upon which identification and testing of microtools is based. A description of this process is given before proceeding to discussion of cell handling and existing micro-tools.

2.3.1 Derivation of oocyte and donor cells.

The example process is of cloning cattle from adult ear fibroblasts (Fig. 3a,b). The first stage of the procedure is the preparation of donor cells and oocytes. The donor cells are obtained by cutting a notch from the ear of the animal approximately 2cm by 2cm. The cells are then transported to the laboratory, diced and placed in a hanging drop culture with antibiotics. The cells are differentially trypsinised removing epithelial cells. They are then passaged 3-6 times. To select cells which are in the G1 stage, cells which are observed to be dividing are selected and separated for use in cloning.

The oocytes are obtained from abattoir ovaries. The ovaries are transported to the laboratory, and individual cumulus oophorus complexes (COC) are aspirated from 3-12mm follicles. The COCs are washed and then cultured for 18-20 hours in in-vitro maturation media. The cumulus cells are dispersed by vortexing in hyaluronidase[7] (SM1 minishaker IKA, Germany) and the oocytes are recovered by sedimentation using a microcentrifuge.

[7]whether the enzyme is useful for cumulus dispersion has been argued against [3]

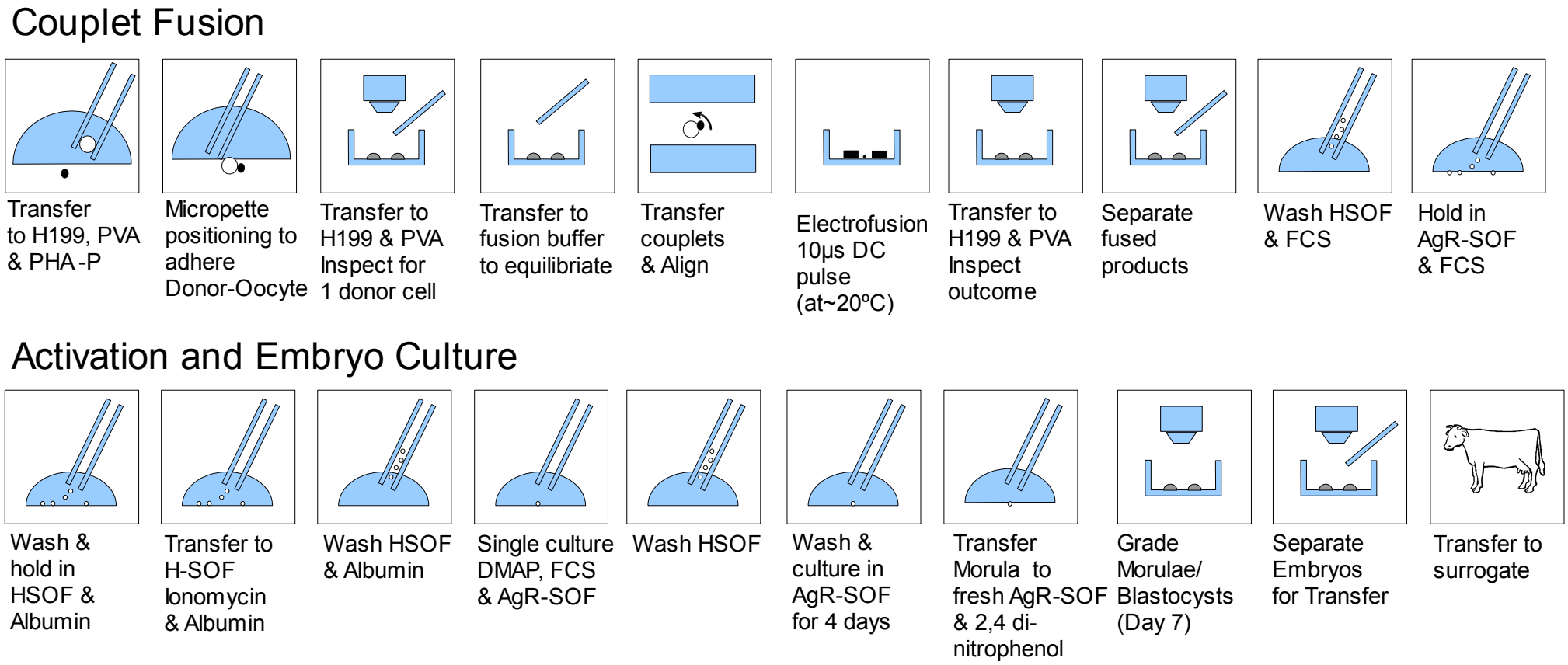

Fig. 3 Cell handling stages in a bovine zona-free NT cloning procedure (AgResearch, 2003)

Stages depicted are: Oocyte and adult ear cell fibroblast preparation, enucleation of recipient oocyte, Electrofusion of donor and cytoplast, activation, embryo culture, grading and transfer.

Donor Cell Isolation

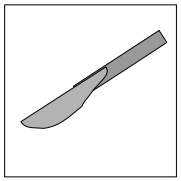
Ear skin tissue sample

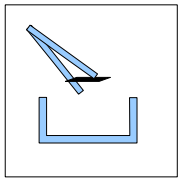
Rinses Ethanol & PBS

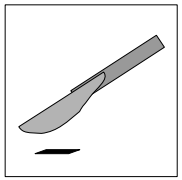
Dice Tissue

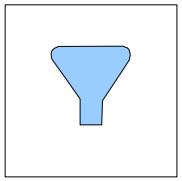
Culture 3-6 passages

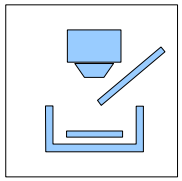
G1 cell selection (in H199 & FCS)

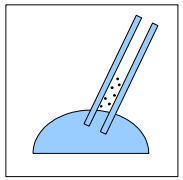
Transfer to H199 & PVA

Oocyte Isolation and Maturation

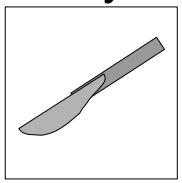
Slaughter-house Ovary extraction

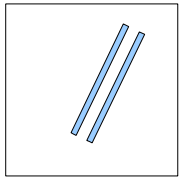
Select &' Aspirate Cumulus oocyte Complexes

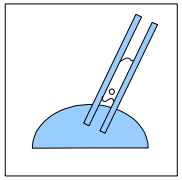
Wash H199 & FCS

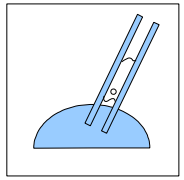
Wash B199 & FCS

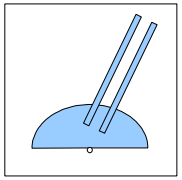
Culture in In-vitro Maturation Media ~19hrs

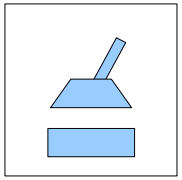
Disperse cumulus Vortex in Hyaluronidase

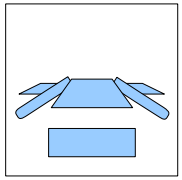
Centrifuge <3s to recover oocytes

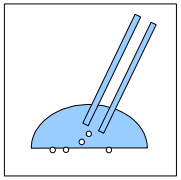
Wash H199 & PVA

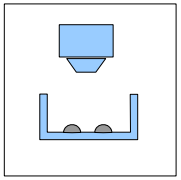
Inspect Oocytes for 1st Polar Body

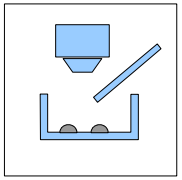
Separate Oocytes with 1st Polar Body

Zona Removal and Ennucleation

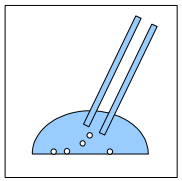
Transfer to pronase (Digest Zona)

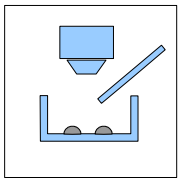
Inspect for start of zona dissolution and remove oocytes

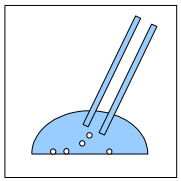
Hold in H199 & FCS (zona dissolves)

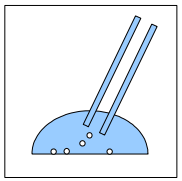
Nucleic Acid Stain

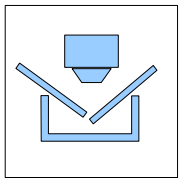
Transfer to Micro-manipulators

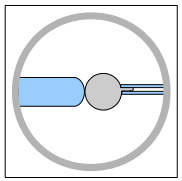
Aspirate Chromosomes

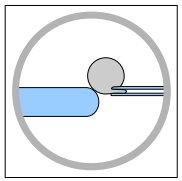
Pinch-off Karyoplast

The zona-intact oocytes with a 1st polar body are then selected, and transferred to a pronase droplet to degrade the zona pellucida. Once dissolution of the zona begins, the zona-intact oocyte is transferred to H199 & FCS and the remaining zona is allowed to dissolve.

enucleation of the zona-free oocyte is achieved by micromanipulators (three-axis oil hydraulic hanging joy-stick MO-188, Nikon Narishige, Japan) and an inverted microscope with epifluorescent illumination. The zona free oocyte is immersed in a fluorescent nucleic acid stain (Hoescht 33342) for five minutes. And then under UV illumination (duration of UV exposure is 10 ± 3 s) the metaphase plate and chromosomes are aspirated using a micropipette and a blunt separation needle (solid, tip radius ~ 75μm in diameter) the aspirated plasma membrane cytoplasm and nuclear DNA is pinched off forming a karyoplast vesicle. The smaller vesicle is removed leaving the oocyte devoid of DNA (i.e. a cytoplast).

2.3.2 Cell Fusion and Embryo Culture

The donor cells are dispersed in a droplet containing lectin (phytohemagglutinin). The cytoplast is then rolled using a mouth pipette over the donor cell to adhere them. The couplets are then transferred to hypo-osmolar fusion buffer and allowed to equilibrate and expand in size. Multiple couplets are then transferred by micropipette to a parallel plate electrofusion chamber containing two electrodes separated by 3mm (section 6.2). The couplet's rotationally symmetric axis is aligned perpendicular with the planar surface of the electrode. For most cells this is achieved using a 22 V (rms) alignment field, although couplets having small donor cells may require manual alignment. Two fusion pulses of 10 μs duration at ~ 600V are then applied to the electrodes. A delay of a few minutes is permitted to allow the membranes of fusing couplets to stabilise, and the products are transferred from the non-physiologically suited environment to H199 & PVA. The couplets are then inspected during the next hour for signs of lysis, detachment and fusion. Fused cells are then washed in HSOF & FCS and transferred for temporary storage to AgR-SOF & FCS (both steps without calcium). Formation of a completely spherical fusion product usually takes less than ten minutes.

While the contents of the cytoplasm have now mixed, the calcium release which occurs during fertilisation is not at this stage replicated. Activation is induced 4 hours post cell fusion by a combination of ionomycin induced calcium release assisted by immersion in 6-DMAP [70-73].

The unactivated fusion products are transferred to HSOF (a HEPES buffered synthetic oviduct fluid [59]) and bovine albumin for 30 minutes. The cells are incubated in ionomycin, HSOF and bovine albumin for 4 minutes to initiate activation. The cells are rinsed in HSOF with bovine albumin, and single cell cultured in 6-DMAP and AgR-SOF for 4 hours.

The cells are rinsed three times in HSOF, and once in AgR-SOF (a chemically defined media [74, 75]). Droplets (5 μl) of AgR-SOF are arrayed on a Petri dish and covered with paraffin oil. The cells are transferred to the droplets for single cell (per droplet) culture They are cultured for a total of seven days. After four days the media is renewed and 2,4 dinitrophenol is added [76]. The embryo development is assessed on day 7, and the embryos are graded for acceptable morphology [77, 78]. Grade 1 & 2 embryos are then transferred to a surrogate cow.

3 Cell Handling

Microfabricated tools were developed to assist the handling of cells during NT cloning. In this chapter background for tool design is presented regarding: NT by cell membrane fusion, and micro-positioning of cells using electric fields. The cell is now briefly discussed as it illustrates the importance of transport mechanisms within a functioning micro-scale process and its construction relates to the membrane fusion mechanism.

3.1 The Cell

The cell consists of a number of unique substructures (Fig. 4) that house specialised chemical processes that must be isolated from other subsystems. Isolation is achieved by enclosing micro-scale quantities of liquid within a membrane. The mitochondria contains a multi-stage catalytic process [79-81] for converting sugar and oxygen into adenosine triphosphate (ATP) that powers most cellular reactions. Data storage, repair, and copying reactions occur within the nuclear membrane. Early production phases of cellular proteins occur within vesicles in the rough endoplasmic reticulum (ER). Membrane bound vesicles often packaged proteins and glycoproteins during intra-cellular transport from the rough ER to the Golgi apparatus or to the cell exterior [82-85]. Post production modification of proteins and glycoproteins occur in the golgi-apparatus. Recycling of many of the building blocks (including amino acids) used for the fabrication of cellular macromolecules occur within lysosomes. Lysosomes contain cytotoxic (~pH 5) reactive species (e.g. hydrogen peroxide) and enzymes (proteases) within a membrane.

A cell membrane consists of phospholipids and cholesterol in a bilayer arrangement (Fig. 5). The hydrophobic aliphatic tail of the phospholipid resides internal to the membrane, and the hydrophilic carboxylic end is located on the external surface of the membrane. Transport and isolation of specific chemicals are two important areas of cell function, which are assisted by membrane containment.

The membrane acts as a barrier that contains and isolates chemical reactants. However, controlled flow of material occurs through the membrane. Particles pass through the plasma membrane (Fig. 4 & 5) by different mechanisms depending on the type of particle. Small water molecules can pass through the plasma membrane by diffusion. Charged metal ions are transported through ion channels by diffusion or by linking with proteins to permit movement (powered by ATP) in an energetically unfavourable direction. Bulk transfer of material from the contents of transport vesicles past the plasma membrane occurs by

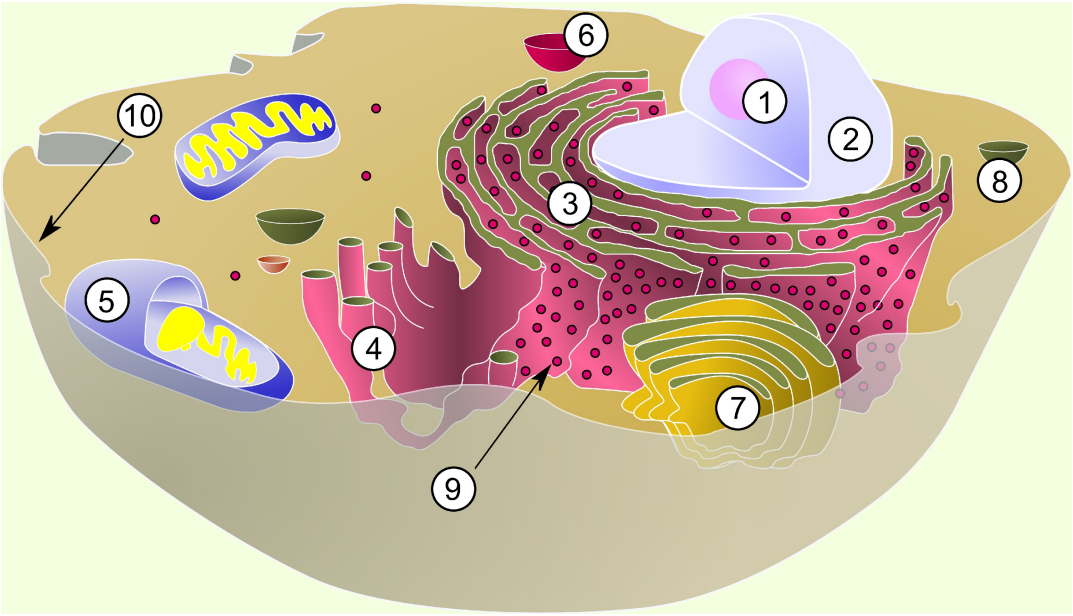

Fig. 4 Cross section of a mammalian cell (Adapted from MesserWoland [22])

(1) nucleolus (2) nucleus (3) rough endoplasmic reticulum (4) smooth endoplasmic reticulum (5) mitochondria (6) lysosome (7) golgi apparatus (8) vesicle (9) ribosomes (10) plasma membrane.

membrane fusion [86]. Membrane fusion, for example, results in the release of the vesicle contents (e.g. hormones such as insulin) from the cell[8]. Transport of material by this last mechanism, membrane fusion, is employed by micro-scale tools for bovine NT.

3.2 Cell Fusion

Cell fusion is a principle step in the base-line cloning process that permits the combination of genetic material. Under normal temperatures and conditions most types of biological cells do not fuse. This is because the carboxylic end of the phospholipids are very hydrophilic and they firmly retain a layer of water molecules that at the nano-scale prevents contact between adjacent cells. The plasma membrane and immobilised water molecules thus form a barrier preventing combination of genetic material.

[8]this process, exocytosis, may also operate in reverse where the cell engulfs extracellular fluid in a process called endocytosis.

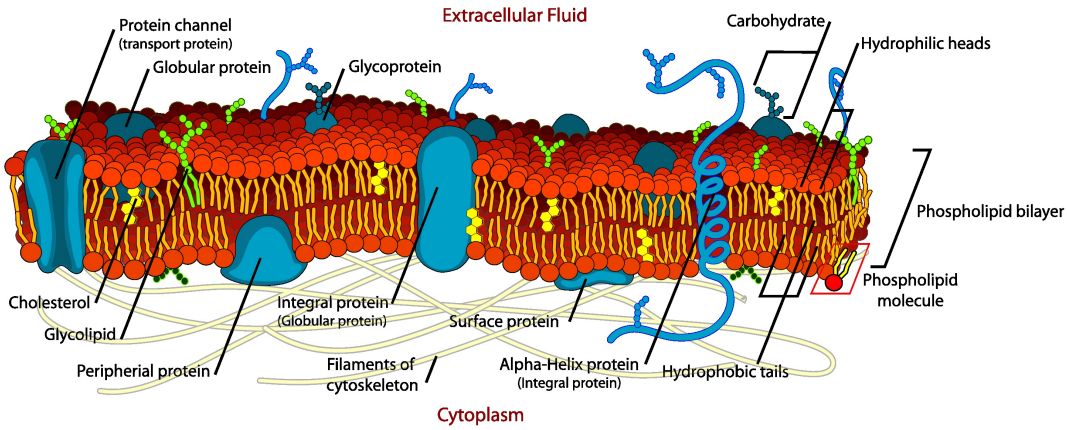

Fig. 5 Cross section of a plasma membrane (Villareal [23])

The plasma membrane is ~8nm thick.

Plasma membranes may be caused to fuse by addition of chemical fusogens (PEG), calcium ions [70], and viral proteins [87, 88]. Polyethylene glycol (PEG) is a chemical fusogen that has been used for many decades. It is a dehydrating agent. Cells placed in polyethylene glycol collapse in the hyper-osmolar solution. When the polyethylene glycol in which the cells are immersed is diluted, the clumped cells rehydrate and simultaneously fuse [89].

Due to the time constraint only one method of cell fusion, electrofusion, was used during tool development. The mechanism for electrically induced fusion of two cells is difficult to observe due to the speed of the neck formation (opening < 1µs [24, 90]) and small scale of the membrane (~8nm thick). However, observations have been made by rapid freezing of cells in liquid nitrogen after pulse application and examining the samples under s scanning electron microscope [91]. The process of membrane fusion has also been observed in artificially created liposomes (Fig.6). Here high-speed camera imaging shows that the fusion process involves the formation of one or more 'hour glass' necks between adjacent vesicles [24] and indicates that the two previous vesicles form a single vesicle encompassing the contents of the former two vesicles.

The transient electric field that induces cell fusion also induces the formation of pores [91] in the plasma membrane. Depending on the field strength and duration, an electrically created pore or electropore will either reseal, or expand until such time as the cell ruptures.

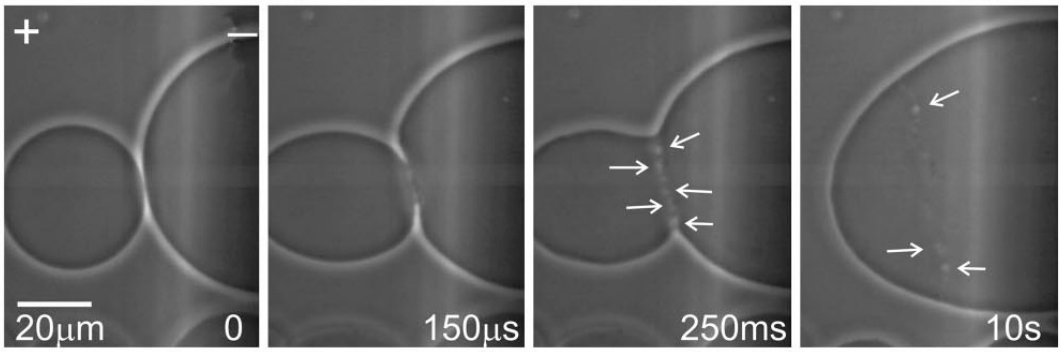

Fig. 6 Fusion of two giant liposomes (Haluska [24]).

DC pulse (width 150 µs) in the absence of salt. Small vesicles in the contact region are visible (arrows).

The irreversible damage to the plasma membrane may not always be clearly visible without dyes (author's experimental observation) as the cells structure may remain reasonably intact due to its internal cytoskeleton.

While in bovine NT the formation of a single spherical fusion product may be complete within 2-15 minutes, the cell takes a longer period of time to recover as it must deal with internalised extracellular media, and the rationalisation of duplicate intracellular material [89]. In plants, the cells are often capable of growing stably with triploid or greater multiples of the genetic complement, and fusion of cells is used for cross breeding [92-94]. A mammalian fusion product with a diploid complement of chromosomes is, in general, a prerequisite for healthy mammalian offspring [95]. The oocyte is therefore enucleated before electrofusion with a somatic (2N) cell in the baseline NT process.

3.3 Cell Polarisation

Cell polarisation due to charge movement is important in the following discussion of cell handling. The polarisation of a biological cell occurs by changes in molecular polarisation and by electrical conduction. Both biological cells, and surrounding liquid media restrict the motion of charges permitting the formation of polarised domains within them when an external electric field is applied [96]. In water based solutions this restriction of charges is commensurate with the length associated with the rotation of a water molecule. Unrestricted movement of ionic charges (ionic conduction) also causes polarisation of the cell.

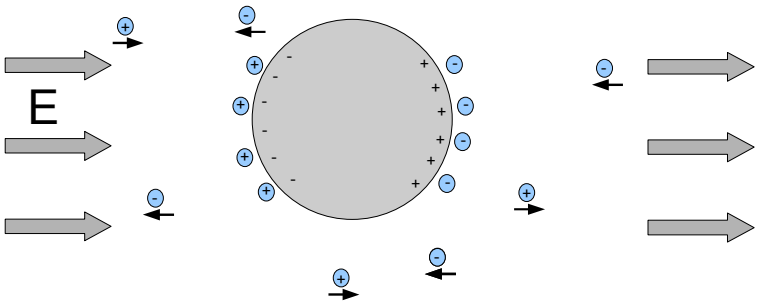

Fig. 7 Polarisation depicted for a cell in conducting media.

Surface charge due to cytoplasm polarisation is depicted inside the cell. Cytoplasm conduction is not shown.

A simple model may be used to illustrate some of the processes that occur when a cell is placed in an electric field. The cell may (theoretically) be considered to consist of an electrically uniform cytoplasm surrounded by a thin shell (the plasma membrane) and external fluid media. These three components are considered polarisable and, with the exception of the plasma membrane, conductive.

We now consider an electric field applied to the cell and surrounding media as shown in Fig. 7. At the moment the electric field is applied, the cell and the media (almost instantly) polarise. The difference in polarisability between the cytoplasm and fluid media results in a net, effective polarisation of the cell. However, as the external fluid media and cytoplasm conduct, ionic charges shift under the influence of the external electric field and gradually build up near the plasma membrane changing the cell's effective polarisation[9].

3.4 Membrane Charging: three time intervals

A cell placed in an electric field is subject to stresses which can cause the membrane to permeabilise. The plasma membrane prevents uncontrolled conduction of most ions and solutes through it provided that it is not permeated by the application of a strong electric field perpendicular to the membrane surface. A discussion of cell polarization and conduction is now made along the lines of that presented by Timoshkin et al [97] and Washizu et al [98].

[9]The charge distribution is unstable and any slight angular displacement, due perhaps to Brownian motion, results in torque being generated. This instability can cause cells to spin in a uniform DC or AC field if the field strength exceeds a certain threshold [4].

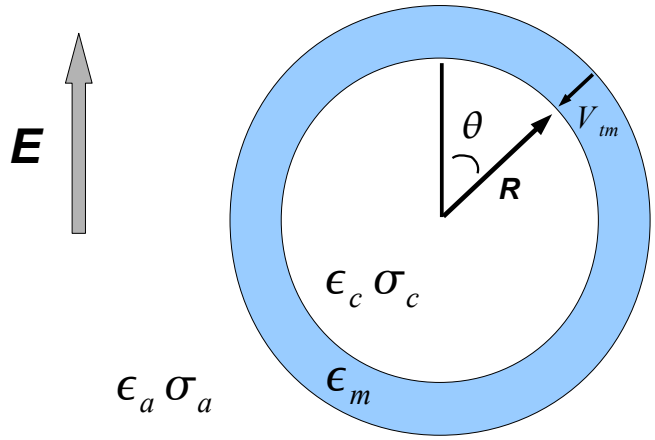

Fig. 8 Transmembrane voltage dependence on angle.

The situation is considered where an isolated cell suspended in a liquid is placed between two parallel plates and a DC step voltage is applied to the electrodes. The membrane conductivity is essentially zero. Polarisation is considered to be of three types: molecular rotational polarisation, internal membrane polarisation due to cytosol ionic charge accumulation and external membrane polarisation due to media ionic charge accumulation.

In the baseline NT fusion procedure the transmembrane voltage V_{tm} (Fig. 8) as a function of time may be split into three intervals in each of which V_{tm} can be approximated as a constant. These intervals are: an initial molecular rotational polarisation interval, the 'cytosol interval' and the 'media interval'. During the initial time period only molecules have time to re-orient and V_{tm} is low. The high conductivity of the cytosol (Table 1) permits charges to migrate more quickly to the inner surface of the cell than does the external media towards the outer membrane surface. The charging time constant of the inner surface is $\tau_c = \epsilon_0 \epsilon_c / \sigma_c$ or 5.9 ns[10] [97]. This marks the end of the initial polarisation interval and the beginning of the cytosol interval. During the cytosol interval the ionic conduction in the media does not have time to accumulate significant charge on the outer membrane surface; the transmembrane voltage V_{tm} is larger than during the initial polarisation interval. At $\tau_a = \epsilon_0 \epsilon_a / \sigma_a$ or 124 ns[10] (hypo-osmolar media) the charge on the

[10]using symbol definitions and values shown in Table 1 and Fig. 8

external surface of the cell due to external media conduction becomes significant. τ_a marks the end of the cytosol interval and beginning of the media interval where V_{tm} increases more rapidly [97] and approaches its steady state maximum value [89, 99].

$$V_{tm(max)} = \frac{3}{2} E R \cos(\theta) \tag{1}$$

Where R is the radius of the cell, θ is the angle given in Figure 8, E is the magnitude of the external electric field in the liquid media far from the cell and the resting membrane potential is neglected. The time constant for completing the charging of the cell membrane is [100]

$$\tau_m = R C_m \left(\sigma_c^{-1} + 0.5 \sigma_a^{-1} \right) \tag{2}$$

Where R is the radius of the cell, C_m [11] is the capacitance per unit area of the cell membrane (F/m^2), σ_c and σ_a are respectively the conductivities of the cytosol and the external liquid media. For an isolated oocyte, given the data in Table 1, τ_m = 53.8 µs.

The plasma membrane of larger cells is therefore according to Equation 1 more easily permeated than smaller cells. The cell membrane breakdown voltage is influenced by the membrane conductivity (especially when the fusion media has a low conductivity), cell line specific membrane proteins, temperature, pulse duration and intra-cellular hydrostatic pressure [89, 101].

3.5 Electroporation and Fusion

The cell membrane which is only ~8nm thick begins to breakdown at a voltage of ~1V. The resistance and ability of the membrane to withstand high field strength is quite remarkable. It can be seen that larger cells will reach the breakdown voltage quicker than smaller cells, and that the transmembrane voltage is highest at the two poles of the cell. The cell is generally internally polarised by ~0.7V relative to the extracellular media. If a

[11] as $C_m = \epsilon_m / d_m$ where d_m is the thickness of the cell's plasma membrane

DC pulse is applied the electrodes of a electroporation chamber, the transmembrane voltage generated by the external field is added to the resting transmembrane voltage and can cause one pole of the cell to rupture before the other [102].

If two cells are placed in contact the expression for the transmembrane voltage is evidently incorrect. It has been shown that allowing the internal and external membrane surfaces to complete charging can shield the region near the membrane contact point, while exposing the opposite ends of the cells to relatively higher transmembrane voltages [98][12]. It is desirable that the maximum transmembrane voltage be reached at the contact point. Reducing the fusion pulse duration increases the voltage at the contact point relative to other points on the membrane surface, but reducing the pulse duration also reduces the transmembrane voltage at all locations on the membrane including the inter-cell contact point. The use of a non-linear field to increase the transmembrane voltage at the contact point has been suggested for improving cell fusion rates [98]. Due to the number of variable factors involved such as cell line dependent membrane properties, both the fusion chamber electrode voltage and pulse duration are usually optimised experimentally (cf. 6.2 Coplanar Electrodes for NT cell fusion).

3.6 Dielectrophoresis

Pohl commented in 1978 that "experiment must accompany or even lead the theory [of non-uniform field effects]"[96]. Much has been learnt since that time, but verification of theory by experiment remains a corner stone of scientific research. In terms of building cell handling devices, it is not possible to merely identify a physical effect and study it on its own. To demonstrate a practical device, many simple aspects must be considered during construction and device operation that are not related to the novel physical principles upon which a device is based. These simple yet critical aspects can easily be overlooked in the design phase, and are easily identified by experiment. Experimental testing therefore holds a central role in tool development, in demonstrating both the principle of device operation and device utility.

Various methods of moving cells and liquids using electric fields are possible (chapter 7). Of these dielectrophoresis (DEP) was the method predominantly used during the course of research for cell handling. Dielectrophoresis was probably first observed when after amber

[12]although this may be offset by electro-deformation of the cells increasing the transmembrane voltage at the contact point [5].

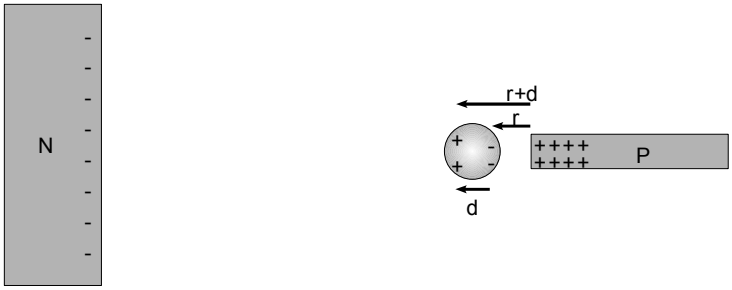

Fig. 9 A polarised particle with net neutral charge.

The force between two point charges (separated a distance r) is proportional to $1/r^2$. The charges on the negative electrode are sufficiently far away to be ignored. The forces on the positive and negative poles of the particle differ causing a tendency for the particle to move.

was rubbed with a cloth, material was attracted to the amber. DEP is defined as "the translational motion of neutral matter caused by polarization effects in a non-uniform electric field" [96]. The cause of the movement of an object with net zero charge in a non-uniform field is due to the redistribution of charge within the object resulting in a separation of charges at opposite ends of the particle (i.e. particle polarisation).

A simple model that indicates a force will be created on a cell in a non-uniform electric field is obtained by comparison with a small electric dipole [103]. In a uniform field the forces on both poles are equal and opposite, and the polarised body does not move. However in a non-uniform field the field strength is usually unequal at the two poles causing movement of the polarised body (Fig. 9).

The force acting upon a dipole in a non-uniform but conservative electric field can be split into rotational (T - torque) and translational (F) components (Appendix B).

$$F = |\boldsymbol{\mu}| \cos(\theta) \nabla |\boldsymbol{E}| \tag{3}$$

$$T = -|\boldsymbol{\mu}||\boldsymbol{E}| \sin(\theta) \tag{4}$$

Where θ is the angle between the dipole direction and that of the electric field and $\boldsymbol{\mu} = q\,\boldsymbol{d}$ is the (turning) moment of an electric dipole

F is proportional to the gradient of the Electric field. A dipole placed between two flat conducting parallel plates will not experience a translational force as the field is uniform and thus $\nabla|\boldsymbol{E}|=0$ in Equation 3. If the dipole is oriented at an angle to the electric field, it will rotate until the angle becomes zero. In a non-uniform field a dipole rotates so that it is not pointing perpendicular to the field before translation occurs (F=0 when $\theta=\pi/2$).

The translational force on an dipole in a non-conducting media can be written [103-105]

$$\boldsymbol{F}=(\boldsymbol{\mu}\cdot\nabla)\boldsymbol{E} \tag{5}$$

where $\boldsymbol{\mu}=q\,\boldsymbol{d}$ is the (turning) moment of an electric dipole and ∇ is the del operator and

$$\boldsymbol{\mu}\cdot\nabla=\mu_x\frac{\partial}{\partial x}+\mu_y\frac{\partial}{\partial y}+\mu_z\frac{\partial}{\partial z} \tag{6}$$

A sphere polarised by a uniform field can be approximated as an infinitesimally small electric dipole in the region external to the sphere and the equivalent dipole moment **μ** calculated (Appendix B).

$$\boldsymbol{\mu}=4\pi R^3\epsilon_a\frac{\epsilon_i-\epsilon_a}{\epsilon_i+2\epsilon_a}\boldsymbol{E} \tag{7}$$

or

$$\boldsymbol{\mu}=3\mathrm{v}\,K\,\epsilon_a\boldsymbol{E} \tag{8}$$

Where v is the volume of the particle, ϵ is the absolute dielectric permittivity of the material and the subscripts 'a' and 'i' denote respectively the material external and internal to the sphere. *K* is the Clausius-Mossotti factor (CM) [96]

$$K = \frac{\epsilon_i - \epsilon_a}{\epsilon_i + 2\epsilon_a} \tag{9}$$

where $\epsilon_i > 0, \epsilon_a > 0$ and $-\frac{1}{2} < K < 1$

Therefore from Equation 5

$$\boldsymbol{F} = (3\mathrm{v}\epsilon_a K \boldsymbol{E} \cdot \nabla)\boldsymbol{E} \tag{10}$$

and as $2(\boldsymbol{E} \cdot \nabla)\boldsymbol{E} = \nabla|\boldsymbol{E}|^2$

$$\boldsymbol{F} = \frac{3}{2} v \epsilon_a K \nabla|\boldsymbol{E}^2| \tag{11}$$

Equation 11 is commonly written

$$\boldsymbol{F} = 2\pi R^3 \epsilon_a K \nabla(E^2) \tag{12}$$

where $E = |\boldsymbol{E}|$.

Because $\nabla E^2 = 2E\nabla E$ [13], if the gradient is retained constant (and excluding the case where E is uniform or $\nabla E = 0$) increasing the field strength will increase the DEP force. This can be explained as it is not simply the difference of electric forces applied at the two ends of the dipole, but the magnitude of the dipole itself which changes when the electric field changes (Equation 8).

The calculation of the effective dipole moment assumes that the externally applied electric field is uniform throughout the sphere. The force is volume dependent $\propto R^3$. The sign of

[13]The direction of ∇E^2 is the same as ∇E .

K, and thus the direction of the force, depends on whether $\epsilon_i > \epsilon_a$ that is whether the cell polarises more than the surrounding liquid [2]. The force is zero when the permittivity of the media ϵ_a and the sphere ϵ_i are equal (K=0). The maximum attainable force is significantly influenced by ϵ_a because $\epsilon_a K \leq \epsilon_a$ irrespective of ϵ_i [96].

3.7 Phase Delay in a non-ideal dielectric

In an alternating electric field, the effective polarisation of a cell changes with the frequency of the applied field depending on the relative influence of conduction and dielectric polarisation.

To introduce commonly used notation describing real dielectric materials, a parallel plate capacitor is considered. Between the plates is a non-ideal dielectric with conductivity σ. An AC voltage of angular frequency ω is applied to the parallel plates, which generates a uniform electric field $\boldsymbol{E}$

$$\boldsymbol{E} = \boldsymbol{E_0} e^{i\omega t} \tag{13}$$

where i is an imaginary number, and t is time.

Two currents will flow. The first is a conduction current due to the unrestricted movement of charges. The second, the displacement current, can be considered due to cyclical polarisation of the dielectric.

The current density due to conduction is

$$\boldsymbol{J} = \sigma \boldsymbol{E} \tag{14}$$

The displacement current density can be found by integrating over the surface of an appropriately selected 3D region containing the surface charges on one plate of a parallel plate capacitor.

$$\oiint D = \rho \tag{15}$$

$$\frac{\partial D}{\partial t} = \boldsymbol{J}_{\boldsymbol{d}} \tag{16}$$

The current density due to the displacement current is (assuming $\boldsymbol{D} = \epsilon \boldsymbol{E}$)

$$\frac{\partial \boldsymbol{D}}{\partial t} = \boldsymbol{J}_{\boldsymbol{d}} = i\,\omega\,\epsilon\,\boldsymbol{E} \tag{17}$$

The total current density is therefore

$$\boldsymbol{J} = \boldsymbol{J}_{\boldsymbol{c}} + \boldsymbol{J}_{\boldsymbol{d}} = (\sigma + i\,\omega\,\epsilon)\,\boldsymbol{E} \tag{18}$$

It has been observed that there are delays between application of the Electric field and the response of the conduction and displacement currents [96, 106]. This delay can be accounted for by the introduction of θ_C and θ_D

$$\boldsymbol{D} = \boldsymbol{D}_{\boldsymbol{0}} e^{(i\omega t - \theta_D)} \tag{19}$$

$$\boldsymbol{J}_{\boldsymbol{C}} = \boldsymbol{J}_{\boldsymbol{C0}} e^{(i\omega t - \theta_C)} \tag{20}$$

A new complex permittivity $\underline{\epsilon}$ is defined

$$\boldsymbol{D} = \underline{\epsilon}\,\boldsymbol{E} \tag{21}$$

$$\underline{\epsilon} = \frac{\boldsymbol{D}}{\boldsymbol{E}} = \frac{\boldsymbol{D}_{\boldsymbol{0}}}{\boldsymbol{E}_{\boldsymbol{0}}} e^{-i\theta_D} = \epsilon_R - i\,\epsilon_I \tag{22}$$

similarly a new complex conductance is defined[14]

$$\underline{\sigma}=\frac{\boldsymbol{J_C}}{\boldsymbol{E}}=\frac{\boldsymbol{J_{C0}}}{\boldsymbol{E_0}}e^{-i\theta_C}=\sigma_R+i\,\sigma_I \tag{23}$$

Thus

$$\boldsymbol{J_C}=(\sigma_R+i\sigma_I)\boldsymbol{E} \tag{24}$$

$$\boldsymbol{J_D}=i\,\omega(\epsilon_R-i\epsilon_I)\boldsymbol{E} \tag{25}$$

$$\boldsymbol{J}=\boldsymbol{J_C}+\boldsymbol{J_D} \tag{26}$$

Comparing equations 18,24-26 (see Fig. 10)

$$\boldsymbol{J}=(\underline{\sigma}+i\omega\underline{\epsilon})\boldsymbol{E}=(\sigma+i\,\omega\epsilon)\boldsymbol{E} \tag{27}$$

and

$$\sigma=\sigma_R+\omega\epsilon_I \tag{28}$$

$$\epsilon=\frac{\sigma_I}{\omega}+\epsilon_R \tag{29}$$

[14]The conductance is sometimes defined in literature as $\underline{\sigma}=\sigma_R-i\,\sigma_I$. This effects, in particular, equations 30 - 34

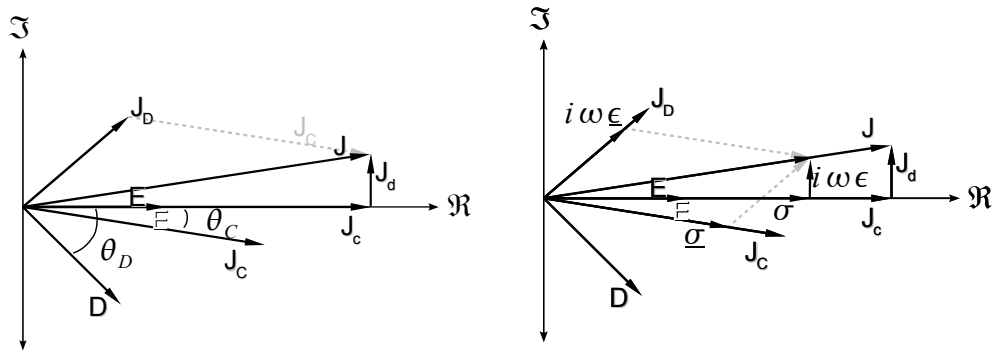

Fig. 10 Vectorial depiction of current density and impedance phasors

The imaginary component of the complex permittivity has the same effect as if the dielectric were conducting. Similarly the imaginary component of the conductivity divided by the angular frequency has the same effect as if the dielectric were polarising. Thus in literature the following are often interchanged:

$$\sigma_R \leftarrow\rightarrow \omega \epsilon_I \tag{30}$$

$$\sigma_I \leftarrow\rightarrow \omega \epsilon_R \tag{31}$$

$$\underline{\sigma} \leftarrow\rightarrow i\omega\underline{\epsilon} \tag{32}$$

Authors write for example

$$\underline{\epsilon} = \epsilon_R - i\frac{\sigma_R}{\omega} \tag{33}$$

and

$$\underline{\sigma} = \sigma_R + i\omega\epsilon_R \tag{34}$$

3.8 Models for DEP force calculation

Models have been derived for ellipsoidal [107], multi-shelled particles [6] , and particle and media with frequency dependent polarisability and conductivity. An often referenced model "the effective moment method" [6] incorporates the effect of frequency on particle and media polarisation[15].

In this model, the time averaged force[16] for a non-shelled spherical particle is:

$$\boldsymbol{F}_{av} = 2\pi R^3 \epsilon_a \Re[\underline{K}] \nabla(\boldsymbol{E}_{rms}{}^2) \tag{35}$$

$$\boldsymbol{T}_{av} = -4\pi R^3 \epsilon_a \Im[\underline{K}] E_{rms}{}^2 \tag{36}$$

where the complex CM, $\underline{K}$ is defined as (8) except with complex dielectric permittivities $\underline{\epsilon_a} = \epsilon_a + \sigma_a / i\omega$ and $\underline{\epsilon_i} = \epsilon_i + \sigma_i / i\omega$ [17], and $\Re[\,]$, $\Im[\,]$ denote the real and imaginary parts of the quantity contained within the brackets. Typical parameters used in modelling the cell and media are listed in Table 1.

3.9 The Debye surface polarisation layer

When a solid and a fluid are placed in contact, the surface atoms of the solid usually have an unmatched charge due to differences in affinities for electrons and ions [105]. A liquid containing ions is under normal circumstances electrically neutral. If a liquid containing ions is placed in contact with a solid surface, the ions migrate to form a diffuse layer of counter charges near the surface of the solid. If the solid has a negative charge (as occurs when glass is placed in contact with water) positive ions are attracted to form a counter charge layer, and negative charges are repelled. The charge density of positive and negative ions within the counter ion layer is dependent on thermal motion, and distance from the solid's surface.

[15]Small modifications to the following equations permit analysis of multi-shelled spherical particles, and application to cases where losses in the dielectric media are significant [6].

[16]The force on the particle with alternating electric fields is cyclical at twice the applied frequency as the DEP force is independent of the sign of the electric field due to the square of the electric field in Equation 12.

[17]cf. Equation 33

Cell Parameter		Value
Dimensions		
Membrane Thickness d_m		8×10^{-9} m
Diameter oocyte		120×10^{-6} m
Diameter fibroblast		20×10^{-6} m
Conductivity σ		
Intracellular (cytosol) σ_i		0.53 S/m
Membrane σ_m		10^{-6} S/m
Culture Media		0.12 S/m
Hypo-osmolar Fusion Buffer†		5.7×10^{-3} S/m
Pure water		5×10^{-6} S/m @ 25 ºC [105]
Dielectric Permittivity (relative) ϵ		
Cytosol ϵ_c		50
Membrane ϵ_m		9.04
Pure Water‡		80
Dielectric Permittivity Vacuum ϵ_0 [18]		$\approx 8.854 \times 10^{-12}$ F/m
Dielectric breakdown (Eukaryotic Cell Membrane [89])		0.5-1.5 V

Table 1 Cell and media parameters

Adapted from Gimsa et al [108]. *†Media in which cells are placed before and during application of the Fusion pulse* [28]. *‡Solutes generally decrease the permittivity* [105]

[18] $\epsilon_0 = \frac{1}{\mu_0 c^2}$ where $\mu_0 = 4\pi \times 10^{-7}$ N/A² and $c = 3 \times 10^8$ m/s [7]

An electrical model[19] representing two parallel plate electrodes in a conducting liquid dielectric (representing the liquid suspending biological cells) is shown in Fig. 11. Application of a DC voltage greater than the electrochemical potential difference causes a chemical reaction to occur. At frequencies above $\tau_D = R_{EC}C_D$ the impedance of the Debye layer reduces and the voltage across the Debye layer drops below V_{EC} preventing electrolysis of the fluid. Operating above τ_D prevents electrochemical reactions and maximises the field strength in the bulk of the liquid.

3.10 Cell Positioning using DEP

Some simple experimental observations serve to illustrate movement of polarised cells. In Fig. 12, polystyrene microspheres (Polysciences™) are placed between two film electrodes coated on a glass substrate. The microspheres are observed to aggregate and form pearl chains.

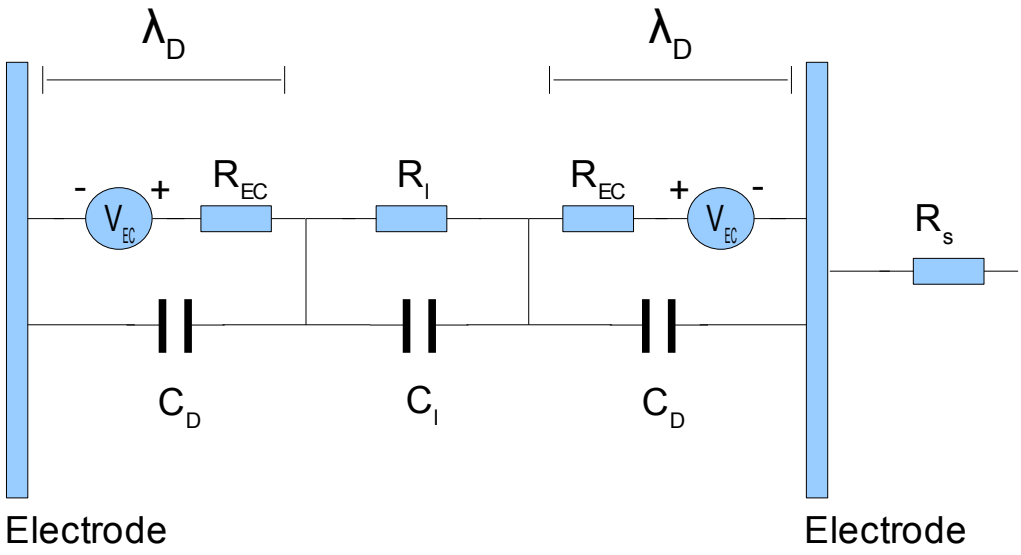

Fig. 11 Electrical model of two parallel plate electrodes immersed in liquid media

Adapted from [25]. λ_D is the Debye length, and is in the order of a few nanometres. C_D is the Debye layer capacitance. R_{EC} is the resistance associated with energy absorbed by electrochemical reactions. V_{EC} is the electrochemical potential (typically around 1V), R_I the liquid media resistance, C_I the liquid media capacitance and R_S the lead resistance.

[19] Model parameters could be evaluated by measuring voltage at which electrolytic dissociations occur and current through the cell as functions of frequency [8]. Parameters are dependent on the liquid and electrode concerned.

Yeast cells (4-6 µm) are observed (Fig. 13) to be attracted at about 20kHz towards electrode edges where field maxima existed and were repelled at about 1MHz. The direction of the yeast pearl chains is perpendicular to the electrode edge for both positive and negative DEP. Yeast cells were often used as positive and negative DEP markers to visualise the direction of the maximum electric field gradient due to their low cost and simple preparation.

During positive DEP the cell is polarised more strongly than the surrounding media, causing the field intensity to increase at the poles. This high intensity region has an associated gradient which causes cell chaining (Fig. 14). The chains orient in the same direction for both positive and negative DEP because during negative DEP it is effectively the fluid, not the cells, that form DEP chains [96].

The rate of aggregation is dependent on fluid drag, which in turn increases with cell velocity. However the dielectric force is independent of the cells velocity, thus a terminal velocity is reached. This terminal velocity can be very low, so that a cell (or bead) in physiological solutions may take half a minute or so to reach its destination. Increasing the particle velocity by increasing the magnitude of the electric field can result in deformation of the cell and membrane poration.

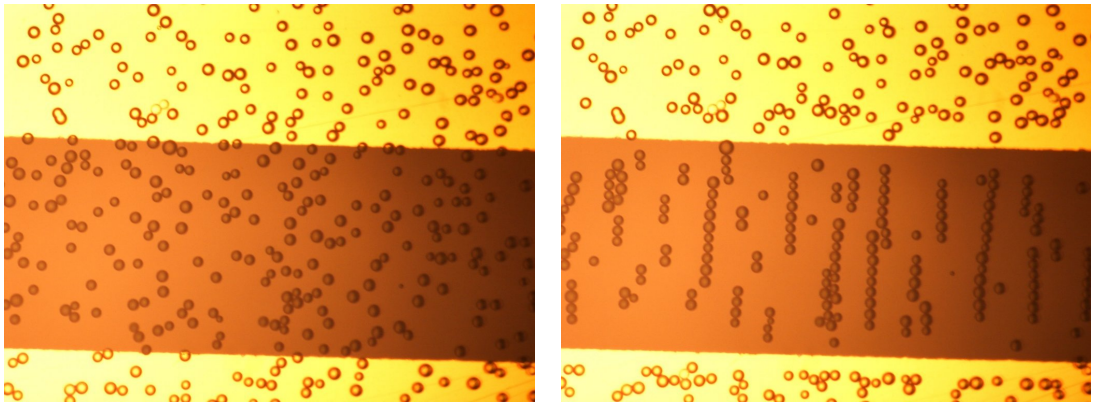

(a) (b)

Fig. 12 Pearl Chaining of 25 µm beads.

Beads were dispensed (a), an AC electric field was applied, and after a short delay (~3/4 minute) the beads formed pearl chains (b). Beads are located away from electrode edges indicating negative DEP.

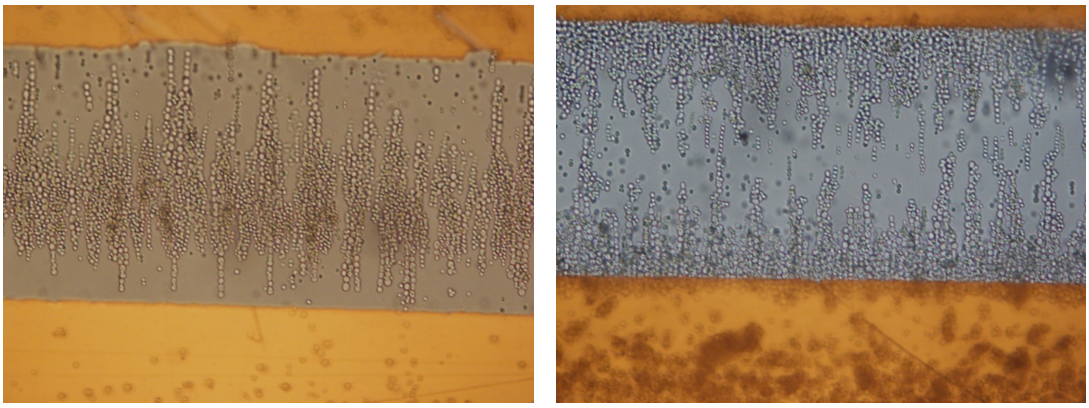

(a) (b)

Fig. 13 Pearl Chaining of yeast cells.

(a) Negative DEP at 900kHz (b), positive DEP at 10kHz. Above the electrodes (right) there is a sparse region that results from attraction of yeast cells towards the high intensity field regions near the electrode edges.

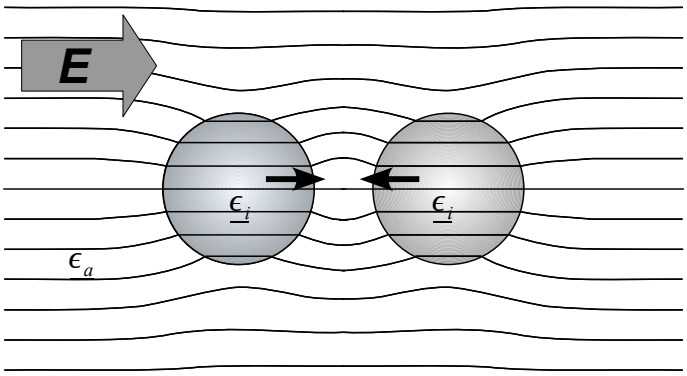

Fig. 14 Positive DEP chaining of two cells.

Perturbation of the external electric field by induced polarisation causes cells to aggregate forming chains. The field is concentrated at the contact point of the cells. The permittivity/conductivity of the cell exceeds that of the surrounding fluid.

3.11 Holding cells at solid surfaces

Dielectrophoresis may be used to attract cells over short range (<1mm) distances and trap them at local field maxima or minima. The trapping of cells using DEP was considered by Washizu et al [109]. It was showed that in an electric field, a cell is trapped at convex surfaces[20], whether they be conducting or not, and conversely they are repelled by concave surfaces[21]. These statements are conditional upon

(1) K>0, i.e. the cell is more strongly polarised than the surrounding fluid.

(2) Conduction dominates in the fluid, i.e. $\epsilon_{media}\rho_{media}<\omega$ (ω is the field frequency)

(3) The external field does not change rapidly throughout the volume of the cell.

That trapping occurs at convex surfaces can be shown by considering the force acting upon a cell in a reference frame aligned with the electric field vector (Fig. 15). The Forces in the reference frame can be decomposed into components normal and tangential to the electric field vector.

The normal component is [109]

$$F_n = k E^2 (\nabla \times \boldsymbol{t}).\boldsymbol{n}' = k E^2 \frac{\partial \theta}{\partial t} \tag{37}$$

where the unit tangent and normal vectors to the electric field are $\boldsymbol{t}$ and $\boldsymbol{n}$ and $\boldsymbol{n}' = \boldsymbol{t} \times \boldsymbol{n}$ and the tangential component

$$F_t = -k E^2 (\nabla . \boldsymbol{t}) = -k E^2 \frac{\partial \theta}{\partial n} \tag{38}$$

[20]Once the cell reaches a solid surface it can continue to move along the surface.

[21]The 'curvature' depends on distance from the surface. From earth, the surface of the moon appears as a convex sphere while standing in a moon crater, the surface appears concave.

Trapping forces exerted upon a cell may be illustrated by considering insulating and conducting surfaces. First the insulating surface is considered. As it is assumed that conduction dominates over the "displacement" current in the fluid (condition [2]), no field lines cross the insulator surface. The electric field and thus F_t are directed tangential to the surface and *n* perpendicular to it. The dielectric force F_n is thus directed towards the insulator if its curvature $\frac{\partial \theta}{\partial t}$ is negative (i.e. convex), and away from it if the curvature is positive[22].

Second a perfect (solid) conductor and its surface are considered where $\frac{\partial E}{\partial t}$ is sufficiently low so as to assume a static charge distribution. In this case, there is no electric field at the surface of the conductor directed tangential to that surface. Therefore the electric field and F_t are perpendicular to the surface[23]. The force F_t is directed towards the surface if it is convex, i.e. $\frac{\partial \theta}{\partial n}$ is negative[24].

A combination of insulating and conducting materials are used in some designs. While a convex curvature is required to trap cells with either insulating or conducting materials, this is not so when the field changes rapidly relative to the dimensions of the cell (condition '3' is invalidated). Objects with dimensions smaller than the cell can cause these rapid field changes and thus cell trapping. Designs such as thin film coplanar electrodes on glass and very shallow micropits are essentially continuous flat (zero curvature) surfaces. These designs have a discontinuity at the interface between the conductor and the insulator that creates a rapid change in the electric field, and are also capable of trapping cells, even though the effective curvature is zero.

---

[22] $\frac{\partial \theta}{\partial t}$ is negative in the case depicted in Fig. 15, in which case the Force F_n is in the $-n$ axis direction

[23] For the conducting case, the normal of the surface reference frame is in the direction of the electric field reference frame's tangent (and vice versa).

[24]One may consider the case where as one moves in the +ve t axis direction, the field lines converge. In this case, when one moves in the +ve n axis direction theta decreases, $\frac{\partial \theta}{\partial n}$ is negative, and $F_t > 0$.

DEP trapping may be used in combination with fluid flow, for separation of cell mixtures based on their electrical properties [110, 111] or for positioning small groups of cells at specific locations [112, 113].

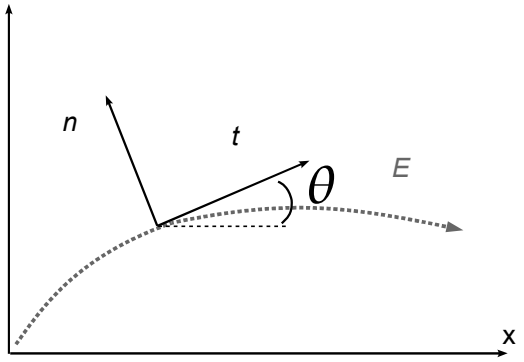

Fig. 15 Reference frame for DEP force vectors

Theta is the angle between the tangent to the electric field vector and the 'x' axis.

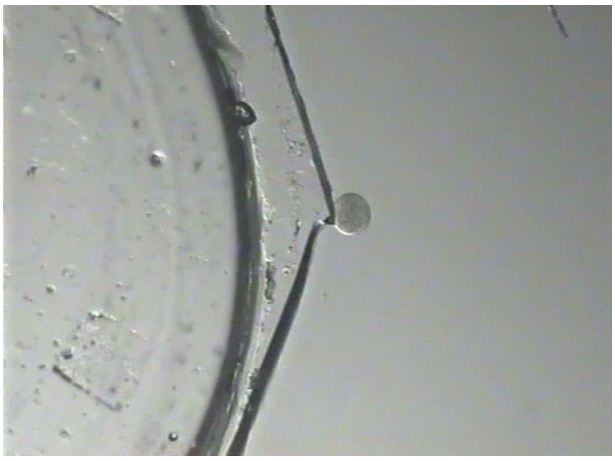

Fig. 16 A cell held by positive DEP near a convex surface

4 MicroFabrication

The concept of a "lab on a chip" became popular around 2001[25]. Early lab-on-chip systems were usually fabricated using tools designed for microprocessors. Microprocessor fabrication tools are based on a UV lithographic process and photoresists for patterning silicon and metal layers [114, 115]. Thicker films (50-500 µm) were sometimes required for micromechanical and microfluidic applications. One of the early micro-electro-mechanical fabrication methods for creating structures with large (>50 µm) vertical dimensions is the use of synchrotron high energy X-ray beams for exposing very thick (1-2mm) polymethylmethacrylate (PMMA) [116]. PMMA is developed using solvents to form a patterned plastic part with a high aspect ratio. Reciprocal metal parts can be made by electroplating and used for plastic injection moulding (LIGA process [117]).

Researchers developed lower cost fabrication methods were developed for prototype fabrication. Photo-Polymer resist SU-8 became important as a relatively low cost thick film (50-500 µm) photo-patternable material which was compatible with existing micro-fabrication equipment. The tradition of moulding to build micro structures from superior materials was continued, in particular PDMS a silicone elastomer was used for enclosed microchannel formation due to its transparency, ease of bonding, and capacity to form high quality mouldings.

At the same time as existing microprocessor technology was modified to permit investigation of the microscale domain, the precision of traditional engineering techniques was also improved. The boundary of traditional manufacturing capability has gradually progressed into the micro-scale domain. Automated milling machines are capable of position resolution of 1nm [118]. Mechanical drills are available with a diameter of 5µm (Performance Microtool Inc., USA). Lathes have been used to fabricate spindles less than 10 µm in diameter [119]. Micro electrodischarge machining has been used to create micro holes smaller than 5µm in diameter [120].

There are a limitless number of fabrication methods. Two other important microfabrication methods are material removal using UV lasers (and also low cost carbon dioxide lasers) to create trenches, slots and micro holes [121] and sintering powders to form polymer and metallic micro-devices [122-124].

[25] the year when the Lab-on-chip journal was first published.

In this chapter, background information is presented on IC technologies that were used in device fabrication: surface coating and UV lithography.

4.1 Surface Coating

An important area of fabrication is creating a surface coating. Surface coatings may be used to modify a surface's thermal and electrical conductivity, dielectric constant (water contact angle), chemical reactivity (including adhesion properties) and to protect parts from heat, abrasion and corrosion.

Methods of coating substrate materials include: dipping, painting, spincoating, spraycoating, wet chemical deposition, electroplating, electrospinning, 'ink' patterning by deformable stamps and vapour deposition. Two methods from the semiconductor industry are now considered, namely vacuum deposition of metals and spin coating of organic polymers.

4.1.1 Vacuum Deposition

It is possible to take a solid material (the source) and with it coat a sample (or substrate) in a vacuum chamber. Removal of material occurs at the surface of the source. Two common ways material may be removed from the source are by heating a solid so that it evaporates or by bombarding it with an ionized gas (plasma) so that source atoms are knocked (or sputtered) from the surface of the source. These methods are known respectively as “thermal evaporation” and “sputtering” and are suitable for depositing a wide variety of inorganic materials.

Evacuated chambers are necessary for many metal deposition processes. At atmospheric pressure and temperature, the mean free path of Nitrogen gas is approximately 65nm [125]. By reducing the pressure, atoms or ions emitted from a solid are able to travel unobstructed from the source to the substrate. Chamber evacuation is also important to reduce the incorporation of unwanted gasses into the surface coating. Higher quality vacuums are generally required for sputtering systems than evaporators, as an ionized gas is used which can promote the chemical reaction of contaminant gasses during the film formation. Various pumps may be used to create vacuums. Vacuums above 0.1Pa (low vacuum) can be produced by rotary vane pumps, rotary piston pumps, roots blowers and sorption[26] pumps [125]. Vacuums from 0.1 to 10^{-4}Pa (high vacuum) can be produced by certain

[26]liquid nitrogen cooled adsorption by porous material

capture pumps (cryo[27]-, getter) and momentum pumps (turbomolecular pumps and diffusion pumps) [125]. Evacuation of the chamber generally occurs in two stages, first by a low vacuum pumping system, and then by a high vacuum system. Both capture pumps and momentum pumps must be assisted by low pressure pumps before they can begin operation. For capture pumps, the pumps have a limited capture capacity and therefore require forepumps. Momentum pumps require pumping assistance both prior to and during operation as they are not efficient in the atmospheric to low vacuum range (101.3kPa to 10Pa[28]).

4.1.2 Thermal Evaporation

Thermal evaporation may be caused by resistive heating. Figure 24 shows a system using an electron beam source to (resistively) heat the source material held in a crucible. The electron gun typically operates at about 10kV, from 0-1.5A, depositing 0-15kW within the source material surface area. The beam is focused to an area of ~ 0.5 cm diameter and is

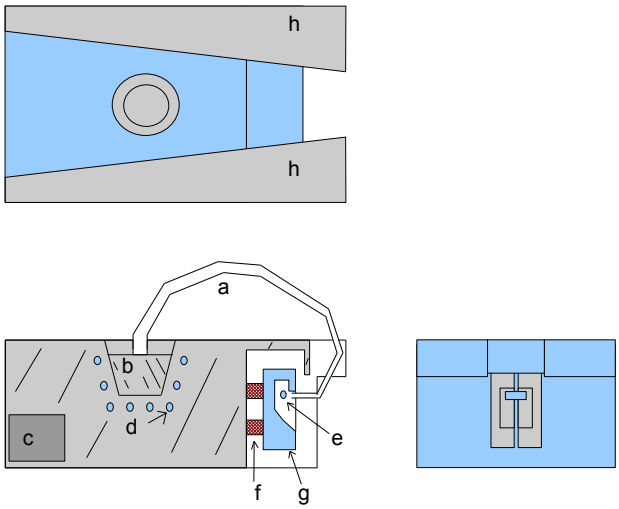

Fig. 17 Electron beam thermal evaporation.

(a) electron beam (b) Hearth (c) Permanent magnet combined with electromagnet (d) Water coolant (e) Filament (f) alumina mounting insulators (g) Two (~500 °C) filament blocks at -10kV below anode hearth ground. (h) Soft iron magnets. Adapted from [26]

[27]helium cooled condensation pump

[28]1 atmosphere = 760 Torr = 1.013 x 10^5 Pa = 1.013 Bar.

incident perpendicular to the surface of the source material. Thermal evaporation systems usually operated at a system pressure of 10^{-5} Torr, where the mean free path length is 5m. Atoms[29] ejected from the source move away in a straight path not interacting with other atoms before they reach the substrate. Interestingly, non-conductive sources such as silicon dioxide may be evaporated by electron beam thermal sources. Water cooling failure during evaporation at 5kV will usually destroy the electron beam gun in under 1 minute (Graper pg. A1.2:4, [26]).

4.1.3 Sputtering

A simplified DC sputtering system is shown in Fig. 18 (Two plates and glow regions). The space (even non-glowing regions) between the plates is occupied by an electric plasma. Argon is commonly used as an inert ionizable gas. Less than 1 percent of the gas is ionized. Positive ions are attracted towards the negatively charged source material (cathode). These ions and a lower concentration of electrons form a net positively charged sheath around the electrode. A continuous flow of ions occurs from the plasma to the cathode. The ions are accelerated across a high potential that occurs between just inside the edge of the negative glow region and the cathode . The ions then bombard the source (target) and material is ejected (Fig. 20) from the target: electrons, X-rays, neutral working gas and source material atoms.

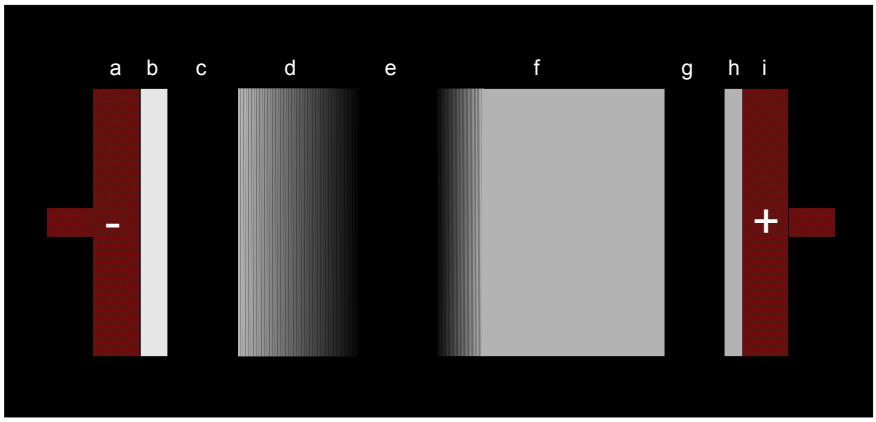

Fig. 18 Simplified DC sputtering system showing glow discharge regions.

(a) Cathode (b) Cathode glow (c) Cathode (Crookes) dark space (d) Negative glow (e) Faraday dark space (f) Positive column (g) Anode dark space (h) Anode glow (i) Anode. The “negative glow” region (c) is essentially at the same potential as the anode.

[29]The evaporant is partially ionized by the electron beam [9]

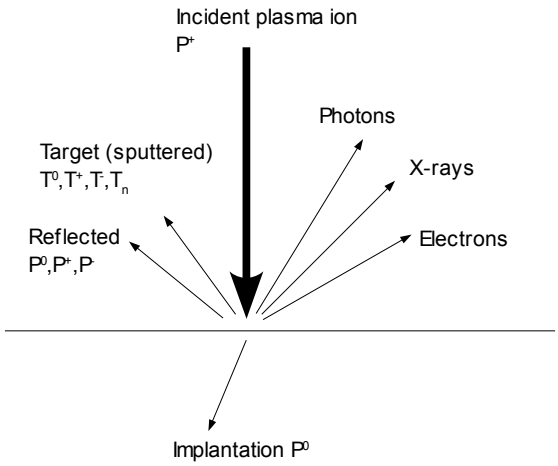

Fig. 19 Plasma source erosion.

Most momentum exchange occurs within 10Å of the surface. P denotes an atom or ion derived from the Plasma, and similarly T from the Target.

The mean free path length of the electrons is shorter than that for the ions, and they collide with gas atoms in the "negative glow" region to cause gas ionisation that sustains the plasma and electrical conduction. DC glow discharge normally occurs at 20-100 mTorr to maximise deposition rate. The pressure used is a trade-off between the working gas blocking incident plasma ions and sputtered atoms, and insufficient plasma bombardment to generate sputtered atoms (Shah pg. A3.0, [26]).

Sputtering offers an advantage over thermal deposition in that alloys may be deposited stoichiometrically. Initially one of the alloy metals may preferentially sputter, however this depletes this metal from the surface layer thereby increasing the sputtering rate of other metal atoms. Equalisation or "target conditioning", taking between a few minutes and an hour, is required to achieve stoichiometric deposition of the target (or source) material onto the substrate. Materials that are DC sputtered must be conductive.

DC sputtering system may be modified to increase the deposition rate and improve film coating characteristics. In the DC sputtering system the control of ion flux (hence deposition rate) and ion energy (film characteristics) can not easily be separated, although some adjustment can be made by controlling the sputtering pressure.

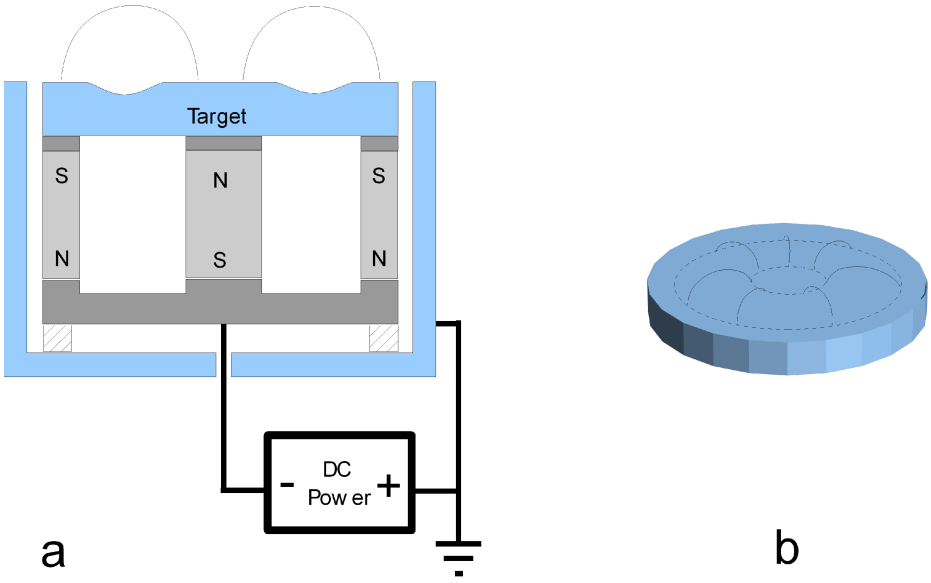

Fig. 20 Sputter Magnetron

(a) Cross section of Target and magnet arrangement. Lines show magnetic field. Electron trapping near the target (and high deposition rate) is dependent on DC operation. (b) 3D view of target, and magnetic field lines. The edges of the eroded sputter track are shown by dotted lines.

The ion flux on the target controls the deposition rate of sputtered atoms onto the substrate. Gas ionisation can be modified by increasing the path length of electrons using a magnetic field or by operating with a RF (instead of DC) voltage source (i.e. a sputter magnetron, Fig. 20). Another method is to have an additional electron source (e.g. triode sputterer). The ion energy can also be adjusted independently by accelerating the source material (Ion beam sputtering) once ionized using electric fields (ion sources e.g. Penning, Knudsen).

The use of RF is advantageous as it permits insulating source materials to be used. A vast amount of literature has been written on these topics [26, 125].

4.1.4 Sputter Etching

Sputter etching is used to remove material from a sample. Sputter etching equipment operates with the same principle as sputter deposition equipment, except that the sample is placed as the target and the destination of the sputtered atoms is relatively unimportant.

4.1.5 Reactive Ion Etching

A reactive ion etcher creates a plasma in a manner similar to an RF sputter etcher. Nominally the principle mechanism of material removal is by chemical reaction. The

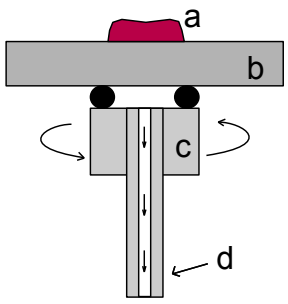

Fig. 21 Spin Coating a sample with Photoresist.

Photoresist (a) was dispensed by pipette onto a wafer (b) that was attached by a vacuum chuck (c) to a rotating electric motor shaft. The motor shaft was hollow forming a vacuum tube (d)

working gas used to generate a plasma often consists of a selected mixture of gasses. Chemically reactive species are formed by the plasma which are then absorbed onto the sample, chemically attack (etch) the sample and are desorped[30]. Ion bombardment of the sample assists the chemical reaction by providing energy for the reaction to occur, and energy to remove the reacted products from the surface of the sample. In practice sputter etching (where atoms are ejected by mechanical bombardment) also occurs simultaneously. Reactive plasmas (generated by RIE equipment) can be used to modify the chemical properties of a material's surface[31] [126] rather than remove the surface material.

4.1.6 Spin Coating

An important class of coatings are etch resists. These protect a substrate or base material from chemical etching. Photoresists are commonly spin coated over silicon wafers, or chips. Typically a few drops of liquid photoresist is dispensed in the centre of the wafer (Fig. 21). The wafer, held by a vacuum chuck, is commonly accelerated at a predetermined rate to allow even distribution of the initial resist. It is then spun rapidly (e.g. 1 minute, 4000 rpm) at a fixed speed to coat the wafer in a film of uniform thickness. The film thickness is dependent on the viscosity of the dispensed liquid and the rotational speed. Films with thickness of 0.5-200 µm can easily be formed If the wafer (a substrate) has previously been etched, and pits have been created in the substrate, it is often still possible to entirely coat the undulating surface using this method. Post spinning, the density of the

[30]formation of complex reactive species is not essential to etching: single gas ions may also chemically react directly with the sample.

[31]oxygen plasma treatment permits quick and effective bonding of glass or silicon with PDMS.

coating may be increased by heating to remove solvent leaving a relatively solvent free organic polymer film. Most coatings are entirely liquid when dispensed but an interesting coating type, a SolGel, contains suspended particles that are spun onto a substrate and heated evaporating the liquid and fusing (sintering) the particles to create a solid permanent coating.

4.2 Optical Exposure

The semiconductor industry has relied on optical light patterning of resist coatings for selectively etching substrates or surface coatings in order to create micro-scale structures. An introduction to the photosensitive materials and equipment used in optical lithography follow.

4.2.1 PhotoResists

Of the etch resists, one of the most useful types are those which are photo-patternable. If the coating is covered (or masked), and part of it is exposed to light, then the exposed part can be selectively removed by immersing the exposed and unexposed coating in an appropriate chemical developer. The remaining coating prevents etching of the underlying substrate or base material. A typical procedure for fabricating microelectrodes on a glass substrate using a photoresist is shown in Fig. 22.

Photoresists generally consist of three components: a base resin, a photoactive compound and a solvent. A common photoresist spin-coating AZ1518 (see Fig. 23) was used throughout microfabrication . This resist consists [127] of two main components dissolved in a liquid solvent: a base resin - Novolak, a group of (usually branched) phenol-formaldehyde condensation polymers[32], and a photoactive development inhibitor Diazonapthoquinone (DNQ) derivative. The inhibitor (DNQ) is inactivated by exposure to light. When the resist (post-exposure) is placed in an aqueous alkaline developing solution, the exposed inhibitor undergoes an exothermic reaction emitting N_2, and thermally breaking hydrogen bonded phenolic links in the resin coating [127]. Dissolution is also dependent upon the formation of carboxylic acid from the photoactive compound and subsequent formation of water after reaction with OH^- ions from the developer.

[32]Novolaks are formed by incomplete reaction of formaldehyde (C_2HO) and phenols (ArOH) (e.g. ratio 0.8:1) with acidic catalysts (Ar=Aromatic ring). Bakelite, a hard black plastic is also a phenol formaldehyde.

To give an indication of coating thickness, resist coatings up to about 10 μm may deposited using AZ4562 (a DNQ photoresist with a modified photoactive compound, MicroChem Corp.) using a single spin coat. Greater film thickness may be achieved using multiple spin-coatings.

A thicker resist, SU-8 2000, was used to coat a layer up to 200 μm thick in a single spin-coat. SU-8, is a UV photosensitive epoxy. The base resin is a non-branched bisphenol A novolak resin consisting of eight aromatic rings and eight epoxide rings (Fig. 24). The photoactive compound is $(Ar)_3SSbF_6$. The solvent in which the resin is dissolved during dispensing is cyclopentanone, and the developer used was 1-Methoxy-2-propyl-acetate. The photoactive compound decomposes to form $HSbF_6$ (an acid polymerisation catalyst [128]) which protonates the epoxide thereby opening the epoxide ring. Oxonium ions (H^+H_20) react with the epoxide when heated. Whereas AZ1518 is normally used as a photopatternable protective coating to permit patterning of other coating layers by etching, SU8 often comprises part of the finished device. SU-8 is transparent to visible light, and not easily removed from most substrates once fully cross-linked.

Due partly to film thickness (solvent evaporation time), the temperature (~95ºC) at which the photoactive reaction is completed, and slow cooling times required to prevent delamination and cracking of the film, the process is more time consuming (2-3 hours for 200 μm SU8 layer) than for AZ1518 (90 seconds for 1 μm AZ1518 layer).

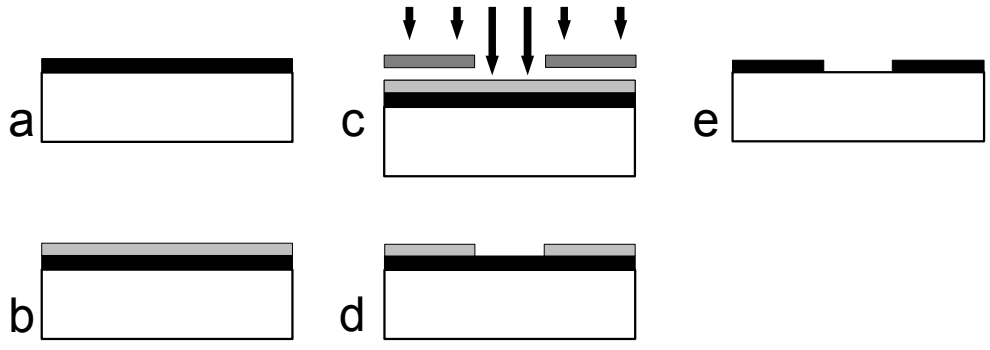

Fig. 22 Patterning a non-photosensitive surface coating.

(a) Coating (e.g. a metal) on a substrate (b) Spin coated photoresist added (c) UV exposure through an optical mask (d) Exposed photoresist removed after immersing in developer (e) Microchip after surface coat etching and a subsequent rinse in acetone (to remove the protective photoresist coating).

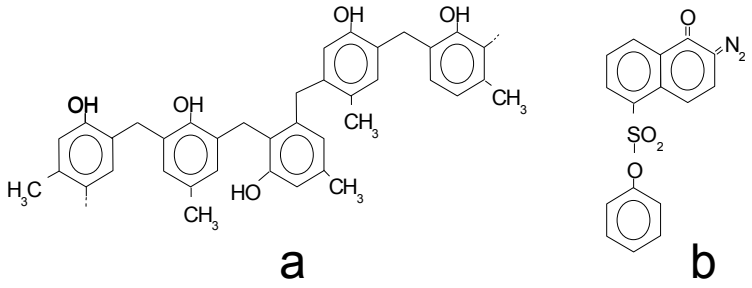

Fig. 23 DNQ-Novolak Photoresist.

(a) part of a Novolak polymer (b) DNQ-5 Sulphonic acid ester inhibitor

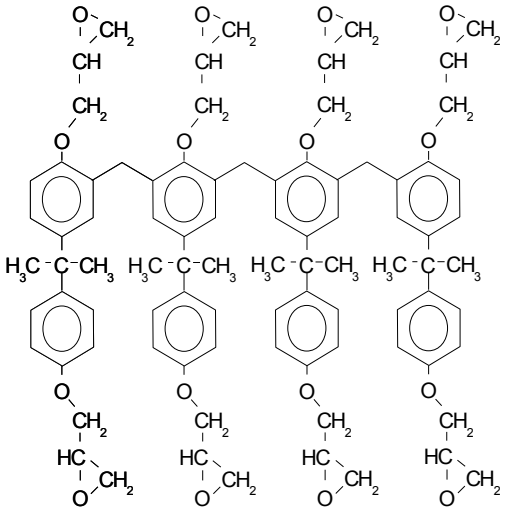

Fig. 24 Base Resin for SU-8 Photoresist.

The epoxy resin contains eight epoxide rings (and eight aromatic rings).

4.2.2 Mask Writer

Photo masks were created using a computer design package (LEDIT, Tanner Research Inc.). A laser mask writer (μPG 101, Heidelberg Instruments, Germany) red laser was then used to expose (8mW, 25% pixel pulse duration) a pre-coated chrome mask (Nanofilm, CA): a 100 mm x 100 mm x 1.5 mm square soda lime glass plate coated with chrome and 5300Å thick AZ1518. After exposure, the AZ1518 was developed and the chrome etched as depicted in Fig. 22 (d,e).

4.2.3 Mask Aligner

Fabrication often consists of repeated cycles of vacuum deposition, photoresist spinning, UV exposure, development and etching. Optical light patterning was achieved by placing a chrome coated glass mask between the photo-resist coated sample and a collimated UV source. After fabrication and patterning of a wafer, subsequent patterning requires alignment of a new mask with existing features on the micro-patterned wafer. The alignment process requires precise control that is often impossible without the aid of mechanical apparatus for positioning the mask relative to the sample with micron scale accuracy. Photo-masks were aligned with micro-patterned samples using a MA-6 mask aligner (Karl-Sűss Gmbh, Germany) which is fundamentally a UV source (350W Mercury Halogen ~4mW/cm^2 at 365nm) with shutters, timers, microscope and a micro-position adjusting mechanism.

4.2.4 Elastomer Mould Micro-Casting

Experimental microfluidic systems often use poly-dimethyl-siloxane (PDMS) as a construction material (reviewed [129]). PDMS is an elastomer which can replicate, by casting onto a mould, features from millimetre to nano-scale dimensions. After casting and curing, it is commonly bonded to other castings of PDMS or glass using ozone treatment without the use of adhesives [13]. The PDMS used in experiments (Slygard Elastomer 184, Dow Corning, Midland, MI, USA) was polymerised by mixing a two part mixture consisting of a base and hardener. PDMS with an acetic acid base can also be purchased as a silicone sealant for commercial and residential building applications. Microchannel fabrication using PDMS is discussed further in section .

5 Microscale Instruments and NT

The objective of research was to develop tangible instruments. The instrument scale-concept in the thesis and chapter titles is related to the utility of the device for handling micro-scale quantities of cells.

Individual cell handling is important in the bovine NT baseline application. Individual cell handling is required to prevent unwanted aggregation of cells (e.g. lectin agglutination of triplets pre-fusion or agglutination of zygotes post fusion). It is also required to achieve and maintain inter-membrane contact without damaging the cell's plasma membrane during cell pairing and electrofusion.

Microscale instruments are classified according to steps in the cloning procedure by specification of categories: (a) system transport (handling of cells and their surrounding liquid media), (b) obtaining disease free isolated oocytes and donor cells, (c) enucleation of oocytes, (d) genetic transfer to the cytoplast, (e) embryo culture, and (f) cell analysis.

Microscale instruments that have previously been applied to cell handling in NT and could be adapted for use in bovine NT are now reviewed. Description of these tools is sometimes incomplete without the context in which they were applied. For this reason background on these applications (which may be considered variations on the baseline process) is also outlined.

A number of existing micro-scale instruments have not been applied to NT and yet are relevant to instrument design. To constrain the scope of background material, the review of such devices is limited to those that are relevant to instruments developed during the course of research. These instruments are considered in the context of specifications made for a particular instrument in subsequent chapters (6 & 7) regarding experimental work. Chapter 6 presents experimental devices for genetic transfer to the cytoplast by electrofusion. Chapter 7 "System transport" concerns devices for on-chip cell relocation over short (< 1 mm) and long range (1-10 mm) distances.

5.1 System Transport.

Transport of cells is an essential step in the baseline cloning process as controlled cell handling is necessary for the various (and numerous) washing stages of the baseline procedure.

Transport of micro-scale quantities of liquid has previously been examined in terms of various micro pumps with operation principles based on mechanical, thermal, electro-hydrodynamic and magnetic effects [130]. Direct actuation of cells using dielectrophoresis has also been examined [89]. However, many lab-on-chip devices either avoid the use of pumping or utilise external pumping sources such as syringe pumps to simplify microchip fabrication and reduce cost.

In the baseline process transport of cells and liquid is effected by the low cost semi-disposable micro-pipette; the microscope is used for counting cells and determining their location. The microscope and the pipette are usually operated in conjunction with each other when selecting, positioning and manipulating donor cells, oocytes, cytoplasts and embryos. Operation of the NT procedure is not possible without these instruments for detection and position control of micro-scale biological cells.

Novel instruments were investigated for transporting cells and accurately positioning cells post transportation in preparation for the electrofusion stage of the baseline procedure. Cell transportation devices and optical detectors for controlled transport of individual cells are presented in chapter 7.

5.2 Separating and purifying oocytes and donor cells.

Separation of cells is an important step for NT as it is in other laboratory procedures [131]. Cell separation methods include adhesives, microscale fluorescent activated cell sorting (FACS) and immunogenic attachment of magnetic particles [132].

The procedure of oocyte preparation differs from that of donor cells. Oocytes can not be cultured, and are therefore very expensive (~ $2 per cell, communication B. Oback) relative to donor cells. In the baseline process the oocyte isolation begins by the collection of ovaries from a slaughterhouse. Follicles (3-12mm in diameter) are separated from the ovary using an 18 gauge needle and negative pressure (40-50mm Hg). A second stage of cell isolation, occurs in the baseline process when the oocyte is separated from the surrounding cumulus cells. This stage of the baseline process is assisted by use of a vortexer (SM1 minishaker IKA®, Germany) and a 'micro' centrifuge. Zeringue et al. [133] developed a microfluidic device specifically for separation of the oocyte from surrounding cumulus cells. It was based on constrictions in a PDMS cast microchannel bonded to a glass microscope slide and fluid actuation by an external syringe pump.

After separation of the cumulus cells, pronase is used to remove the zona pellucida surrounding the oocyte (Fig. 2 & 3). Tools for manipulating the zona pellucida have been investigated for zona removal (in zona-free NT) and zona weakening (in zona-intact NT). Artificial weakening of the zona of in vitro produced embryos can be achieved by: zona drilling (microneedle dispensing of acidic Tyrode's solution), laser cutting of the zona (ultra-violet to infrared wavelengths) [134], threading a microneedle needle through the zona (subsequently rupturing the zona) and piezoelectric perforation [135-138] .

Donor cells are extracted by cutting a two centimetre notch of ear tissue from a donor animal. Disease free fibroblasts are isolated by culturing and passaging cells with antibiotics. Culture of cells occurs in a humid, 5% CO_2 atmosphere. Fibroblasts are manually separated from epithelial cells at the first passage. Trypsinization lifts off the fibroblast cells more rapidly, and the fibroblasts are then aspirated by Pasteur pipette [28].

Post isolation, donor cells are often selected for a particular cycle stage (G0 or G1). G0 stage cells may be obtained by serum starvation or culture to confluence. G1 stage cells can be obtained by manually observing dividing cells under a differential (or phase) contrast microscope and selecting recently divided cells using a micropipette. This process is slow, taking 15-30 minutes to obtain 60 individual cells [28]. Donor cells are then (by micropipette) dispensed onto the bottom of a Petri dish and dispersed in preparation for 1:1 donor-cytoplast agglutination.

5.3 Enucleation of oocytes

Elimination of nuclear DNA from the oocyte is an essential step in NT cloning (reviewed [139, 140]). After in vitro oocyte maturation and dissolution of the zona, the MII oocyte is dyed (Hoechst 33342) and placed under a UV light to locate DNA. This is then extracted using the micromanipulators and a 0.2-ml Gilmont® micrometer syringe (Cole-Parmer Instruments, IL) by puncturing and 'aspirating' with a blunt aspiration pipette (Fig. 3a).

A volume of cytoplasm containing the nuclear DNA is identified and extracted from the oocyte. Loss of 50% of cytoplasm volume is probably detrimental to embryo development [69, 141]. Accurate identification of the DNA spatial location is therefore used in most oocyte enucleation procedures to minimise the amount of cytoplasm that is extracted with the DNA.

A number of methods have been used for locating chromosomal DNA. One method is to note the location of the extruded PB1 itself [142], however care must be taken to ensure the polar body is not, after extrusion, moved relative to the oocyte during handling. Location of the nuclear DNA can also be achieved by observing deformations in the plasma membrane. Deformations can be initiated due to the stage of the cell cycle, as protrusions occur at the start of the extrusion of the first and second polar bodies [58, 143, 144]. However, the use of TII oocytes (second polar body extrusion) hinders the electrofusion stage in the baseline process [145]. Deformation of the plasma membrane near the chromosomes can also be formed through weakening the cytoskeleton by centrifugation [146, 147] or chemical induction (e.g. demicolcine) [148]. Artificial extrusion of polar bodies can be induced by general UV irradiation of the oocyte [149] or the application of a laser pulse to the spindle of AI/TI bovine oocytes [58].

The POLscope [150] utilises polarised light and an adjustable liquid crystal to adaptively enhance the optical image. This method is capable of identifying the position of the DNA without the use of UV, which with high exposure doses may damage the oocyte.

Nuclear DNA may also be removed by cleaving the cytoplast in two with a scalpel (Ultra-Sharp splitting blades, Bioniche Animal Health, NSW, Australia) blade [69]. The scalpel blade is a micro-scale instrument, the thickness of which is smaller than the cell diameter. The division of the oocyte in two is particularly well suited to automated miniaturised systems due to the relatively low positional accuracy required in the horizontal plane and simple positional control required in the vertical direction (the blade is stopped by the base of the Petri dish to within micron tolerances). As a result, the technique is functional without specialised micro-actuators and is aptly named the "Hand made cloning" technique. In this technique, the cleaved vesicles are stained to detect cytoplasts and the cytoplast volume is subsequently increased by fusing multiple cytoplasts during the electrofusion stage of embryo reconstruction [39].

5.4 Genetic transfer to the cytoplast

In nature chromosomes are usually isolated by enclosure within sealed membrane vesicles: the plasma or nuclear membranes. The transfer of DNA through the plasma membrane is not a normal action for most mammalian cell types. NT cloning involves the transfer of the entire nuclear DNA between cells, requiring the cell membrane to be breached.

Many genetic transfer methods have been used to breach the membrane barrier although not all of these (for example: the shot gun approach, nano-scale viral delivery packages, calcium ion induced DNA uptake and electroporation) are in their current form suited to transfer of the entire set of chromosomes. Artificial liposomes have been used to transfer small quantities of DNA [151] and may in the future be used for DNA storage, on-chip transport and genetic transfer.

In the baseline process, the donor cell plasma membrane is used as the containment vesicle for genetic information. Transfer of a complete complement of DNA is accomplished by electrofusion of the fibroblast with the cytoplast using a parallel plate fusion chamber (section 2.3.2).

Microdevices may also be used in DNA transfer. The ubiquitous micropipette is used for intracytoplasmic injection of nuclear DNA. A micropipette in a lab-on-chip form has been developed [152] by anodic bonding of glass and deep RIE of silicon. This could be be used for DNA injection instead of a micropipette.

Either the nuclei or a whole donor cell may be injected. Injection may be assisted by piezoelectric actuation of the micropipette [153]. In the case of nuclei injection, dissolution of the nuclear membrane after injection occurs spontaneously. After whole cell injection into the cytoplast, lasers may be used to assist release of DNA by lysing the donor cell [58].

Genetic transfer by cell fusion can be achieved through various means. Chemical reagents (fusogens) may initiate fusion of cells in close mechanical contact [154, 155]. Naturally occurring fusion proteins are found in Sendai virus [156] and in the gamete cell fusion process [157]. Proteins from the Sendai virus [158] have been used to induce bovine cell fusion [156] although this is no longer commonly used (discussion B. Oback). Laser beams may also induce cell fusion [159].

The baseline process uses the most common method of transferring entire sets of bovine chromosomes, electrofusion, due to its high fusion yield, lack of introduction of contaminants, ease of use and reproducibility. Various electrode geometries have been used including parallel wires [160, 161] and parallel plate electrodes [162]. Electrodes are normally separated by less than a few millimetres and do not contact the cells, as there is a possibility that the plasma membrane will adhere irreversibly to the metal surfaces.

Microscale electrodes attached to micro-manipulators have been positioned directly in contact with the zona pellucida of a zona-intact oocyte and used to fuse a donor cell injected within the perivitelline space to the oocyte [163].

5.5 Heterogeneous Cell Fusion

Cell pairing is an important physical prerequisite that must occur before effecting cell fusion. In the baseline process, fibroblasts and oocytes are incubated in lectin, an agglutinating substance. Post lectin treatment, donor cells must be kept isolated to prevent unwanted agglutination. Cell pairing is there-after achieved by rolling the oocyte with a pipette over a donor cell.

A common mechanical method of cell pairing which achieves close contact of membranes before electrofusion is the injection of the donor cell into the perivitelline space.

The following devices are noteworthy in that they fuse many heterogeneous cells simultaneously. Application of these devices to bovine NT has not yet been reported. Devices developed by Schaper et al [164] were designed to produce dentrite- tumour hybrids for cancer vaccines. One of the designs utilised laminar flow to interleave cells of differing types to increase the fusion of heterokaryons. Dielectrophoresis was used to align the cells into chains, and an electrofusion pulse was applied. The second device was based on forming parallel stripes of antibodies ~10um wide on a substrate by either micro-stamp printing (deprecated) or by linking antibodies to a monolayer self-assembled on micro-fabricated gold patterns. Cells dispensed onto the second device adhered to antibodies. Excess cells were subsequently washed away and another cell type was then dispensed onto the chip causing cells to be alternated (Fig. 26a). A feature of Schaper's micro-chip fabrication method was the rapid construction of enclosed microchannels by CO_2 laser cutting of medical double sided tape. Rates of heterogeneous fusion of cell pairs were not reported.

Skelley et al [165] developed a high throughput device for cell pairing and fusion based upon microfluidic weirs, which were used not only to alternate the position of differing cell types as achieved by Schaper et al, but also to isolate heterogeneous cell couplets (Fig. 26b). The figure indicates high rates of cell pairing. Additional cell pairing and electrofusion devices are presented in chapter 6 and are considered in relation to experimental work.

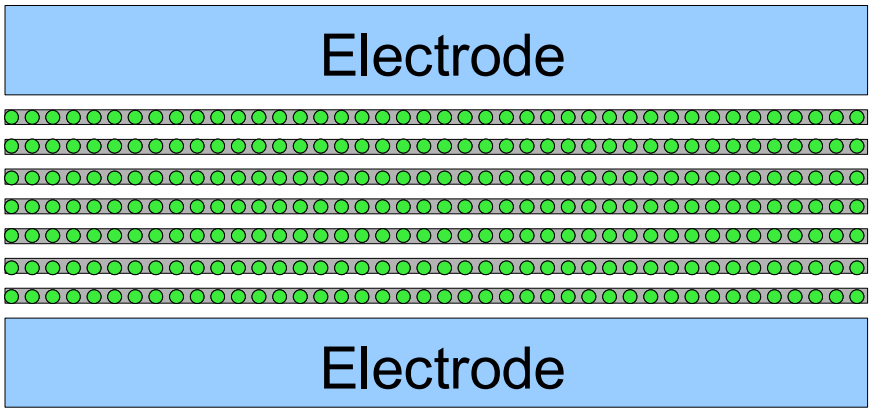

Fig. 25 A Heterokaryon cell fusion system.

Micro contact printed antibodies trap cells on a substrate (adapted from Schaper et al [164]). Excess cells are removed by washing, and an alternate cell type (not shown) is dispensed.

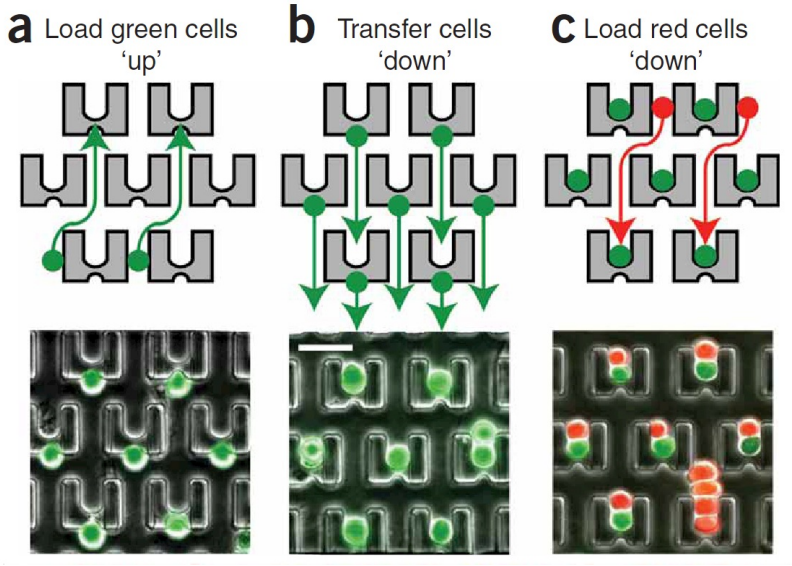

Fig. 26 Heterokaryon cell fusion array.

Reproduced from Skelley et al [165]. Three stages of cell loading are shown (a,b,c). (Top) Arrows indicate trajectory of cells. (Bottom) Photos show fluorescently labelled NIH/3T3 mouse fibroblasts. Each of the cell traps consists of a bridge like structure that permits fluid, but not cells, to pass under it. The device was formed by plasma bonding a multi-level PDMS casting to a glass cover.

5.6 Oocyte Activation

In the baseline process, electrical pulse application is designed to fuse cells. Activation, which occurs subsequently, is by chemical means. Electrical methods may be used to activate oocytes [166] or reconstructed embryos. However, microscale devices for embryo activation were not investigated.

5.7 Embryo culture

Many of the stresses that a cell must withstand are of a chemical nature. It is evident that the correct in vitro microfluidic environment must be maintained post reconstruction. In vivo the fluid surrounding the developing embryo alters over time modified both by the oocyte itself and by the external environment. A single media change is made in the baseline process during embryo culture to compensate for these changes. Cultivating the embryo in a small V shaped well (~250 um deep) improves blastocyst development compared with the single drop culture method used in the baseline system [167]. In the well of the well culture system [167], a well is formed by imprinting a micro-well into a plastic dish using a ground steel rod. The dish is then rinsed thoroughly to remove any toxins generated by the melting process. The improved development is thought to be due to the retention of autocrine factors in the micro-environment surrounding the cell while still permitting entry of nutrients and dilution of metabolic products through the well opening to the microdrop covering the well.

5.8 Micro-tools for Cell Analysis

A large group of tools that can be applied to bovine NT are those for non-destructive cell and micro-environment analysis, and subsequent cell selection [168-170]. Micro-scale instrument design for cell testing and micro-environment analysis was not conducted during the course of the PhD due to the limited time available.

6 Micro-Devices for cell Fusion

Micro tools were developed for handling and fusing cell pairs. NT of the entire cellular DNA to the cytoplast is achieved in the baseline process by electrically induced fusion. Variations on this method of cell fusion were considered for tool development and testing.

The first experiment involved the fabrication and testing of coplanar film micro-electrodes to demonstrate similar fusion efficiency to commonly used macro-electrodes. As discussed later in section 6.2, this demonstration was important to future development of lab-on-chip systems that incorporate a range of microscale instruments.

Following the co-planar experiments investigation was directed towards devices for automating cell pairing and cell fusion in a single device. In this second stage of tool development, fabrication was more complicated and device designs were selected considering available fabrication equipment. Selected fabrication processes were evaluated for device fabrication time, quality and yield. A few of the devices fabricated were tested in the baseline NT process.

6.1 Baseline process for NT cell fusion

The baseline process for NT involves two steps. Donor cells are incubated in lectin to enable attachment to oocytes. Donor cells and oocytes are adhered (or positioned) manually to form couplets (Fig. 27) using micropipettes. The couplets are then transferred into a hypo-osmolar fusion buffer. The oocyte and donor cells swell as a result of the osmotic pressure imbalance which facilitates better cell fusion rates [162, 171] . The long axis of the couplet must be aligned with the direction of the electric field vector to effect cell electrofusion. In the baseline procedure, this is achieved through the application of a low voltage AC waveform (~70 Vrms/cm, 1MHz) [28]. The couplet undergoes positive DEP and torque is induced (cf. Equation 4), which causes the couplet long axis to align with the electric field vector. Because the field is otherwise uniform ($\nabla E = 0$), no translational force acts upon the couplet. After alignment, two 10 µs DC electric field pulses are applied at 2kV/cm. The low voltage AC sine wave is reapplied to reinforce the pressure of the two agglutinated vesicles towards each other during membrane fusion (cf. Fig. 14).

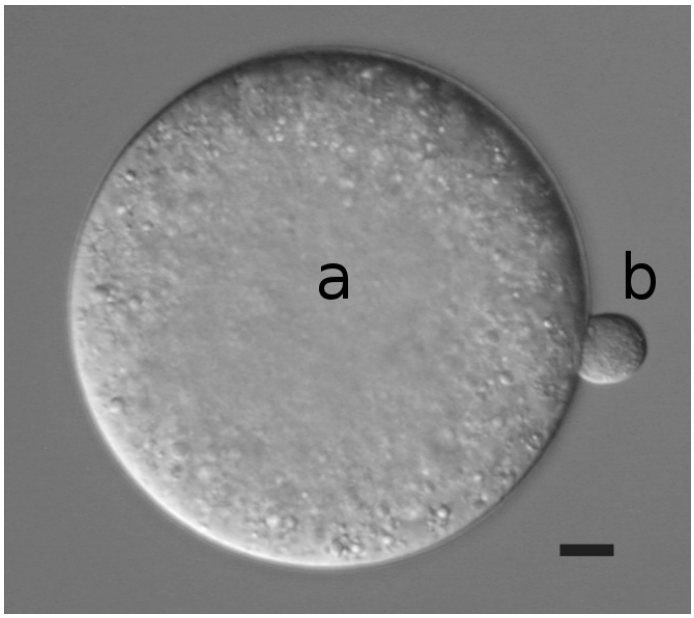

Fig. 27 Cells adhered by lectin in preparation for electrofusion (baseline procedure)**.**

(a) Zona-free cytoplast (b) fetal fibroblast. Scale bar 10 µm.

6.2 Coplanar Electrodes for NT cell fusion

In the interest of developing a lab-on-chip system, it is useful to consider the mechanical fabrication of the elements of which it is comprised. One system element, an electrode pair, is used for effecting cell fusion in the baseline process. Both parallel plate (baseline procedure) and parallel wire systems are commonly used in NT systems. However parallel wire and parallel plate electrodes are (arguably) unsuited to miniaturisation and integration with other system devices.

A microsystem could be fabricated with circular cross section wire electrodes embedded in plastic or glass, but this may be difficult (e.g. a micro-array of individually addressable electrodes). Experimental parallel plate micro-electrodes have been constructed by electroforming [172] and by RIE and glass bonding [173] but both of these methods are expensive. An electrode pair formed by two thin conductive coplanar films separated by gap (Fig. 28) was investigated, as it appeared that: its fabrication is simple, rapid and low-cost; it is easily miniaturised; its use would permit a wide variety of fabrication techniques to be employed during lab-on-chip manufacture; and it is easily integrated with other devices in lab on chip systems.

Coplanar electrodes are however not generally used in NT and the edges of coplanar electrodes generate high electric field gradients that have been suspected of preventing cell fusion [172, 173]. For these reasons, it was considered worthwhile to investigate whether coplanar film electrodes were useful for bovine cloning.

Investigation began [160] by considering a simple case where the coplanar electrodes were widely spaced (2-3mm) and evaluating couplet fusion rates. Two sets of experiments were conducted: one with coplanar electrodes, and the other with a control set of electrodes. Parallel plate electrodes were chosen for the control experiment as they provide a uniform electric field (Fig. 29) and are used in the baseline NT process. In both sets of experiments it was expected that an approximately uniform field would be created in a region midway between the electrodes (Fig. 30). The co-planar field is however evidently non-uniform and cells were placed in the coplanar electrofusion chamber away from the electrode edges to avoid high field strength regions and DEP induced drift towards the electrode edges.

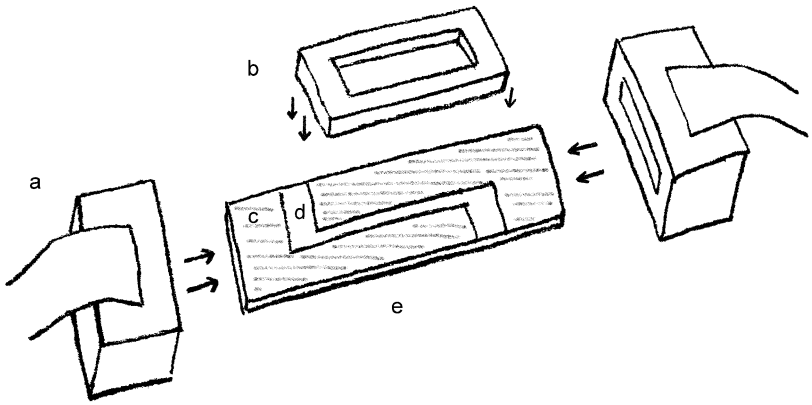

Fig. 28 Coplanar Electrode Fusion Apparatus

(a) Printed circuit board edge connector. (b) rectangular plastic ring milled from 2mm thick PMMA plastic (c) gold film (d) Gap between the film electrodes (e) glass microscope slide, 75x25x1mm. The rectangular plastic ring is sealed to the glass microscope slide using synthetic rubber putty (Blu-tack™, Bostik) forming a small chamber to hold the fusion buffer media. The glass slide is plugged into two printed circuit board edge connectors.

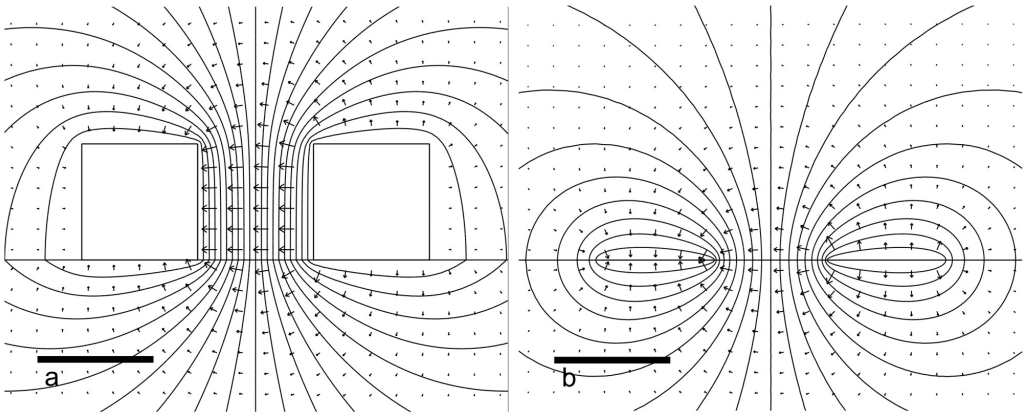

Fig. 29 Electric field near (a) Parallel plate and (b) coplanar electrode pairs.

Electric field vectors and equipotential lines are shown. The parallel plate chamber provides a larger region of uniform field, than does the coplanar chamber.

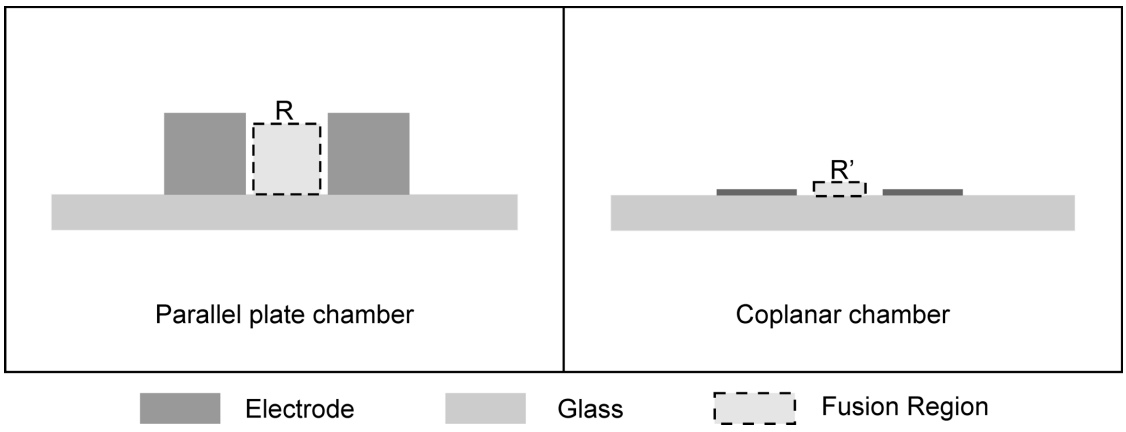

Fig. 30 Regions of uniform electric field near parallel plate and coplanar electrode pairs.

The parallel plate chamber provides a larger region of uniform field, than does the coplanar chamber.

The electric field surrounding coplanar microelectrodes was examined numerically and analytically. The electric potential in the gap between the electrodes for infinitely wide coplanar film electrodes is [174]

$$\phi = V - \frac{2\mathrm{V}}{\pi}\sin^{-1}(u) \quad , \quad 0 \le x \le a \tag{39}$$

$$\phi(x) = -\phi(x) \quad , \quad -a \le x \le a \tag{40}$$

where

$$u = \frac{1}{a\sqrt{2}}\sqrt{[a^2 - x^2 - y^2] + \sqrt{[a^2 - x^2 - y^2]^2 + 4\mathrm{a}^2 y^2}} \tag{41}$$

and x and y are Cartesian co-ordinates, the two electrode potentials are +V and -V and the electrode edges are located at $\pm a$.

Therefore

$$\boldsymbol{E}(x, y=0) = \frac{-2V}{\pi a}\frac{1}{\sqrt{1 - \left(\frac{x}{a}\right)^2}}\boldsymbol{i} \quad , \quad -a < x < a \tag{42}$$

The electric field magnitude midway between the electrodes (x=0,y=0) is therefore

$$\boldsymbol{E}(x, y=0) = \frac{-2V}{\pi a} \tag{43}$$

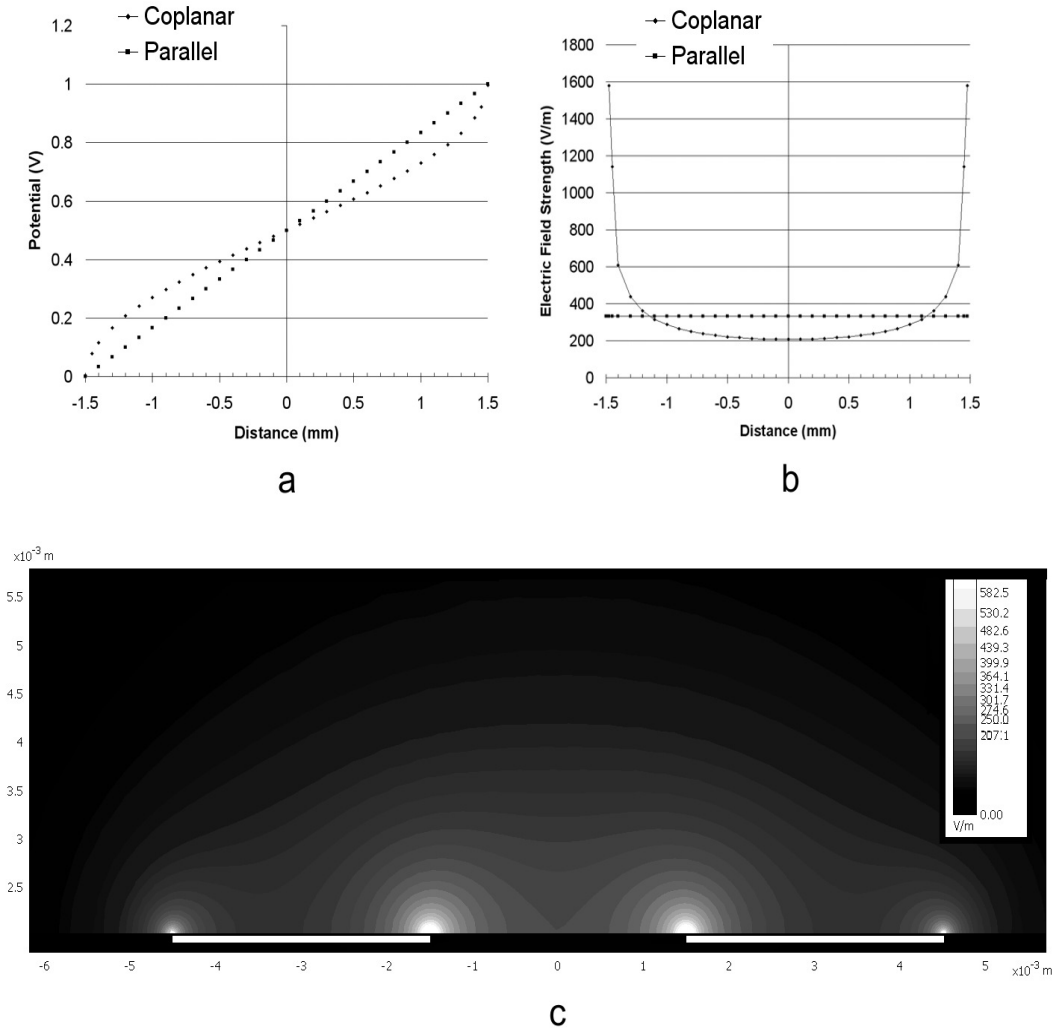

Fig. 31 Electric field simulation of coplanar electrodes.

(a) Electric potential on the surface of the glass in the gap between the electrodes and (b) the corresponding electric field strength (c) Electric field strength map at unit electrode voltage (Vel=1 V). White bars indicate location of 3 mm wide thin film electrodes. The electrode gap Gel=3 mm

The electric field throughout the coplanar electrode fusion chamber was modelled. It was found that provided the width of each the two electrodes (W_{el}) exceeded the inter-electrode gap, the field strength midway between the electrodes was not significantly influenced (<4%) by the electrode width [160]. The theoretical electric field strength along the bottom of the electrofusion chamber is shown for the coplanar and parallel plate electrodes in Figure 31 a&b. As is seen, the gradient of the field is relatively constant midway between the electrodes. A high field gradient and large voltage drop near the edges of the coplanar electrodes can be observed (Fig. 31c). This causes a drop in the field magnitude midway between the electrodes. Based on Equation 42, fusion voltages for coplanar voltages were

increased by $\approx\pi/2$ to compensate for the reduction in field strength. This was then experimentally tested through varying the fusion voltage to detect changes in fusion rate.

Experimental cell fusion tests were conducted to determine whether the fusion rate differed from the baseline parallel plate electrodes. Disturbances causing variation in fusion rates were observed, however considerable variations are not uncommon in fusion trials [147, 175]. The lysis rates were assumed to be independent of electrode type as lysis rate variations were large between trials with both types of electrode. To reduce the influence of these events on the fusion rate estimate, individual lysis events were discarded. The results of the fusion trials are shown in Table 2. Coplanar electrodes were proven to achieve useful rates of fusion: fusion rates >90% having been achieved for all the cell lines tested (fetal and adult fibroblasts, embryonic blastomeres and follicular cells). Coplanar electrodes are thus an option for most cell fusion applications. In both the parallel plate and coplanar cases the optimum fusion rate obtained was at an estimated 2.3kV/cm, consistent with the calculated electrode voltage compensation. The fusion results were also consistent with the hypothesis that coplanar electrodes with a 3mm gap effect the same fusion rates as parallel plate electrodes. There may however be a small (but undetected) reduction in fusion rate. For example 3mm electrodes at 2.0kV/cm gave lower fusion rates (4.3% EFC1, 6.3% FSH and 6.7% LJ801) but these rates were not statistically significant[33]. There was however a significant reduction in the fusion rate for the 2mm coplanar electrodes in one of the two trials for fetal cells, where the fusion rate was 88.9% which was down from 96.3% for the 3mm gapped parallel plate electrodes, a difference of 7.4 %. The reduction in fusion rate for the 2mm gap coplanar electrode may be negligible depending on the application.

Fusion devices constructed using coplanar electrodes within closed microchannels formed from insulating materials would tend to improve field uniformity as the electric field direction is parallel to insulating surfaces. This would permit inter- (coplanar) electrode spacing to be significantly reduced.

The coplanar fusion chamber was observed to have practical advantages over the existing baseline parallel plate electrodes without further miniaturisation. The coplanar electrodes were easier to use as they allowed easier access with the micropipette to cells that are placed between electrodes. They are also easier to clean, as the chamber surface is flat to

[33]Binomial distribution. Fisher exact test, $P<0.05$.

Donor cell	Electrode	n	Gap (mm)	Applied voltage (V)	Field strength† (kV/cm)	No. fusion attempts	No. fused	% Fused	95% C.I.
4-cell	parallel	1	3	450	1.50	24	24	100.00[a]	88-100
4-cell	coplanar	1	3	675	1.50	28	28	100.00[a]	89-100
16-cell	parallel	1	3	450	1.50	17	17	100.00[a]	84-100
16-cell	coplanar	1	3	675	1.50	27	27	100.00[a]	88-100
EFC1b	parallel	1	3	600	2.00	76	73	96.05[a]	90-99
EFC1b	coplanar	1	3	900	2.00	73	67	91.78[a]	84-97
FSH	parallel	4	3	600	2.00	410	395	96.34[a]	94-98
FSH	coplanar	2	2	400	1.33	137	115	83.94[b]	77-90
FSH	coplanar	2	2	600	2.00	72	64	88.89[b]	81-94
FSH	coplanar	1	3	900	2.00	60	54	90.00[ab]	83-96
LJ801	parallel	1	3	600	2.00	30	25	83.33[a]	68-93.5
LJ801	parallel	1	3	700	2.33	56	55	98.21[b]	92-100
LJ801	coplanar	1	2	400	1.33	43	34	79.07[a]	65-89
LJ801	coplanar	1	2	600	2.00	30	23	76.67[a]	60-89
LJ801	coplanar	1	3	900	2.00	30	23	76.67[a]	60-89
LJ801	coplanar	1	2	700	2.33	46	46	100.00[b]	93-100
LJ801	coplanar	1	2	800	2.67	28	21	75.00[a]	58-86

Table 2 Coplanar and parallel plate fusion rates for various cell types

n = number of independent fusion experiments; † predicted from the electric field model; ab Within each donor cell type, rows with different superscripts differ P<0.05.

within 0.1µm. The chamber used in trials (cf. Fig. 30) also used less than 1/20th of the reagent used in the baseline process.

A convenient Petri dish based electrofusion device was created to facilitate manually placed fusion of cell couplets (Fig. 32). Fabrication was similar to that of the planar electrodes. A laser print on plastic sheet was used as a mask and placed inside the dish during electrode optical patterning. Adhesive tape was used to mask and subsequently lift off (remove) photo resist from the walls of the glass dish as this region was not easily patterned by optical means.

Fig. 32 Coplanar film electrodes fabricated on the base of a Petri dish

Electrode spacing is 2.5 mm. This distance minimised the fusion voltage while still preventing cells drifting by DEP toward the electrode edges.

6.3 Cell Pairing and Fusion

Bovine NT is slow in part because manual handling is required to position cells before effecting electrofusion of cell pairs. Tools were sought that could be used to automate the process of positioning bovine cells prior to their fusion. Literature was searched for information relevant to the application of pairing and fusing cells. This information was found scattered throughout a variety of disciplines including applied physics, cell biology, and MEMS. The reason for this is that the motives for conducting research concerning these two topics are varied. Cell fusion has been investigated for scientific knowledge concerning the fusion mechanism [157], for explanation of cell motion in electric fields [176] and for various applications requiring generation of fused cell products.

Fusion (and hence pairing) of cell couplets is recognised as an important stage in laboratory procedures for development of monoclonal antibodies [177], tumour vaccines [164, 178] and for crop improvement [92-94, 179]. Mammalian NT cloning requires cell pairing, as do (in general) these other fusion procedures. However in mammalian NT cloning the financial cost of failing to achieve cell pairing is much higher, and post fusion cell culture is also significantly more costly. Therefore in the baseline NT process individual cells are paired and later checked to determine whether couplet fusion has occurred.

In 1989, Masuda presented the first results demonstrating both automated formation of isolated couplets and their electrofusion [180] using a micro-instrument. The principle of operation was named field constriction and devices based on this principle are the subject of ongoing research [181-183]. Cell fusion and pairing devices presented in this thesis are based on the field restriction method.

Cell pairing by field constriction may be illustrated using Masuda's original microfluidic device (Fig. 33). In this device, individually controllable on-chip piezoelectric micro-pumps pressurised two reservoirs filled with cells. These cells, due to their dilution, flowed one at a time down micro-channels. When a cell passed the junction between the channels, it moved due to the electric field gradient towards an area where the field was constricted and was trapped at the junction. Subsequent activation of the alternate micropump caused another cell on the opposite side to arrive, and become trapped, in contact with the first cell. A high voltage pulse was then applied to two parallel plate electrodes located either side of the junction causing the two cells to fuse. Since that time, the main development for the field constriction device has been the creation of an array of such trapping points so that many cells may be paired and fused simultaneously. Work also continued with other methods of cell pairing and fusion, using adhesive micro-patterning [164] and microfluidic flow [164, 165].

Three designs were developed and used in attempts to create a functional device for bovine cell positioning and fusion. The first design was an open channel 'Hour-Glass' fuser. The second was a 'T junction' PDMS microchannel pressure driven device. The third design was a micropit fuser. Fabrication of these pairing and fusion devices is now discussed.

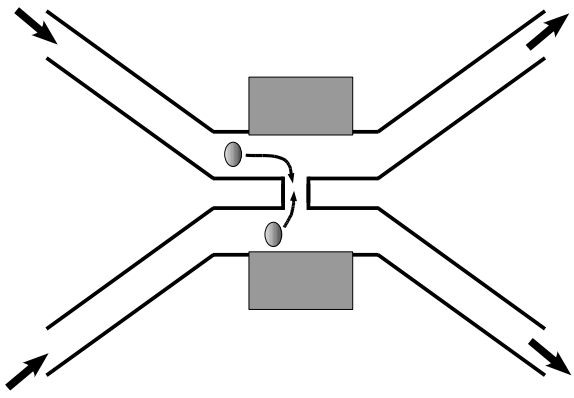

Fig. 33 Masuda's Field Constriction Cell Pairing and Fusion System (refer [180])

Parallel plate electrodes are grey.

6.3.1 Microfabrication of devices for Bovine Cell Handling

The requirements of a bovine NT cell pairing and fusion system differ from those of other systems. Oocytes are considerably more valuable than other cell types due to limited supply, and cost of preparation. Thus, unlike other cells (including most bovine donor cells), loss of an individual oocyte is of importance. This is partly because their population can not be increased by cell culture. In many cell hybridisation procedures, defective cell fusion products can be rejected at little cost. Rejecting embryo reconstructs is however considerably more expensive. More effort (usually manual cell handling and inspection) is expended to prevent situations that generate defective fusion products. Such situations occur due to failure to detect cell location or inaccurate micro-positioning that leads to defective cell pairing (an unpaired oocyte, or agglutination of a cell triplet). Oocytes and embryo reconstructs are therefore individually tracked throughout certain stages in the baseline process.

Oocytes are considerably larger than most mammalian cells (e.g. red blood cells ~15μm, fibroblasts ~10 μm) being ~120 μm in diameter. The size of the cells requires the fabrication of deep microchannels, which lie below sizes commonly used in engineering and above those used in microfabrication. The size also influences cell handling. The tendency for oocytes to settle more quickly to the bottom of a Petri dish than smaller cells makes them difficult to transport. Physiological conductions must also be considered during device design as they can not be loaded in a syringe (in fusion buffer) and stored for more than approximately half an hour.

6.4 HourGlass Fuser

The first design used in an attempt to automatically position cells prior to fusion was a field constriction open channel 'HourGlass' Fuser. A diagram of the insulating component of an HourGlass design is shown in Fig. 34a. This design requires two cells to be deposited, one either side of an opening or 'neck' of the HourGlass. The cells are then moved by DEP towards the opening. The task consists of two stages: (a) automatically position two cells in contact and (b) cause the cell couplet to fuse.

Three geometrical variations on this design were fabricated. The first was a simple pair of insulation regions that formed an acute angle near the field constriction region (Fig. 34 a&b). In the second two small structures were added to allow the larger oocyte to reach the opening without being obstructed by the V shaped walls and also to position the smaller donor cell (Fig. 34c). The third device was built to increase the range over which the cell would travel towards the orifice (Fig. 34d) and has a shape, an approximation to an isomotive geometry [27], that generates a force that is less dependent on cell position than the other designs.

Three objectives were set during the design phase. First was that the device should increase the throughput of cells fused. Second that the feature size of the 'neck' of the HourGlass be equal to the diameter of the donor cell (~15um) and third that it would be manufacturable[34]. The second objective was subsequently rejected due to difficulty in fabrication and lack of evidence that it was essential to an effective cell handling device. The manufacturability constraint was diminished to the constraint that a prototype be produced. A new objective was later introduced that the devices be suitable for rapid fabrication due to the delay in research progress caused by fabrication.

6.4.1 HourGlass Fuser Fabrication

A number of fabrication problems were encountered. The method used in construction was to investigate fabrication obstacles only where they prevented construction of the device. If an investigation provided sufficient information to continue construction, then further investigation of the fabrication process was halted. Time (and possibly suitable test

[34]The last two objectives are in retrospect design constraints.

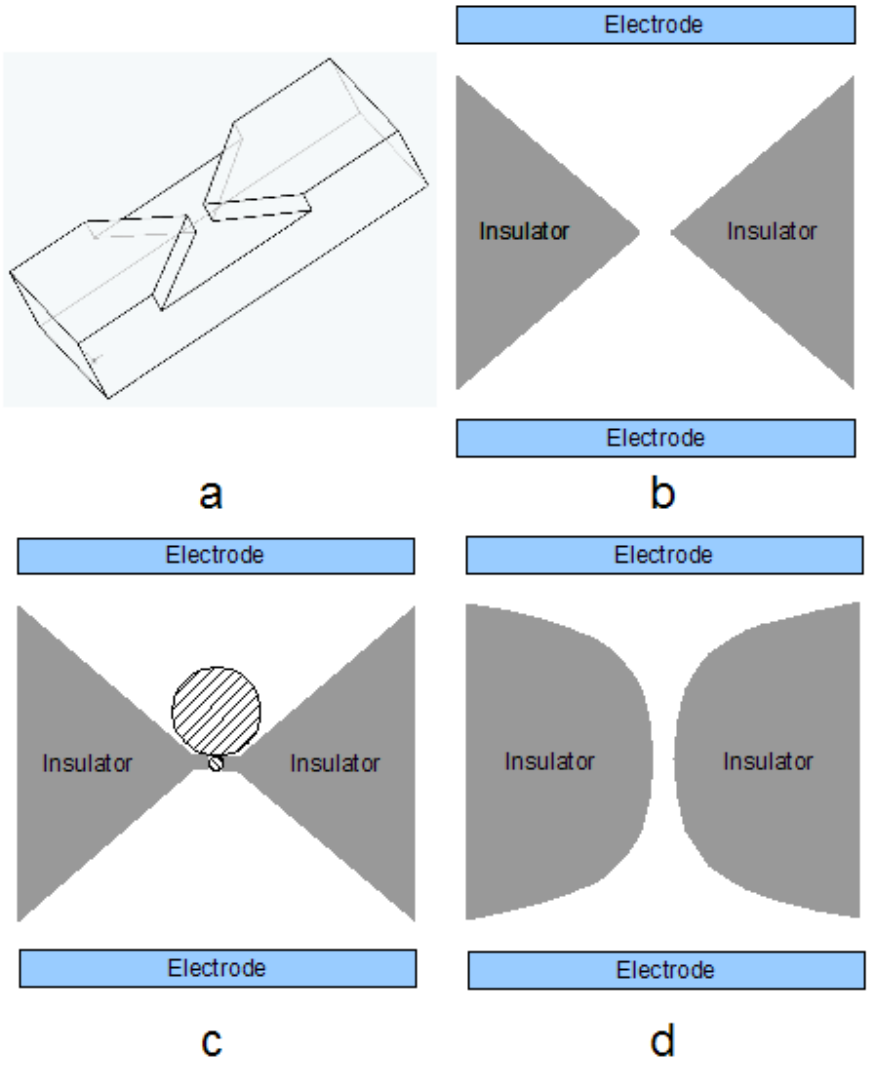

Fig. 34 An HourGlass Fuser

(a) 3D view of the insulating structure. (b-d) Top views of three types of insulator geometry: (b) A simple V field restriction geometry (c) Modified V restriction for positioning small cell while still permitting access of large cell (d) A rough approximation to an isomotive geometry [27] which was built to increase range over which cells were attracted.

equipment [184]) was not available for testing and modelling of the SU8 polymer. Discussion of profile simulations and experimental test results for SU-8 may found in [184, 185].

The primary patternable material used was the photosensitive insulating polymer SU8. Coplanar electrodes were used as they permitted device miniaturisation, and eliminated the requirement (e.g. device shown in Fig. 35a & Fig. 38) for external electrode apparatus.

One of the first problems encountered was the size of the features. Initial attempts were made to fabricate structures with dimensions similar to the donor cell. The photo reduction procedure for creating masks was at the time available only every two to three months. The mask photo-reduction process produced an acceptable feature resolution but was rejected due to the mask iteration interval[35]. 'High precision' laser prints on transparent plastic sheet were trialled, however these were examined and found to have a resolution of around 30 μm, roughly twice the diameter of the donor cell, and the contrast ratio between mask regions and 'transparent' regions was questionable due to the toner ink being translucent. A chrome mask was created from the laser print using a higher contrast AZ1518 photoresist (cf. [186]) to improve the mask quality. In addition over etching of the chrome mask permitted a narrower (<30 μm) region in the HourGlass to be created by under-etching the resist coating.

Photo-patterning of an SU8 film is a multi-step process which has many factors that require optimisation such as: exposure length, solvent concentration (pre-bake), polymer cross linking time and development time. All these parameters influence the minimum feature dimensions that can be obtained. While some parameters that influenced film quality are available, due to their dependence on unspecified parameters, the manufacturer's initial parameters (SU-8 2000 datasheet, MicroChem) required optimisation. The adjustable fabrication parameters that influence the quality of the film patterning are not independent. For example, the necessary exposure times depend on solvent concentration (pre-bake time) and can be partially compensated by adjusting the cross-linking reaction time (post bake time).

A number of film characteristics (cracking, delamination, wrinkling of the SU8 during pre-bake) depend on the exact temperature profile of chips during processing and the relationship between them was not investigated due to time constraints.

Some fabrication faults[36] are shown in Fig. 35. Parameters affecting film quality were not always easily identifiable, nor reported in literature. For example 'bench-top researchers' use different covers during baking, to prevent contamination with dust, each having differing abilities to evolve solvent. Another example is film heating during UV exposure.

[35]Since that time a laser mask writer was purchased, reducing the turn around time for 4” mask fabrication to ~4 hours.

[36]A particularly interesting event (not depicted) occurred when the UV filter was removed, creating a buried SU8 channel in a single exposure.

Solvent evaporation during exposure can cause differences in solvent concentration at the surface of the SU8, and possibly thermal differences throughout the thickness of the film. As these effects influence the reaction rate during exposure, the temperature of the devices was measured post exposure using an infrared temperature sensor. A delay of 20 s every 10 s exposure was used to permit cooling[37]. This short cooling period may not produce the best resolution, but it decreased the time required to optimise process parameters.

To prevent an oocyte from moving in a vertical direction, the vertical component of ∇E should be minimised. It was estimated that a film thickness of ~400 μm would be required. The SU8 process was however time consuming. Part of the reason that SU8 thick film devices are slow to prepare is the time taken for the solvent to be removed from the film prior to exposure. The solvent evaporation time increases with film thickness (50 μm layer is ~6 min, 500 μm layer ~ 120 minutes, datasheet SU8 2000 series photoresist, MicroChem).

A thinner film minimises fabrication turn around time and consequently time to determine usable fabrication parameters. To reduce fabrication turn around time and optimise process parameters rapidly, a film thickness of ~150 μm was used. The time to develop a device entails checking multiple parameter combinations by manually processing samples at approximately 5 samples per four hours for thick film work. Each change in film thickness required re-optimisation of fabrication parameters. Choosing a film thickness of 150 μm was a trade-off between rapidly obtaining rough parameter estimates and not departing too far from the fabrication parameters required for an estimated film thickness of ~400 μm.

To minimise cost and permit the use of standard microscope bottom light sources during device testing, standard glass microscope slides were used as substrates. However early devices showed problems developing (removing) the resist in the neck region of the hourglass shape (Fig. 35). It was noticed that samples which were labelled on the rear surface with ink developed cleanly near the neck region of the HourGlass (cf. Fig. 35a & Fig. 36a). This was identified as a problem with reflected light. While it was known that reflection from the substrate influenced the exposure time (manufacturers datasheet, MicroChem), most substrates are flat mirror like surfaces and therefore, as the light source (Suss Mask Aligner) is collimated, the effect of reflected light is to alter the required

[37]measurements indicated the use of a 60sec delay however, with multiple samples this would have increased turn around time by 10 minutes per sample. No multi density exposure masks, which would have expedited exposure optimisation, were available.

exposure time. However, the support under the glass was not optically flat, and a diffuse light source was created beneath the glass substrate. The rear surface of the glass microscope slide was reduced by coating it with removable black ink. Further investigation into whether the roughness of the glass slide to air interface might create diffuse reflections was not made, as this interface was replaced with an ink - glass interface which was effectively non-reflective.

Other effects suspected of influencing the quality of the completed SU-8 structure were: solvent concentration variation with depth (especially near the surface), variation of the refractive index as a function of exposure dosage and solvent concentration, refractive index variations in the film near the mask edge causing bending of the light away from the vertical normal.

Delamination of the SU8 film from the substrate was caused by differences in thermal expansion coefficients of the substrate and the SU8 (Fig. 35). SU8 has a fairly high thermal expansion coefficient of ~50ppm/K relative to silicon (2.6 ppm/K), quartz (8.5 ppm/K) and borosilicate glass (0.6 ppm/K). As the SU-8 cools below its glass transition temperature (~50 °C) it contracts placing the film under tensile stress. Stress in the film depends on the position co-ordinate with respect to the perimeter of the film as stress fractures are position dependent in the completed device (Fig. 35). Thermal contraction also had a tendency to induce cracking of the SU8 film, even if delamination did not occur (Fig. 35b).

Adhesion of SU8 to the substrate may be improved by selection of the substrate thermal expansion coefficient. The bonding force between SU8 and the substrate also depends on the substrate material. PMMA has been shown to adhere well to SU8 [187]. Adhesion may be improved by treating a silicon surface with an RCA1 clean, or by plasma 'ashing' (O_2 reactive ion etching) and then baking the sample (~150 ºC) to remove water trapped on its surface.

Dissolution of unexposed SU8 around small structures during development was not easily achieved. It was assisted by placing the chip, immersed in developer, in an ultrasonic bath. Unfortunately this also has a tendency to cause film delamination from the substrate and can shatter fine SU8 features (Fig. 35c). Adhesion strength varies depending on the material SU-8 is adhered to [184].

One solution used for improving the adhesion of patterned SU8 structures to the substrate was to form a thin SU8 base layer. This increased interlayer adhesion and may have shifted

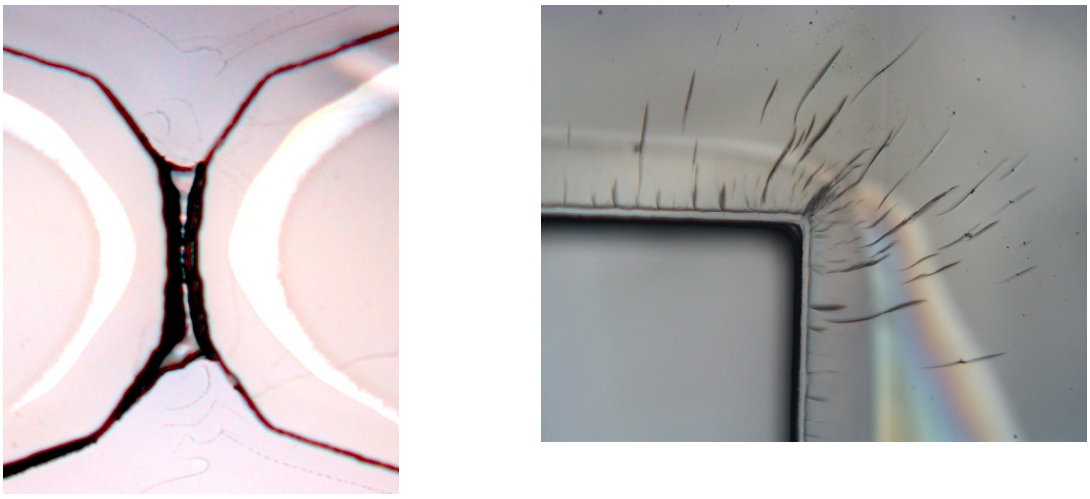

Fig. 35 Examples of SU8 fabrication defects

(a) unremoved SU8 blocking the neck of the HourGlass Fuser. This can be caused by improper UV spectrum and diffuse reflection (b) Cracking due to thermal expansion is dependent on mask shape (c) Shattering of fine features by use of ultra-sound. (e,f) SU-8 interface delamination from glass substrate. The edge of the squares in (e,f) are 100 µm.

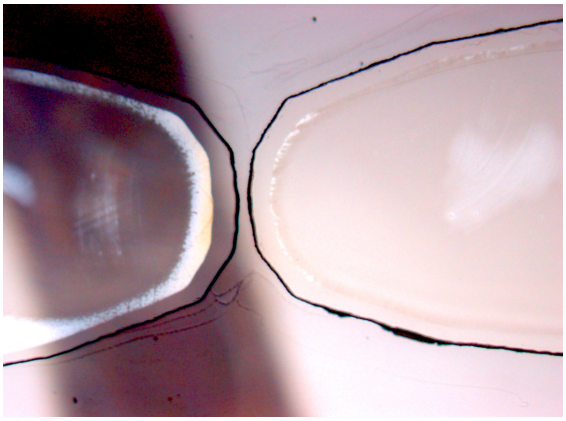

a

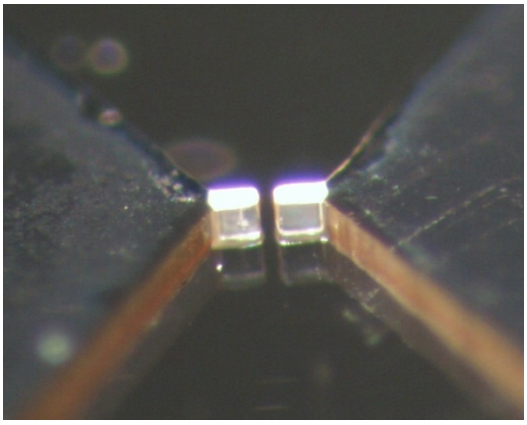

b

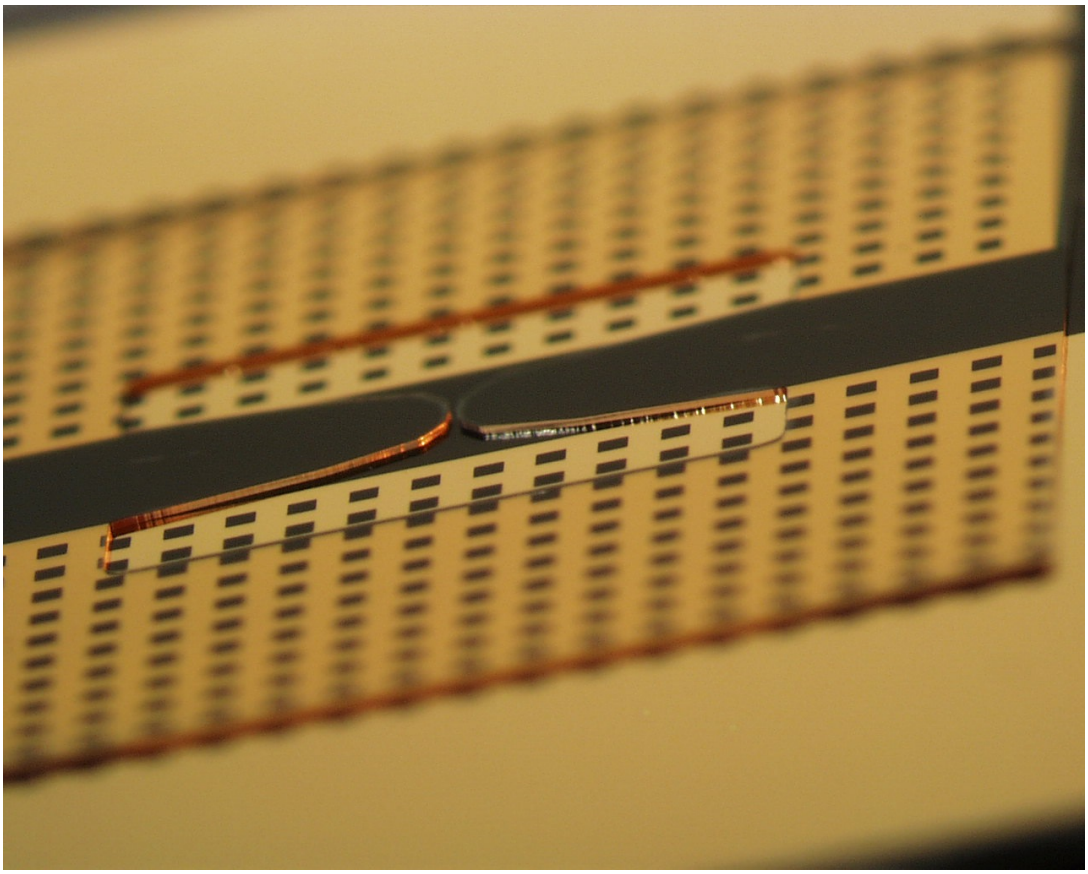

c

Fig. 36 Examples of HourGlass microfuser fabrication using SU8.

(a) Ink covering the rear of the slide improved development of fine SU8 features. (b) SU-8 insulator without film electrodes (gap ~20 µm) (c) SU-8 HourGlass insulator with film electrodes (film thickness 62µm, gap 50 µm).

thermal related stress away from patterned SU8 structures to the interface between the base layer and the substrate. Delamination of the SU8 base layer from the substrate was reduced. This is presumed to be due to the SU8 - substrate contact surface area of a base layer being larger than that of a patterned SU8 layer, where the film is discontinuous. Adhesion promoters such as Hexamethyldisilizane (HMDS) [188] and AP300 (Silicon Resources Inc.) were not used.

Introduction of metal electrodes into the device increased complexity by increasing the interfaces between different materials from one to three: Gold-glass, gold - SU8 and SU8-glass. Each layer was required to adhere firmly for the device to operate (Fig. 35d,e). To improve the adhesion, a cross hatched metal layer was used (Fig. 35e,f). However as fabrication parameters were estimated more accurately adhesion strength increased and it was not necessary to evaluate the relative strength of adhesion to gold or glass, or whether the grid structure enhanced adhesion by 'keying'.

Introduction of metal electrodes also brought a new reflecting surface which prevented optimal exposure being achieved across the entire device. A trade-off was required between SU8 exposure above gold, and that above glass. It was more important that the UV dosage be optimised in the region of the neck area of the HourGlass fuser than at other locations as it was critical to achieve adhesion in that region. The best device constructed is shown in Fig. 36c. Unfortunately during testing it was verified that the film layer at 100 µm was too thin: the gravitational force acting upon the oocyte was overcome by a DEP force towards the top edge of the film.

While a perfected process may take four hours to fabricate a single layer, a substantial amount of time was spent repeating the process to optimise parameters such as: exposure time, solvent concentration in the film prior to exposure, cooling times, developing time, and often determining the duration of ultrasound that could be used before delamination occurred. Due to the extended length of time spent adjusting process parameters, attention turned to the development of alternative fabrication methods and designs that were simple and rapid.

6.4.2 Rapid Fabrication

Due to the long SU8 fabrication time and the large number of process parameters that required optimisation other fabrication methods were examined. As there are an enormous number of possible fabrication methods, a few were selected as prospects for decreasing

fabrication time, taking into account the cost of materials and equipment involved. Material cost was generally not problematic. However, some types of equipment were expensive to use or purchase. UV laser ablation machining equipment [189, 190], and deep reactive ion etching [191] both of which would simplify fabrication significantly do not exist in the department of electrical and computer engineering at the University of Canterbury.

Initial tests were made to gain practical insight into the methods selected. Rapid fabrication methods that underwent initial testing included: imprinting a micro-milled aluminium sample into 2mm acrylic by (a) heating and (b) using solvents; microbead blasting of glass

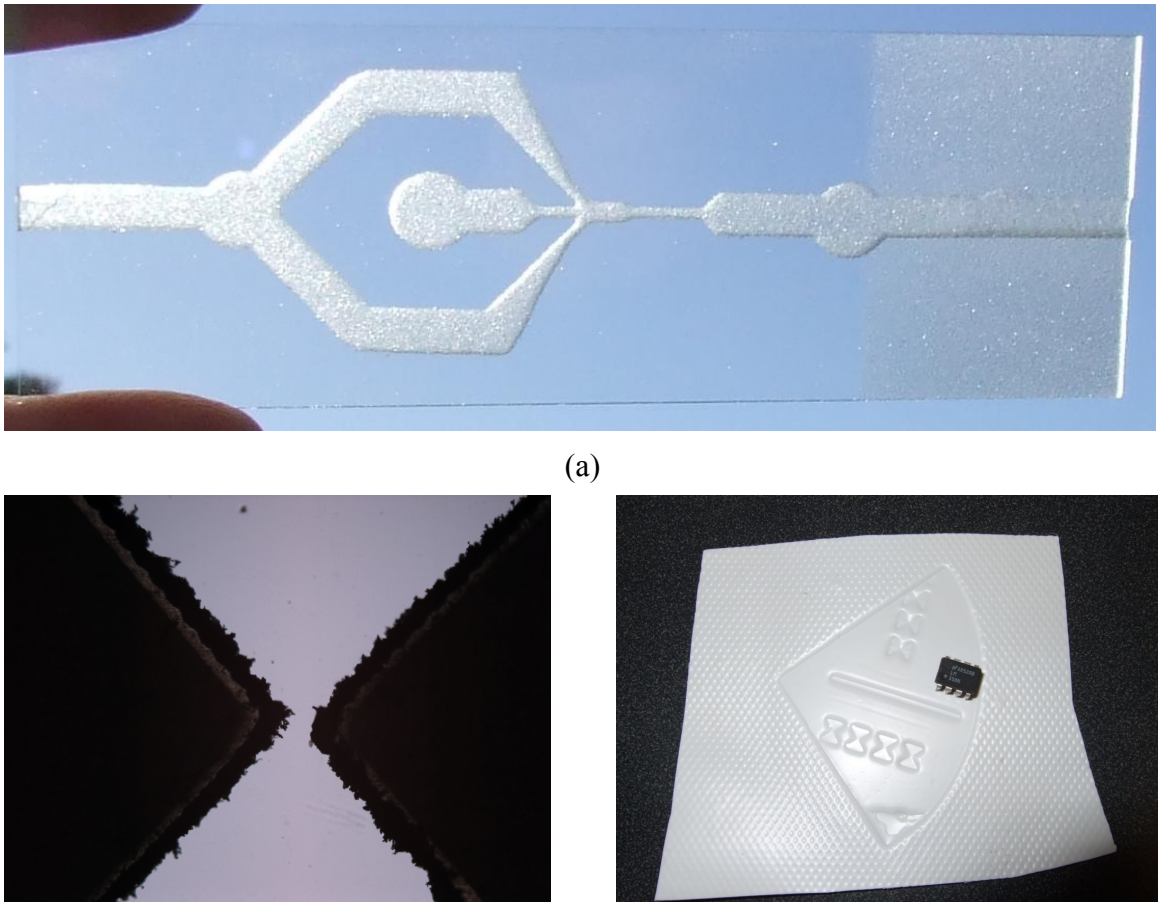

(a) (b) (c)

Fig. 37 Micro-devices fabricated by various rapid prototype techniques.

(a) Glass bead blasted microchannels (smallest channel width ~300 µm). Minimum channel dimensions were limited by bead diameter. (b) Desktop Laser Milled HourGlass (120 µm gap), ~140 µm thick (c) HourGlass fabricated by vacuum moulding of styrene onto an SU-8 master. Oocytes were invisible against the styrene background.

using a UV pattern-able adhesive protective film (Fig. 37a), CO_2 laser milling of plastic film (Fig. 37b) and vacuum forming of styrene onto an SU8 micro-mould (Fig. 37c). The following discussion concerns device fabrication methods that were developed to the stage where particle positioning could be tested.

The first (and in some respects most rapid) fabrication method that was suitable for device testing was constructed by separating two glass microscope coverslips by aluminium foil to obtain a micro-scale gap of around 30 µm. The glass coverslips (100 µm thick) were glued[38] perpendicular to a glass base, and the foil removed. This was tested with an oocyte, which was observed to drift (due to field restriction) towards the opening from approximately 1mm away. In retrospect a variation on this fabrication method could have demonstrated cell pairing and fusion, however at this stage research was directed towards 'design for manufacture' and (as it was conjectured that this would be difficult to integrate with other lab-on-chip devices or even multiple copies of itself) other fabrication methods were sought.

3D printing

The next method that was used to fabricate an HourGlass Fuser and be tested at AgResearch in Hamilton, was 3D printing. This is one of the traditional additive plastics based fabrication processes which include fused deposition modelling, stereo lithography and selective laser sintering [192]. A rapid prototyping company was approached to produce micro-scale prototype parts using a 3D printer. The 3D printer that was evaluated functioned by a micro-mirror reflector array (DLP, Texas Instruments) projecting a 2D image through the transparent base of a container onto a movable platform immersed in a proprietary photosensitive polymer. Exposure to light caused the polymer to cross-link. The platform was then raised, and consecutive layers (Fig. 37a) of polymerised resist were formed.

The pixel dimensions were 100 µm square, and layer thickness was 50 µm. A device 35x20x5mm was fabricated with an hourglass shape 1mm deep patterned onto the top surface (Fig. 38). Due to the fabrication method, the thin devices (5mm) were curved due to differences in layer expansion during formation. Failure under bending did not cause layers to delaminate: the device split perpendicular to the plane of the layers. Development (removal of unpolymerised resist) did not occur reliably if a groove was less than 300 µm

[38]this was done at points far from the gap to prevent adhesive obstructing the gap.

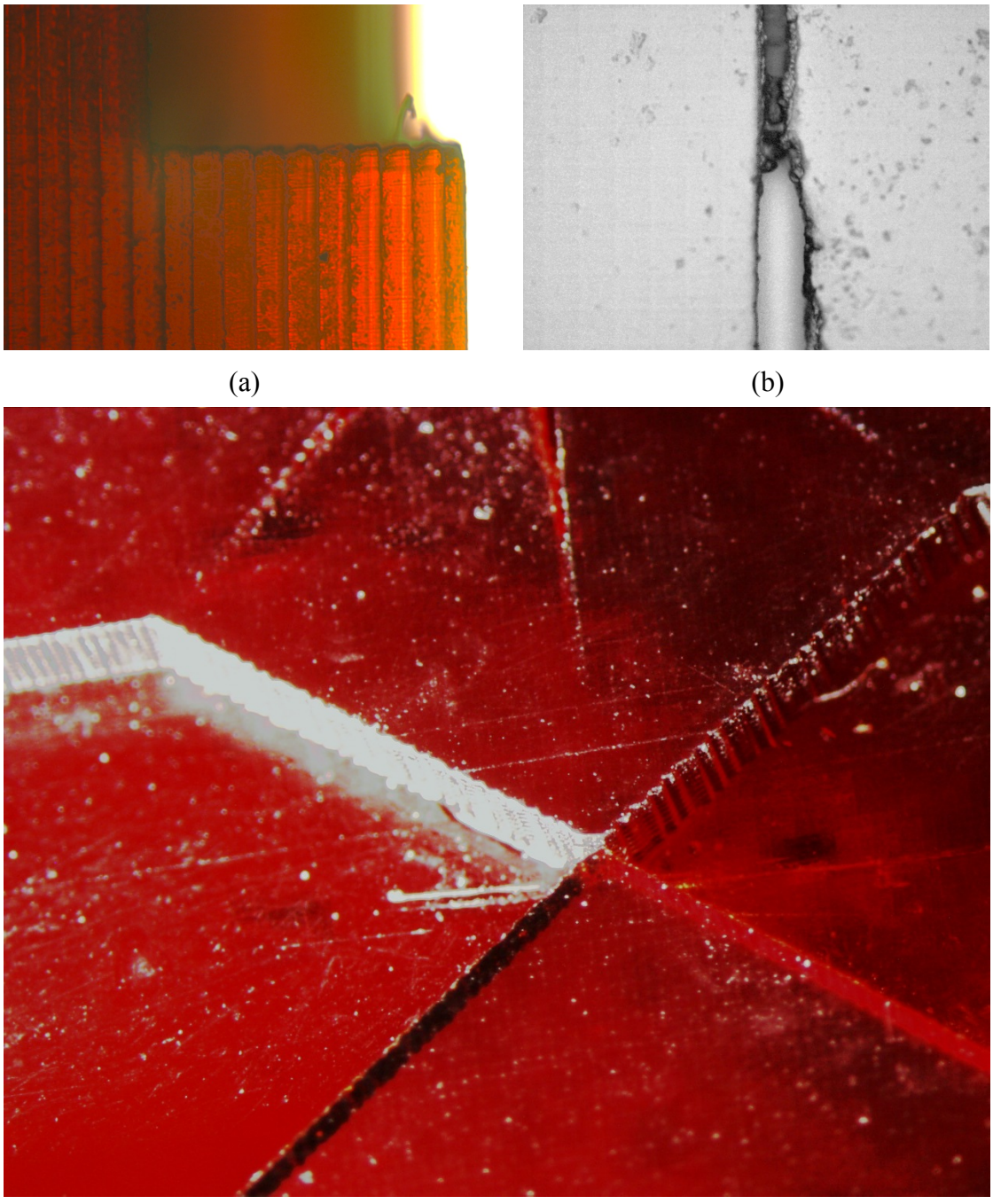

(a) (b)

(c)

Fig. 38 Photos of a 3D printed sample.

(a) layers of photo-polymerised polymer (b) Shallow 200 µm wide channel and partly developed 100 µm channel (c) HourGlass neck (1mm deep). A scalpel blade was used to clear remaining photo resist from the 100 µm 'gap'.

wide and depended on the aspect ratio[39] of the channel. Channels having a 200 μm width with a low aspect ratio might have been fabricated by controlling the micro-mirrors individually. Programming of the machine and mechanical adjustments to it were not possible, as the machine was not university equipment.

The device was cut to a width of 3mm and two electrodes were placed either side of it. An oocyte was then placed on one side of the HourGlass. The oocyte was observed to move slowly to the neck of the HourGlass. Although automated positioning of the oocyte at the channel neck was achieved, optically it was difficult to distinguish the semitransparent oocyte from the dark red polymer. Detection may have been improved using (expensive) polarising filters, however donor cells would be much harder to detect. This method was rejected as a basis for tool development due to the optical characteristics of the plastic and the cost of the devices.

MicroMilling

Endmill tools are commercially available at 25 μm and drills at 10 μm (Performance Micro Tool, USA). Acrylic[40] was machined using a Protomat H100 PCB prototyping machine (LPKF Laser & Electronics AG, Germany). Protomat H100 position accuracy was 0.25 μm. The smallest endmill size tested was 25 μm and used to create microchannels. Tests were conducted to determine feed rate and shaft rotational speed for micromilling[41]. Acrylic sheet was oxygen plasma treated and titanium was vacuum deposited onto the acrylic. The adhesion of the titanium film to the acrylic was considered adequate although the tape-pull test [125] was marginal. It was hoped that electrodes could be milled from the coated transparent acrylic.

Unfortunately, timely access to the milling machine was unavailable and, in addition, a machine fault caused relatively expensive micro endmills to break. The machine was eventually sent for repair, and was unavailable for many months. Due to the need for optimisation of the milling process (which could not be completed during an evaluation time-frame), micro-milling was discounted as a fabrication method.

[39]height/gap of the HourGlass neck

[40]Poly-methyl-meth-acrylate (PMMA); trade names include: acrylic, perspex, plexiglas.

[41]Process parameters for micromilling acrylic using two flute endmills are (endmill diameter <μm>, rotational speed <x1000 rpm>, feed rate <mm/s>): 1000, 20, 8; 400, 30, 5; 100, 40,1; 25, 80, 0.5. Optimisation of parameters was not completed (see text).

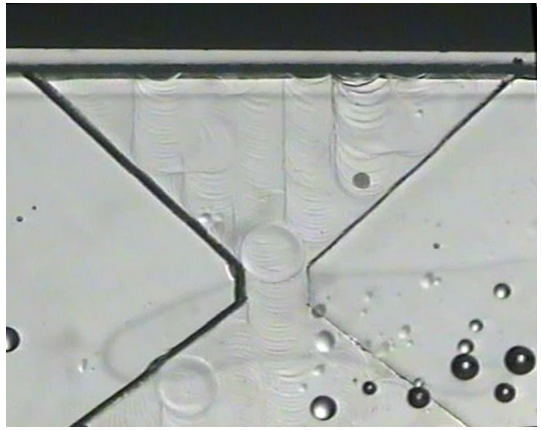

t=12s

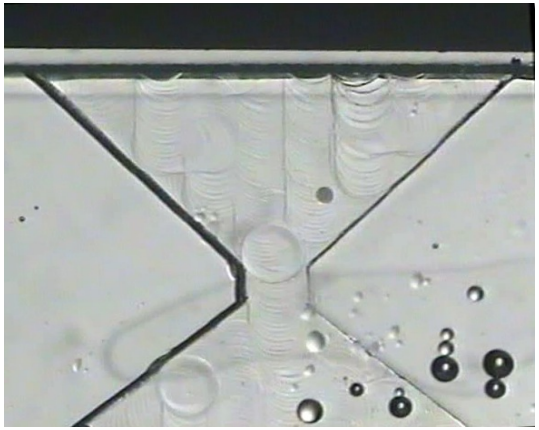

t=15s

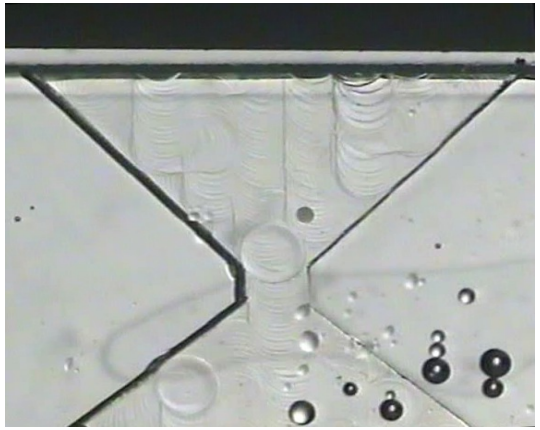

t=18s

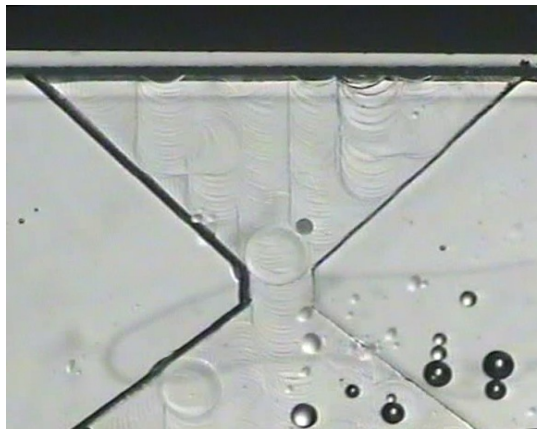

t=19s

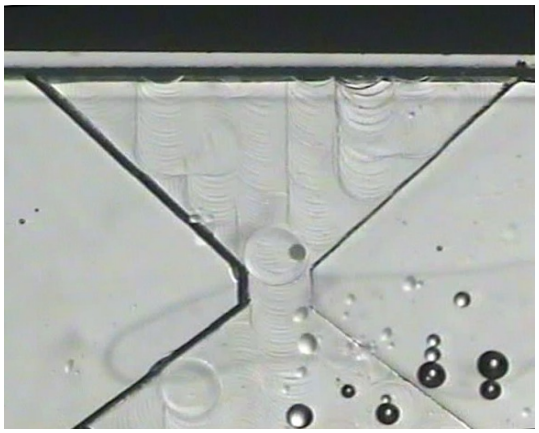

t=19.5s

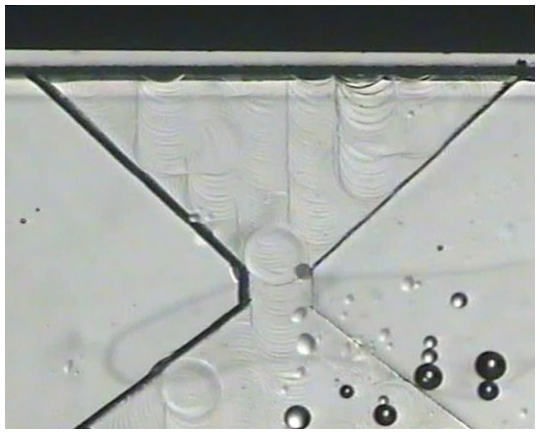

t=20s

Fig. 39 Time sequence photographs of Oocyte movement to HourGlass Fuser opening

Oil droplets floated on the surface or stuck to the acrylic (bottom right of photos). The apparatus was formed by placing a milled acrylic piece (cf. Fig. 34a) between two parallel plates. At the top of the photo can be seen one of the parallel plate electrodes (top black strip) and the edge of the milled acrylic piece. HourGlass 'neck' is 400 μm.

Movement of the oocyte towards the neck of the HourGlass was achieved (Fig. 34), using diascopic illumination. Oil droplets visible in the photographs unavoidably adhered to the external surface of the micropipette and were transferred from the paraffin oil (Squib, Princeton, NJ) covering the oocyte storage drops.

PDMS cast Fusers

Fabrication of the field constriction insulator was separated from the fabrication of the electrodes because separating device fabrication into components permitted a defect part to be discarded without loss of the corresponding electrode or insulation layer. Two different PDMS mouldings were made in a manner similar to [13]. PDMS mouldings were used to constrict the electric field, and to form microchannels. The first moulding was a perforated stencil-like film cast from an SU-8 master. The second was a solid PDMS block ~ 2mm thick (similar to Fig. 34a) that was cast from a milled aluminium block (Fig. 42).

Fig. 40 illustrates the preparation of a perforated PDMS film from a photo-patterned SU-8 film formed on a silicon wafer Briefly, PDMS base and hardener (Slygard 184, Dow Corning) are stirred in a beaker, and placed in a vacuum chamber to remove trapped air bubbles. PDMS is then poured onto the mould, and a plastic film is placed on top of the mould and weighted down so that PDMS is excluded from the interface between the SU8 and the transparent film. The PDMS is then cured at 150 °C for 4 hours, and the insulating film removed from the mould.

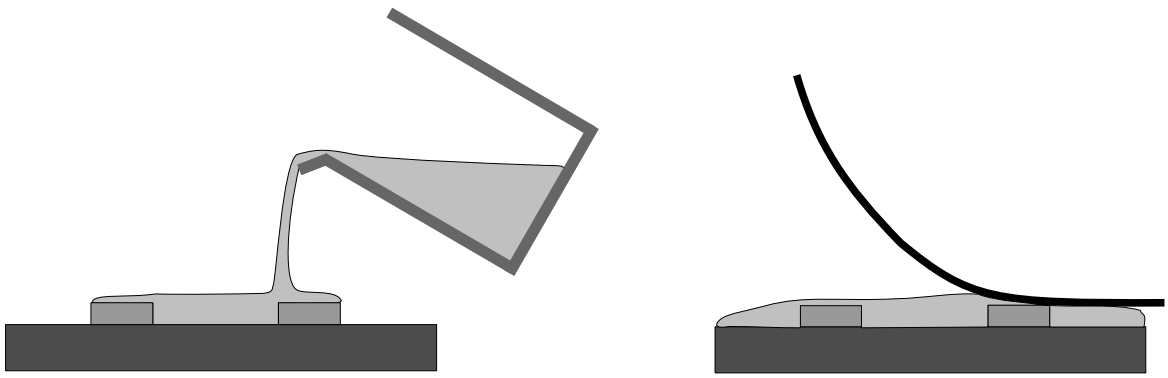

Fig. 40 'Stencil' PDMS casting on SU8 master

(a) PDMS is poured onto a SU8-silicon wafer master (b) Transparent plastic film is used to form the other side of the mould.

The 'Stencil' PDMS Fuser was tested (Fig. 40). The insulator was laid on the surface of a microscope slide having coplanar film electrodes. The film remained on the slide (without air bubbles trapped underneath it) as its density is 1.03 g/cm^{-3}. The elastomeric film had to be laid carefully to obtain the desired gap width at the HourGlass neck. The oocytes levitated and rested on the top edge of the PDMS indicating that the height of the PDMS layer was too low (~100 μm) for the device to operate[42].

An aluminium mould was outsourced, and machined using a 1 mm diameter endmill. A thick (1-2mm) non-perforated PDMS casting was made. The gap at the neck of the HourGlass (Fig. 42) was almost identical to the mould, not suffering significantly from the dimensional inaccuracy of the stencil mould. The curvature of this outsourced mould was limited to the size of the endmill used, which was 1mm diameter. The neck width (Fig. 42) of the fabricated structure was much lower (100 μm) than the tool diameter (1 mm). The mould height (280 μm) was sufficient to prevent oocyte levitation and motion of the oocyte to the field restriction region was observed.

Interlayer adhesion problems that were present with the HourGlass Fuser were simplified by using PDMS. The elastomeric nature of the insulating film eliminated cracks and film delamination that were due to thermal expansion. Adhesion of PDMS to glass by ozone bonding, while not necessary during cell positioning tests, was routinely done in subsequent experiments. A higher bond strength was achieved than the bond strength that occurred between SU-8 and glass. The PDMS HourGlass device required the PDMS to be immobilised on the surface of the glass for fusion tests.. However, it did not require formation of a fluid tight seal and so a functional bond was rapidly obtained.[43]

PDMS replica moulding facilitated dissolution of the unpolymerised SU-8 as the narrow neck region was exposed to large quantities of developer solvent: the neck was formed of SU8 whereas in the non-replicated SU8 fuser, the narrow neck region was surrounded by SU8 hindering dissolution of undeveloped SU-8 by the developer.

Separation of the device into two parts: insulator and electrodes, significantly increased device throughput, and rework-ability but did not alter the critical path (time) for device

[42]SU8 and PDMS device testing occurred on the same trip to AgResearch.

[43]Bond adhesion is impaired in humid climates.

construction. Device throughput was important for testing, as contaminated devices could be disposed of and many replicas were available for replacement. Re-workablilty (replacement of unbonded PDMS) extended the useful life time of devices during testing.

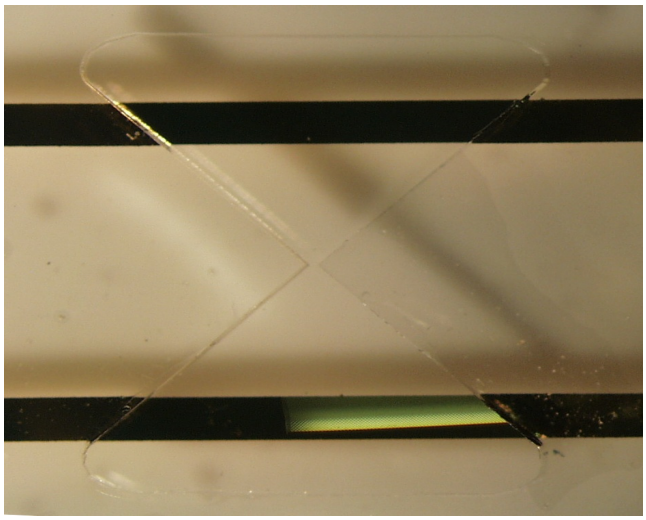

Fig. 41 PDMS 'stencil' insulator over coplanar film on glass electrodes.

The insulating film was too thin and caused the oocyte to levitate and trap on the top edge of the film.

Fig. 42 PDMS cast from a micro-milled mould.

Oocyte is visible below the neck of the HourGlass Fuser. and was attracted towards the neck of the HourGlass.

PDMS HourGlass Fuser status at project termination.

The SU-8 stencil mould was desirable as the next simplest options were to either: (a) use electrodes on an opposing cover, sealing the channel and thereby preventing pipette access to oocytes loaded into the microchannels or (b) cut non-perforated casting into narrow (~2mm wide) strips prior to placement between electrodes as was conducted with the PDMS casting ofthe Aluminium mould.

A thicker SU8 casting was required for the SU-8 stencil mould (between 100-280 µm) which is not impractical. The Aluminium mould also required modification. The aluminium mould required an increase in the gap to ~130 µm to achieve positioning of the oocyte at the centre of the micropit.

The time allocated for the HourGlass project expired. As a termination date had been set for implementing the HourGlass Fuser and microfabrication tools were not available in Hamilton, work on HourGlass Fusers was discontinued.

Newer designs were to be based on the principle of utelising the inherent field distortion around the oocyte to complete the donor - oocyte cell pairing over the final 50-100 µm (PDMS cast 'T' fuser, next section) reducing the smallest feature size required in the moulds.

6.5 'T' junction Fuser

6.5.1 Supra-scale Features and Fluid-assisted cell-positioning

Research into devices for integrated cell positioning by DEP and electrofusion was continued. At around this time a field constriction fusion system similar to the HourGlass Fuser was demonstrated (unpublished results[44]). Work continued regarding automated dispensing and removing of cells from the microchip as the HourGlass Fuser would require manual dispensing of individual donor cells which are small, and difficult to handle.

It was decided to consider:

(a) Pressure actuated fluid flow in combination with DEP to assist deposition and removal of cells (i.e. long range transport between the micropipette dispense location and the fusion site).

(b) Enclosed (sealed) microchannels to isolate donor cells, oocytes and fusion products during dispensing and removal of cells from the chip.

(c) A tool having a smallest feature size considerably larger than the donor cell size.

(d) Separation of the device into different assemblies to mitigate defects occurring at any particular stage of fabrication.

An oocyte will distort an otherwise uniform field so that a donor cell in the near vicinity will be attracted to it (experimentally confirmed by B. Oback, cf. Fig. 14 pearl chaining). Therefore, a field restriction cell positioning device does not necessarily need to position the cells in contact but merely to position the cells in close proximity. Consequently, the dimensions of a cell positioning device may be increased greater than the dimensions of the donor cell. The use of supra-scale device feature size was important to reduce the depth to width aspect ratio of the device constriction region. This permitted larger tolerance in SU8 process parameters, simplifying and expediting prototype completion. It was also conjectured that having two methods of placing cells could facilitate cell micro-positioning.

[44]a design by Paul Gaynor with fabrication carried out by Ling Lin

6.5.2 PDMS Cast 'T' junction Fuser

In the new PDMS 'T' junction fuser design, the final placement of cells in contact is assisted (in addition to the field restriction method employed by the HourGlass Fuser) by fluid flow. Fluid flow would also be used for long-range transport of the cell from the micropipette dispense location to the fusion site.

Because of the cost of a single oocyte (~$2), it was desired that individual oocytes could be easily placed in and removed from the channel. Donor cells are relatively inexpensive and donor cell recovery was not required.

The operation of the single cell serial PDMS fusion device is described in the caption of Fig. 43. Oocytes are entrained and if necessary are expelled (recovered unfused) from port 'a'. Donor cells enter port 'c'. The donor cells exit via port 'a' if fusion is successful or are removed from port 'b'. Flow reversal is not required in port 'c' as donor cells are expendable. Although the prototype device is serial in operation, multiple devices could theoretically be fabricated on-chip and operated, concurrently and automatically, using cell detection devices (optical detection, chapter 7.4).

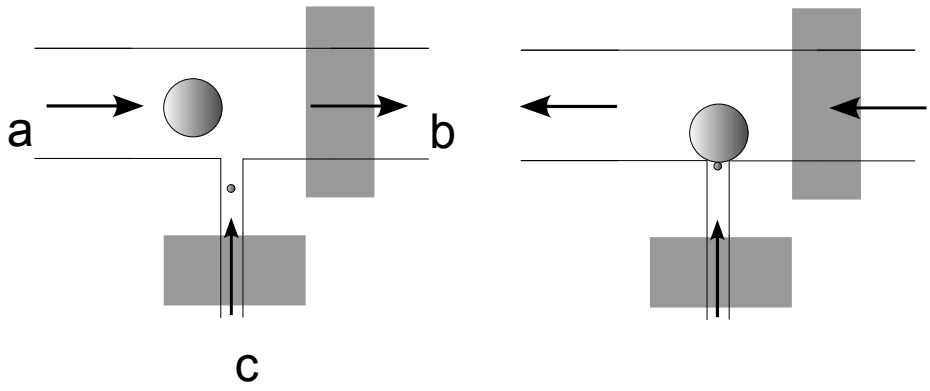

Fig. 43 T fuser device operation.

Oocyte enters port 'a'. Donor cell enters port 'c'. Cells are attracted to the T junction by DEP. Fusion pulse is applied. Fused cells exit port 'a'. Ports b and c are driven. Port a is at atmospheric pressure. Coplanar electrodes grey. Diagrams are approximately to scale. Note the dimension of the donor cell is ~4x smaller than the width of port 'c"

6.5.3 Ports and Transport Lag.

Entrainment of heavy particles (including the oocyte) in a horizontal syringe pump (and in vertical microfluidic ports) was problematic due to cell settling. Cell entrainment resulted in the device operating below atmospheric pressure. Channel sealing was also problematic due in part to the use of a fluid system pressure lower than atmospheric pressure. Many experiments are conducted at positive pressure and improper sealing results in loss of fluid from the system. In such cases small leaks can be unimportant. In this experiment a leak while the device was subject to a negative pressure causes ingress of air rendering the device inoperable. Surface tension at the air-fluid interface causes clogging that prevents the passage of fluid and cells [193]. Channel clogging also traps cells at the air-fluid interface (Fig. 44).

Transport lag between the syringe pump and capillary tubing is often not a problem in single liquid phase systems, as there may be no practical difference between the fluid at the tube entry and tube exit. In a NT system, the oocytes and fusion products can not be stored

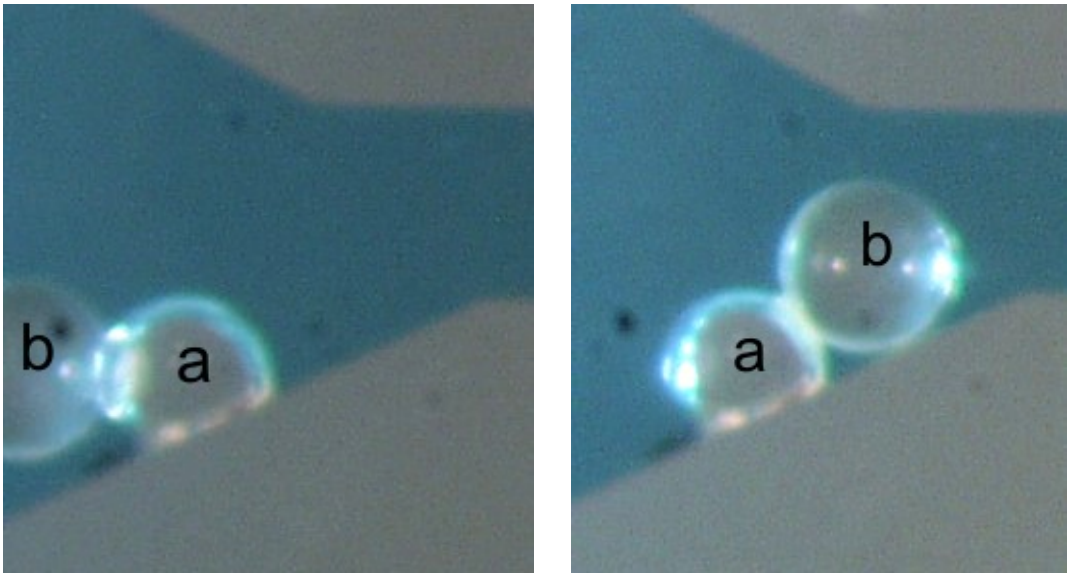

a b

Fig. 44 A trapped (~120 µm diameter) microbead pivots on an air bubble.

The air bubble 'a' is attached to the channel wall (a) flow direction to left (b) flow direction to right. PDMS is permeable to air, and bubbles can diffuse out of the micro-fluidic channel.

for long lengths of time in the capillary feeder tube as the fusion media is not physiologically suitable. It is therefore desirable to load a single cell and traverse the entire feeder capillary tube.

To reduce the transport lag, the velocity of the fluid may be increased at the expense of increasing channel pressure, and consequently the pressure rating of the channel seal. The method used for reducing the transport lag was to minimise the length of the channel. A minimum fluid velocity was required even with short channels to entrain test beads. This also required use of high pressure differentials. Increasing the velocity of the particles

a

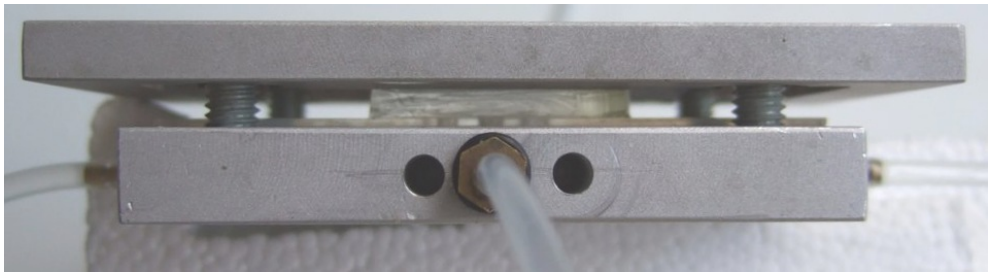

b

Fig. 45 Mechanical Clamp for reversible channel sealing.

(a) Photo of clamp viewed from the top. (b) Side view. The dimensions of the base (50x75mm, or two standard microscope slides) permitted the clamp to be mounted and operated on a microscope translation stage.

however introduces another problem in that the particle velocity is too high for human visual microscope observation. Particles passed out of the field of view within milliseconds undetected by the operator. The relatively slow human response time and the fluid transport lag also hindered placement of a particle within the field of view by adjustment of the fluid pumping rate (cf. 7.4 Automated Cell Detection).

6.5.4 Channel Sealing

A significant obstacle to pressure driven micro-positioning of cells was sealing of microchannels. Sealing of mechanical layers to form microchannels is part of the wider mechanical task of bonding structures. Bonding can be achieved: by fusing two materials using heat or solvents; by using an intermediate adhesive layer that forms chemical bonds with the two materials [194, 195]; and by mechanical means such as threading a material and use of bolts or by external clamping. Bonding two layers together to form microchannels by fusing materials may require optimisation of solvent or adhesive formulation, pressure or temperature as it is a simple matter to irreparably deform a microchannel or clog it with adhesive [196]. Clamps permitted reversible channel sealing. This was beneficial because if the microchannel clogged, the device could be disassembled and either cleaned or part of the device replaced. Mechanical methods also have shortfalls that are discussed presently.

As with the SU8 HourGlass fusion device, mechanisms for a particular fabrication failure (in this case channel sealing failure) were examined using experimental trials only where a selected but diverse range of simple fabrication methods had also failed.

The most rapid and simplest methods for achieving a seal were evaluated first. Three of the sealing methods trialled were: mechanical clamping, magnetic clamping and bonding through surface modification by ozone treatment [13].

Mechanical Clamp

A diagram of the mechanical clamping arrangement is shown in Fig. 46. Fluidic ports were formed in the base of the clamp. Initially glass was used as the optical cover, however stress caused the glass to fracture. A plastic transparent flexible cover was used instead. Titanium coplanar electrodes were vacuum deposited on the plastic microscope slide and etched using a process similar to that described for glass electrodes (Appendix C: MicroPit Fabrication).

The microchannels were tested in two locations, either the patterned side of the PDMS block was up or down. The upward orientation required holes to be formed in the PDMS. The PDMS was observed to tear and split easily if it was pierced. Drilling created a rough surface that trapped air bubbles (Fig. 50c) which rendered the device unusable[45].

The down orientation was then trialled, eliminating holes in the PDMS. This required the placement of the film electrodes at the base (Fig. 46). Having the plastic slide supported entirely (compared with the upward orientation where, when it was located across the view port, it was only partially supported) reduced flexing and improved channel sealing. Double sided adhesive tape was used to seal the plastic slide to the aluminium block. Use of an acrylic substrate (part c Fig. 46) made the task of drilling ports simpler than it was for glass substrates. Tracking individual polystyrene beads (105-125µm diameter, PolySciences) was impractical using a microscope because from the time cells were loaded in the syringe until the cells reached the view port various objects obscured them from view. Settling of beads and bubble trapping were suspected in the vertical ports: These characteristics are attributable in part to the size of the microfluidic system.

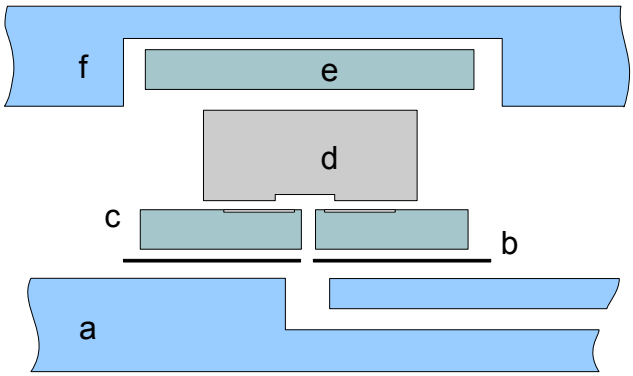

Fig. 46 Cross section of the mechanical clamp and downward oriented PDMS moulding

(a) Aluminium base with fluid ports (b) Double sided adhesive tape seals between aluminium ports and plastic slide (c) Plastic slide provides electrical insulation between the vacuum coated coplanar film electrodes and the aluminium base (d) PDMS block (e) Transparent plastic slide distributes clamping pressure (f) Aluminium top plate with view port. Clamping bolts not shown. The plastic slide 'e' is recessed into the top plate to accommodate the focal length of the objective lens.

[45] A smooth surface could be created using an insertable tube, and filling the intervening region with uncured PDMS. However this tube required rigidity to enable insertion into the PDMS. It was consequently not compressible in the axial direction and unsuitable for use under compression.

Channel sealing was not achieved. The PDMS appeared to form a poorer reversible seal with the acrylic plastic than with the glass microscope slide. Adjusting the PDMS thickness and area, and improving clamp pressure distribution may have permitted channel sealing. Sealing using this method was not pursued further.

Magnetic Clamp

A clamping arrangement using neodymium ring magnets (Fig. 47& 48) was designed and built to improve clamping and device operation. Pressure was distributed in a continuous circular ring and the device was smaller than the mechanical clamp system in order to reduce cell settling and bubble trapping. The tubing diameter was reduced, as was the vertical port height. The 9mm thick aluminium base was replaced with transparent 3mm thick acrylic. Two annular magnets were used to provided an even pressure between the two magnetic rings. The clamping force increased significantly as the distance between the magnets decreased. For this reason a thin layer of PDMS was used.

Adequate sealing was not achieved with this clamping method. Minute flexing of the acrylic may have caused uneven pressure distribution at the centre of the device where the PDMS-acrylic channel seal was located. Uneven pressure distribution may also be related to the PDMS thickness: a thicker film may have redistributed localised areas of high pressure so that a more even load distribution is attained at the PDMS-acrylic layer interface.

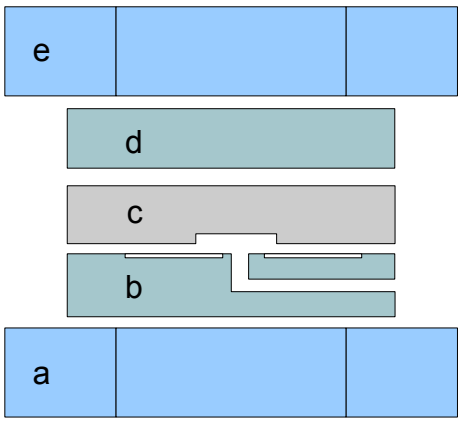

Fig. 47 A Magnetic Clamp used for reversible channel sealing (cross section).

(a) Annular magnet. (b) Acrylic base with vacuum deposited electrodes and fluidic port. (c) PDMS block (d) Acrylic disc to distribute compression load evenly (e) Annular magnet.

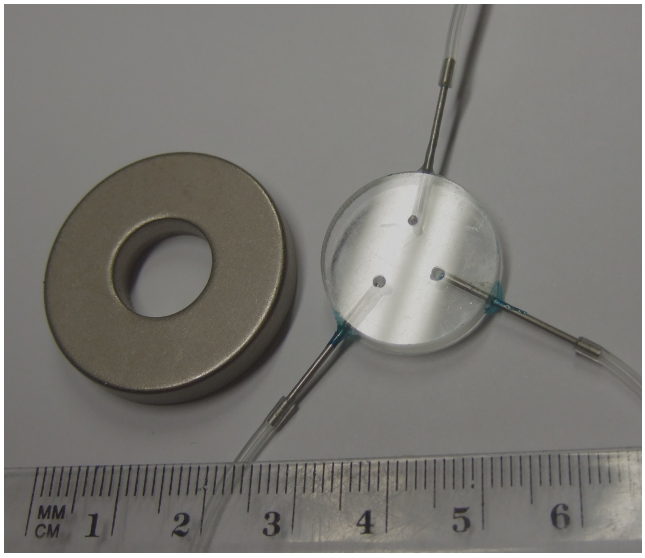

Fig. 48 Photo of Magnetic Clamp Fusion Device

(Left) Annular Magnet (Right) Acrylic base and fluidic ports

Immersion of the entire device was tested as a means to prevent air ingress and bubble formation. Liquid immersion was however not always beneficial for viewing cells under a microscope. The short focal distances of a high magnification microscope results in the liquid being close to the objective lens. Exposed fluid at physiological temperatures caused condensation on the objective lens preventing observation of the microchannels and cells. If the device was partially immersed, the liquid curvature near the vertical view-port wall (annular magnetic ring) diminished the usable view-port area.

6.5.5 Composite 'T' junction Fuser

Chemical Bonding

Ozone bonding is known to form a very good seal between glass and PDMS. In addition titanium electrodes[46] could also be bonded to PDMS. Sealing of the channel was achieved using this irreversible bonding method.

Port miniaturisation and channel sealing

One of the important, yet often overlooked components of a microfluidic device is the connection of capillary tubing to the lab-on-chip [197, 198]. To minimise settling within ports, the vertical distance of the port was reduced. However, ports were still placed

[46] Precisely, the oxidised surface of the titanium bonded to the PDMS.

underneath the chip to permit viewing using a standard 'non-inverted' microscope. The volume of trapped bubbles was reduced, by reducing the port diameter compared with the mechanical clamp. To obtain an effective interface between capillary tubing to the syringe pump and the microdevice, a composite material was formed by adhesion of a microscope glass coverslip to a small square of 2mm thick acrylic. This laminate is easily machined and has surface properties compatible with ozone bonding.

Various adhesives were tested for adhering the acrylic substrate to the glass coverslip. Silicone (multi-purpose sealant 732; Dow Corning) was selected although it did have a long curing time (>24 hours).

A multi-stage Assembly

Fabrication of the device occurred in stages. The acrylic base was drilled edge on and a thin ~1 mm diameter stainless steel tubing (needle, Kahnetics™ KDS2012P, Cooper Industries[47]) was coated with quick setting (~5 minute) epoxy and inserted into the acrylic base. Although the epoxy did not adhere to the steel insert a pressure tight fitted seal was formed[48].

Electrodes were vacuum deposited onto a microscope glass cover slip that was 0.1-0.2mm thick to form part 'c', Fig. 49. Part 'c' was then bonded to the acrylic base (part 'a') using the multi-purpose sealant and left to cure for 24 hours.

A 1mm diameter diamond grinding bit was then used to form small holes in the glass layer of the laminated base above the inlet ports (Fig. 48). The plastic beneath the small holes was subsequently drilled vertically to meet with the horizontal drill hole. This completed the laminated base and fluid ports.

[47] or Part 412-2689, Farnell NZ

[48] The metal tube insert could be removed from the base assembly and replaced without damaging the fitted seal.

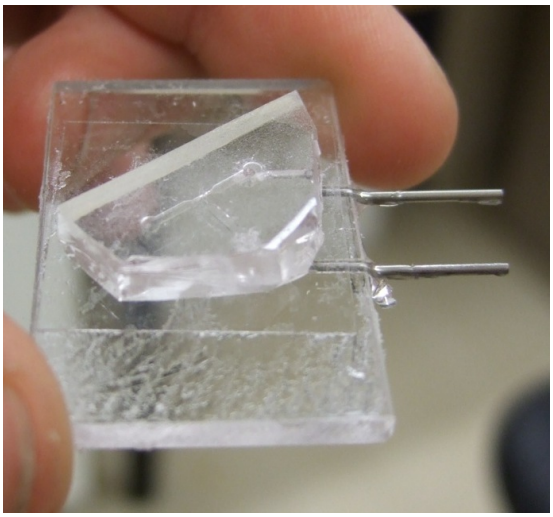

(a)

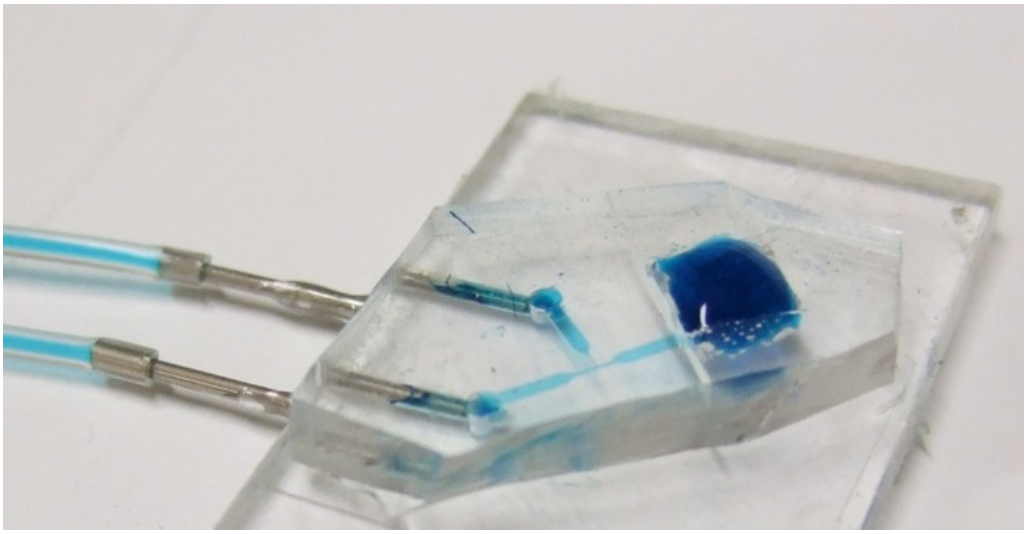

(b)

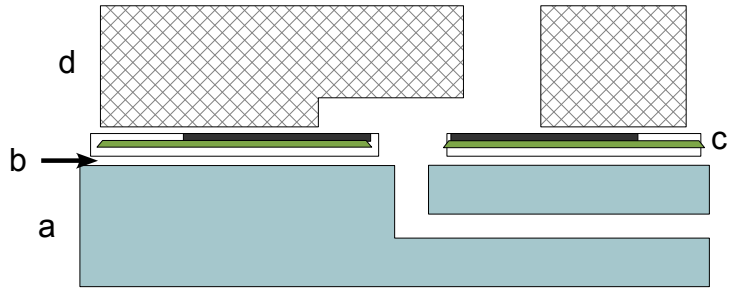

(c)

Fig. 49 Composite 'T" junction Fuser

(a) & (b) photos of device (without electrodes) (c) Device construction: 'a' acrylic base with drilled side port , 'b' Multi-purpose Sealant 732 (Dow Corning), 'c' Glass cover slip ~0.1mm thick and and vacuum coated electrodes, and 'd' PDMS casting.

A master was formed by spin coating and photo-patterning a single 150 µm thick layer of SU-8 on a 100 mm diameter silicon wafer. The PDMS block (Fig. , part 'd') was formed by casting ~ 5 mm of PDMS prepolymer onto the SU-8 master (cf. section 6.4.2, PDMS cast Fusers).

A small 5mm square hole was cut in the PDMS with a scalpel (Fig. 49)[49]. Microchannels were formed by ozone bonding the PDMS layer to the glass [199, 200]. After assembly plastic tubing was then expanded over the metal port inserts.

Separation of the device into different assemblies mitigated defects occurring at any particular stage of fabrication. A defect in the fabrication of the PDMS insulating structure for example did not damage the microelectrodes, as occurred in the fabrication of the HourGlass SU8 insulator. By mitigating damage during fabrication, yield increased. After a specification of the process was completed, a single device (vacuum deposited electrodes, SU-8 mould, PDMS casting and acrylic base and ports) using the specification could be built in 3-4 days. Multiple devices could thereafter be built at a rate of 2 per day, limited by manual assembly of the base. Part 'd' (Fig. 49c) could be prepared in batches of 10-15 and the SU8-silicon master was reusable, although casting release from the mould was reduced after multiple castings[50].

6.5.6 Composite Fuser Fabrication

While channel sealing was excellent and electrodes were correctly (and manually) positioned[51], it was extremely easy to clog the microchannels (Fig. 50b). Contamination with airborne dust was due to the design incorporating an unsealed oocyte inlet port, and partly due to the stickiness of the PDMS material at the inlet port. Use of a filtered air cabinet would eliminate this problem. Other causes of unwanted material ingress were related to the fabrication quality of the inlet. The silicone adhesive between the glass and acrylic layers may be torn (by grinding, glass fracture or drilling). The high pressures used

[49]If the PDMS is bonded before the hole is cut in it, the PDMS can not be easily removed during construction . Without removing all the PDMS from the base of the reservoir, cells and air bubbles are trapped rendering the device inoperable.

[50] Vapour deposition of HMDS (hexamethyldisilizane: $[(CH_3)_3Si]_2NH$) and TMCS (trimethylchlorosilane) on the SU8 master has been used [10, 11] to facilitate release of the PDMS casting. Another method for obtaining more castings per SU-8 master would be to use rapid replication of master structures in PDMS [12]

[51] methanol could be used to assist and delay bonding while positioning ozone treated PDMS [13]

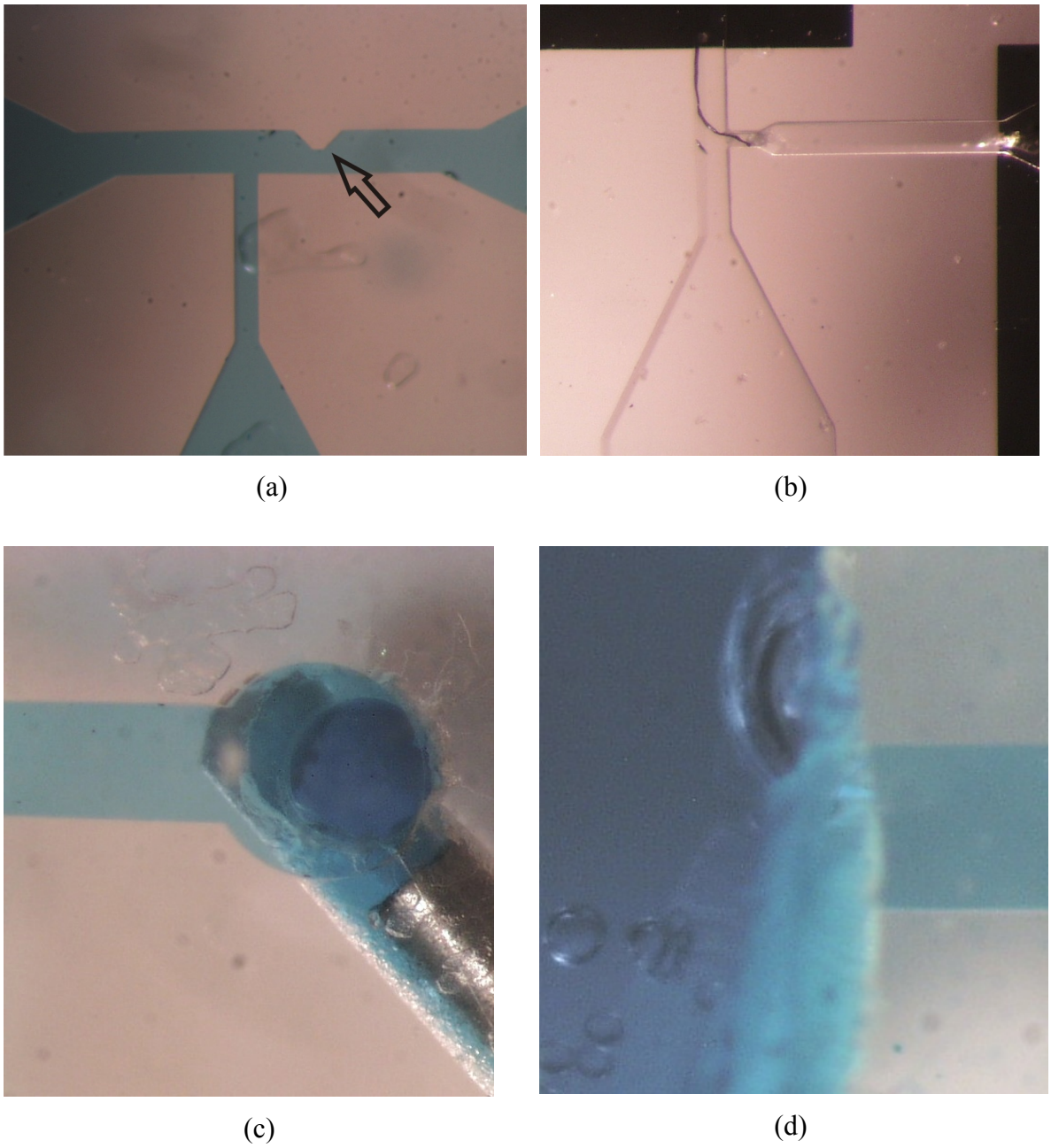

Fig. 50 Photos of Composite 'T" junction Fuser during testing.

(a) T fuser. The bump visible (arrow) in the design is useful for trapping the oocyte if during entrainment (Fig. 43) it should overshoot the T junction. (b) clogged T Fuser. Vacuum deposited electrodes are visible top and right (c) Base inlet Port. Air bubbles trapped between the acrylic base - glass interface are visible. Discontinuous sealing of the acrylic base- glass interface did not hinder device operation because the multi-purpose sealant did not form part of the microchannel seal. Continuous sealing was significant only at the port connection (d) Side inlet Port. Air bubbles and microbeads are attached to the manually cut surface of the oocyte reservoir.

may then cause pieces of detached silicone to enter the microchannel and clog it. The thickness of the adhesive silicone may influence glass fracture and silicone tearing during cover slip grinding. Flushing of each base assembly port was therefore conducted in both directions to remove material remaining from construction. Glass fracture near the inlet port was not of great importance, as it was subsequently reinforced through its bond to the PDMS.

While clogging due to fabrication faults or contamination did not occur in most devices, if it occurred after ozone bonding, the device could not be repaired. The prototype production rate was too low for these losses to be accepted.

Composite Fuser testing and conclusion

Preliminary tests with beads showed that entrainment and recovery of individual oocytes would not be easily achieved using the side port into the oocyte reservoir. The reservoir level required careful monitoring. Increasing the collection range near the port required a reasonably large flow rate. The high flow rate for collection was too fast for manual optical detection of beads. This led to multiple beads being trapped at the bump trap (Fig. 50a).

The oocyte reservoir had a rough surface which trapped air bubbles and particles. Improvements to device cell loading could be achieved by having a smooth inlet reservoir surface with an inlet at its base.

Clogging due to detached silicone might be eliminated by replacing the acetic acid based silicone adhesive and cover slip glass with a thin photo-patterned SU8 film coating[52]. SU8 adheres to PMMA [187] and can be ozone bonded [201]. However, new fabrication processes: SU-8 to PDMS and SU-8 acrylic bonding; SU8 on acrylic photo-lithography; and conical port construction [133] would incur delay due to inevitable optimisation of new fabrication techniques. The estimated projected completion date exceeded the project deadline therefore development of the composite 'T' junction fuser was discontinued.

[52]refer PDMS to SU-8 bonding [14] and section 6.5

6.6 Micro-pit Fuser

6.6.1 Redesign of Field Restriction device

The main obstacle to achieving a functioning prototype within a short time was the total time spent fabricating devices. Faults discovered during fabrication or in device testing are usually corrected by fabricating a new device. Reducing the fabrication cycle time was therefore important to reduce time spent fabricating devices.

A new design was selected to reduce the time to fabricate a single device. As it is time consuming to develop and test new fabrication processes, a design was chosen to accommodate the SU8 fabrication method used previously. It was decided to rotate the direction in which the cells were attracted from the horizontal to the vertical plane. This would permit the use of thinner layers of SU8. The associated reduction in the solvent evolution time to (~5 minutes) would reduce the process length.

A diagram of the device concept is shown in Fig. 51. Total fabrication process time was short at ~12 hours. Yield after optimisation was 100%. Reduction in device dimensions allowed miniaturisation of the chip, and more devices to be created per wafer increasing fabrication throughput (~3 device per hour). In experimental testing, devices were treated as disposable, although they were on occasion re-used. Elimination of external syringe pumps removed the requirement for port interconnects simplifying device construction. Elimination of microchannels (apart from the micro-pit, which is a vertical channel with a closed end) also eliminated bubble trapping.

The objective of developing a tool for positioning cells and subsequently fusing them remained unaltered.

6.6.2 Demonstration of Cell Fusion Capability

The micro-pit had been used previously for positioning cells according to an array pattern (positive DEP [202, 203] [53], negative DEP[54] [113]) . There was however an uncertainty entailed in the micropit cell pairing and fusion design. No reports were found documenting the use of micropits for cell fusion.

[53]These pits may have also used the pit depth and hydrodynamic flow to assist particle trapping.

[54]The micropit geometry is also known as a microwell.

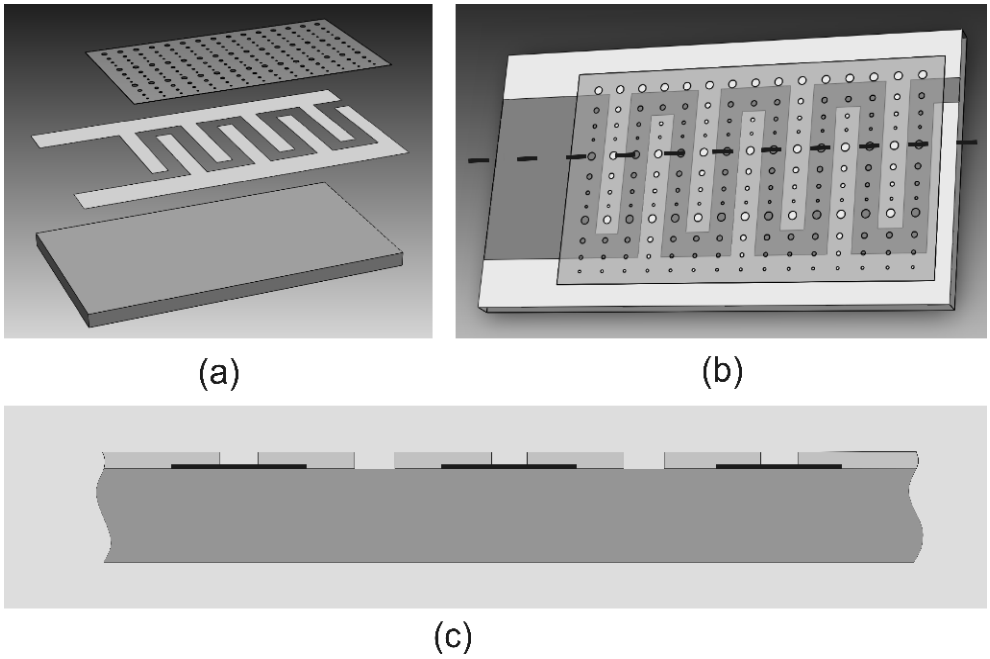

Fig. 51 Construction of a micropit array.

(a) Exploded diagram of device layers: (Bottom) borosilicate glass substrate, (Middle) Titanium film microelectrodes and (Top) Epoxy polymer electrical insulation (SU-8)

(b) Device as built, Dashed line indicates location of cross-section

(c) Cross-section through the microchip. (not to scale). Titanium microelectrodes (black). Borosilicate glass substrate (grey). SU8 (light grey)

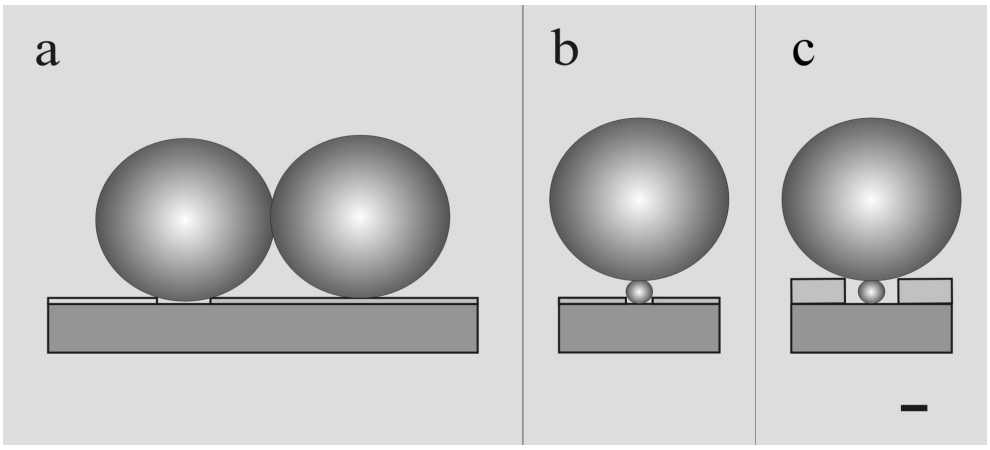

Fig. 52 A Scale drawing of the micropit and the location of paired cells.

Drawing shows the location of various cell pairs immediately prior to fusion. Three of the configurations tested are shown. (a) Oocyte-oocyte and (b,c) oocyte-small donor . Scale bar 20 μm.

The electric field strength at appropriate field strengths can cause of disruption of the phospholipids in the cell membrane. Electrical disruption of the phospholipids can result in pores in the membrane, cell lysis and membrane intermingling that results in cell fusion. To achieve cell fusion, the electric field should ideally be highest at the point where membrane contact occurs between cells. Possible cell and electrode arrangements are shown in Fig. 52. Modelling of the device (section 7.1) indicated that the highest field region might not occur at the point of intercellular membrane contact (Fig. 53).

The aim was to determine if cell fusion could be initiated without irreversibly permeating the plasma membrane. A secondary question regarded a problem that can occur with retrieval of intact fusion products: the plasma membrane can adhere permanently to electrodes during electric pulse application [204].

The obstacle to demonstrating a cell pairing and fusion instrument (time consuming fabrication) had now been removed and replaced with an unanswered question: Was it possible for a micropit to fuse cells. Demonstration of the new devices capability to achieve cell fusion was a pre-requisite for demonstrating that the device was a useful tool in Bovine NT. While modelling might assist formulation of predictions about membrane fusion and permeation, the best (and quickest) method for determining if cells could be fused was to conduct an experiment.

An array of differing micropits was fabricated on a small device 20 by 15 mm. It consisted of a glass substrate, coplanar electrodes and a thin insulating film of SU8 (Fig. 51). Details of the fabrication process are in Appendix C. As the objective was to form fusion products using the device, and only two geometrical parameters- the pit height and depth could enhance the fusion rate, a number of differing pits were fabricated.

Trials were conducted in AgResearch in Hamilton. Devices were prepared for testing with variations in depth (4μm or 22 μm thick film) and diameter (20,30,40,80 μm). These devices would permit testing of variety of geometries that could potentially achieve cell fusion (and pairing). Variation in geometry would influence the electric field distribution the cell pair experienced and also the area of plasma membrane in contact with the surface of the insulator and coplanar film electrodes.

Three cell types were used for testing: zona-free oocytes as described in [205]; mural granulosa cells (EFC) from ovarian antral follicles [161], adult ear skin fibroblasts (AESF-

1) [205]. These cells were cultured with and without reduced quantities of serum. Serum-starved cells were cultured in medium containing 0.5% fetal calf serum (FCS) as described in [32]. Non-serum starved cells were cultured in 10% FCS.

Donor cell-oocyte couplets were formed by DEP without the use of the lectin adhesion agent used in the baseline process [28]. Fusion was performed in hypo-osmolar fusion buffer (nominally 172 mOsm, comprising 164 mM mannitol, 50 μM CaCl2, 100 μM MgCl2, 500 μM HEPES, 0.05% fatty acid-free BSA, pH 7.3) with a conductivity of 57 μScm^{-1} (Cyberscan PC300 series, probe 8090).

A DEP voltage of 3 Vrms at 1MHz created a force strong enough to consistently attract small donor cells from a distance of approximately 100 μm of the pit edge and did not appear to damage the cells. This DEP voltage was used for most experiments.

Results

A circular region of attraction around each pit was observed for both somatic donor cells and oocytes. Within ~45s, small donor cells (Table 3, trials 1 & 2) were observed to position themselves entirely within the pit circumference. The 4 μm thick SU-8 film shielded cells from significant attraction to underlying electrode edges. Additionally, some donor cells were observed to be repelled away from the micropit through negative DEP. Oocytes automatically centred directly on top of the micropit.

The results of the experiment are shown in Table 3. An example of two oocytes positioned for electrofusion is shown in Fig. 54. All of the pits tested were capable of fusing cells. The fusion rates in the trials were: oocyte - oocyte 69% (n=13), oocyte - embryonic follicular 60% (n=10) and oocyte - adult fibroblast 75% (n=12) are consistent with efficiencies (60-80%) generally regarded acceptable [206].

Both delicate embryonic cells and robust adult cells were fused. While some cases of cell adhesion to the SU8 were observed, this was minor and may be reduced or prevented by inorganic or organic surface coating (serum, albumin) of the electrodes [206].

6.6.3 Significance of a MicroPit to Bovine Cloning.

The micropit is part of a class of devices for cell pairing and fusion (CPF). CPF devices such as the micro-orifice field constriction array [207] and hydrodynamic CPF [164, 165] are primarily designed for high fusion throughput, and generating a high percentage of fusion products from heterogeneous cell couplets.

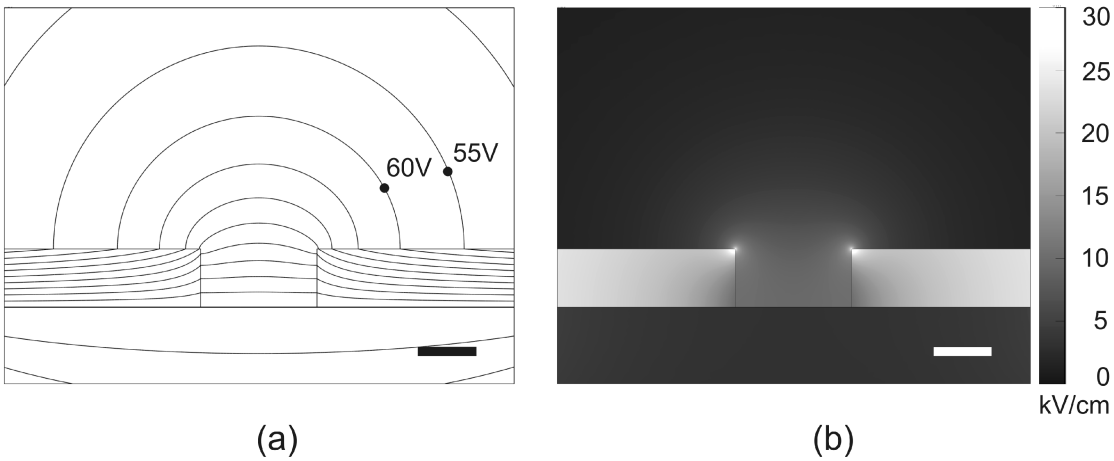

Fig. 53 Micropit Electric Field Simulation results.

(a) Electric potential (b) Electric field magnitude. The electrode voltage was 100V DC. Only the central micropit is shown. Scale bar 20 μm

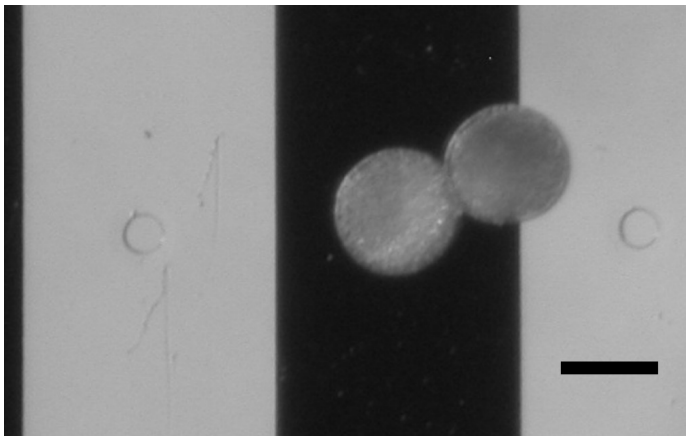

Fig. 54 Oocytes at a 40 μm pit.

The titanium electrodes (width 250 μm) are black, and the borosilicate glass appears white due to transmitted light. Scale bar 100 μm

Trial	Donor Type	DC Pulse Voltage	Pit width (w)	Pit depth (h)	w/d	h/d	n	Fused	Lysed	Fused (%)
1	AESF-1(s)	160	40	22	2	1.1	3	0	3	0
2	AESF-1(s)	120	40	22	2	1.1	20	12	3	60
3	AESF-1	100	20	4	1	0.2	3	0	0	0
4	AESF-1(s)	120	20	4	1	0.2	3	1	2	33
5	AESF-1	115	20	4	1	0.2	12	9	1	75
6	EFC(s)	110	20	4	1	0.2	10	6	3	60
7	Oocyte	120	80	22	0.7	0.2	2	2	0	100
8	Oocyte	120	40	22	0.3	0.2	3	2	ND	66
9	Oocyte	120	40	4	0.3	0.0	13	9	ND	69

Table 3 Micropit nuclear transfer (fusion) results

The cross sectional width (w) and depth (h) of micro-fabricated pits were varied in the attempt to fuse bovine cells. Donor cell diameter (d) was approximately 20 µm. Serum starvation is denoted by (s) and the number of fusion attempts is denoted by (n). "ND" = not determined.

Cell pairing for electrofusion can be considered to occur in two stages: (a) couplet formation and (b) couplet micro-positioning for electrofusion. The final previously untested stage of cell fusion was also demonstrated. All three stages of CPF operation using the prototype were demonstrated without interruption or manual intervention.

The micropit increased fusion throughput. Concerning couplet formation, the baseline procedure was simplified and streamlined by eliminating transport of cells to lectin media, and eliminating the holding time (5-10 minutes) in lectin. Reduction in the baseline process complexity, by utilising the micropit (both the removal of the requirement for media exchange and the minimisation of the number of reagents used) the fabrication cost of bovine NT lab-on-chip devices could be reduced.

Throughput increases can be achieved by concurrently fusing cells. Adhesion of donor cells to oocytes by manual rolling (section 2.3.2) was eliminated, permitting increase in throughput. It also removes the commensurate increase in laboratory personnel for the labour intensive baseline procedure.

Adjustment of the couplet main axis is part of the baseline procedure and most other NT electrofusion procedures. This is usually achieved automatically by application of a low voltage electric field for couplet alignment (section 2.3.2). It however is not effective for small (low volume, cf. Equations 11&35) donor cells attached to oocytes. The micropit was demonstrated to position small donor cells and oocytes and electrofuse them, increasing throughput.

Automation of cell handling in the baseline procedure is important to researchers concerned with the genetic aspects of bovine NT. Manual handling of cells that occurs during transferral of donor cells to lectin, adhering cells and adjusting couplet axis orientation can be considered uncontrolled disturbing factors in experimental trials that hinder identification of genetic characteristics studied in the bovine NT process. The micropit reduces manual cell handling and is therefore conjectured to improve experimental repeatability.

Automated simultaneous positioning of many donor cells above a micropit array might also be achieved using this device, in a manner similar to that demonstrated with pituitary cells [202, 203]. This would further increase production rate of reconstructed embryos. To characterise cell handling using the micropit, the DEP force applied to cells is considered further in the following chapter (section 7.1).

7 System Transport

Transport is an important element that integrates various biochemical functions into a whole system. In a living cell, mechanisms transport nano-scale chemical building blocks such as amino acids for protein synthesis, fatty acids for membrane construction, and tubulin monomers [208, 209] for assembly of the cytoskeleton. In a NT laboratory system, micro-scale transportation concerns individual cells and fluid flows.

In bovine NT the transportation is effected by the manually controlled micropipette. This ubiquitous tool is utilised in the baseline procedure for exchanging fluid media, transporting cells, removing zona pellucida, enucleating oocytes, separating aggregated donor cells, 'sticking' donor cells to cytoplasts and aligning couplets with the electric field. Although the pipette is a versatile instrument, manual cell handling is time consuming and introduces operator dependent variation within experimental trials. This variation hinders identification of biological factors influencing blastomere production and calving rates [69]. Automated transportation devices are hoped to reduce the manual component of the baseline process and thereby also reduce variation in cloning trials.

Tools for transport of cells to the fusion site were investigated. Transport mechanisms were classified according to actuating cell movement over short (<1mm) and long (>1mm) distances. The previously encountered micropit, a short distance positioning and cell trapping device, was examined regarding the force exerted on a cell near the pit. Two on-chip long-distance transportation devices were also tested to obtain experimental familiarity with their operation and shortcomings: travelling wave DEP and open-channel capillary transport.

Misdirection of an individual cell during transportation is detrimental to the operation of some miniaturised systems. Such systems include those that effect cell sorting, counting [210], DNA extraction, individual cell analysis and mammalian NT [211]. Actuator testing was complimented by demonstration of a laser based cell detection device designed to further reduce operator involvement by facilitating automated tracking of individual cells.

7.1 A MicroPit for Cell Positioning

Aim

Experiments and computer simulations were conducted concerning automated positioning (moving and trapping) of cells without manual assistance. The micropit was examined regarding the force exerted on a cell located near a DEP micro pit, in particular the effect of the pit dimensions upon the DEP force in the vicinity of the pit.

Method

The electric field $\boldsymbol{E}$ surrounding the pit was modelled for pits of two differing depths (4 µm and 20 µm) and diameters (10 µm and 40 µm). Comsol multiphysics software was used to simulate the electric field pattern created by the micropits. The relative dielectric permittivity of the liquid media was assumed to be 80 (i.e. that of water). Simulations assume that the rate of change of the electric field ($\underset{\sim}{\boldsymbol{E}}$) is negligible $\partial \boldsymbol{E}/\partial t \simeq 0$ [212] and thus $\nabla \cdot \boldsymbol{E} = 0$ and $\boldsymbol{E} = -\nabla \phi$, where ϕ is the electric potential.

A 1 µm thick layer of AZ1518 was used to form the insulating layer from which micropits of diameter 5, 10, 20 and 40 µm were fabricated (Spin Coating, section 4.1.6). AZ1518 was used due to two advantages over SU8. First, the processing time for AZ1518 is about 5 minutes compared with about an hour for SU8 (due to the slow temperature ramping times required during SU8 processing). The second advantage is that the AZ1518 is reworkable, whereas an SU8 layer is not: an AZ1518 layer may be removed and reformed within 20 minutes, permitting salvage of devices with a damaged or biologically contaminated insulation layer

Due to the difficulty in shipping donor cells to the South Island, saccharomyces cerevisiae (bakers yeast) cells were used as inexpensive test particles suitable for positive and negative DEP tests. The yeast cells were spheroids approximately 3-6 µm in diameter. Saccharomyces cerevisiae was prepared by adding 1-2 g of yeast pellets and 10g of sucrose to 100 ml of filtered deionised water and culturing for 5-6 hours in a conical flask.

The effect of pit diameter and force direction on cell position was examined. The fluid and cell suspension was transferred onto the surface of the microchip and diluted with deionised water to form a reasonably flat droplet of water covering 25-50% of the 20 by 15 mm chip. Two AC frequencies, ~1MHz and ~25kHz, at ~8.5 Vrms were used to effect

respectively positive and negative DEP. The AC field was applied first and cells were subsequently dispensed. To permit time for DEP induced movement to complete, a delay of greater than 1 minute was allowed before subsequent experimental steps. For the positive DEP test, an additional step was made where a gentle rinse was applied using a wash bottle to remove untrapped cells. The cells were then photographed.

Simulation Results

The 2D simulation provided information on the dielectric force exerted upon cells as a function of pit diameter and depth. This was due to the 2D nature of the simulation non-quantitative. The field pattern was dominated by conduction and the capacitance of the insulating layer was negligible.

The following symbols are defined: radial distance from the centre of the micropit (r), pit cross-sectional width (w), pit depth (h), the distance (g) from the centre of one micropit to the centre of the nearest micropit on an adjacent electrode (cf. Fig. 51c) and the cell diameter (d).

The inter potential line spacing (or field strength) can be considered in three regions: near, intermediate and far from the pit centre. The results of the simulation over 'close' and 'intermediate' distances from the pit are shown in Fig. 55. Close to the pit (r<w) equipotential lines are flattened in the vertical direction as the lines begin to conform to the horizontal potential lines within the pit. At intermediate distances from the pit centre (w<r<g/3), the electric potential lines are approximately hemicircular. Further from the centre of the pit (not shown), the equipotential curves become elongated in the vertical direction and are no longer hemicircles.

Varying the micropit depth linearly scales the field magnitude $\boldsymbol{E}$ surrounding the pit (r > w). In the intermediate region (r>w) the direction of the field does not alter as the pit depth is changed. The deeper the pit, the more potential is dropped within the pit, and the lower the field magnitude is at points surrounding the pit. Adjustment of the electrode voltage can therefore compensate for variations in pit depth when r > w.

Altering the pit diameter also influenced the electric field generated by the micropit. Two characteristics of the equipotential lines were observed to vary: the distance between the lines and the curvature of the lines. From observations of these variations, some predictions may be made.

(a) A smaller pit diameter increases the trapping force exerted on cells located at the micropit (r < ~w).

In the region r < ~w, the potential lines are closer together for smaller diameter pits (Fig. 55 a & b). Thus the cells effective dipole moment and the surrounding field strength are and therefore DEP force acting upon the cell can be expected to increase.

(b) The electric force (and the DEP force[55]) is less for smaller diameter pits at intermediate distances from a pit.

This is due to the observation that the equipotential line spacing is greater for smaller diameter pits than for large diameter pits (Fig. 55: a vs b; c vs d).

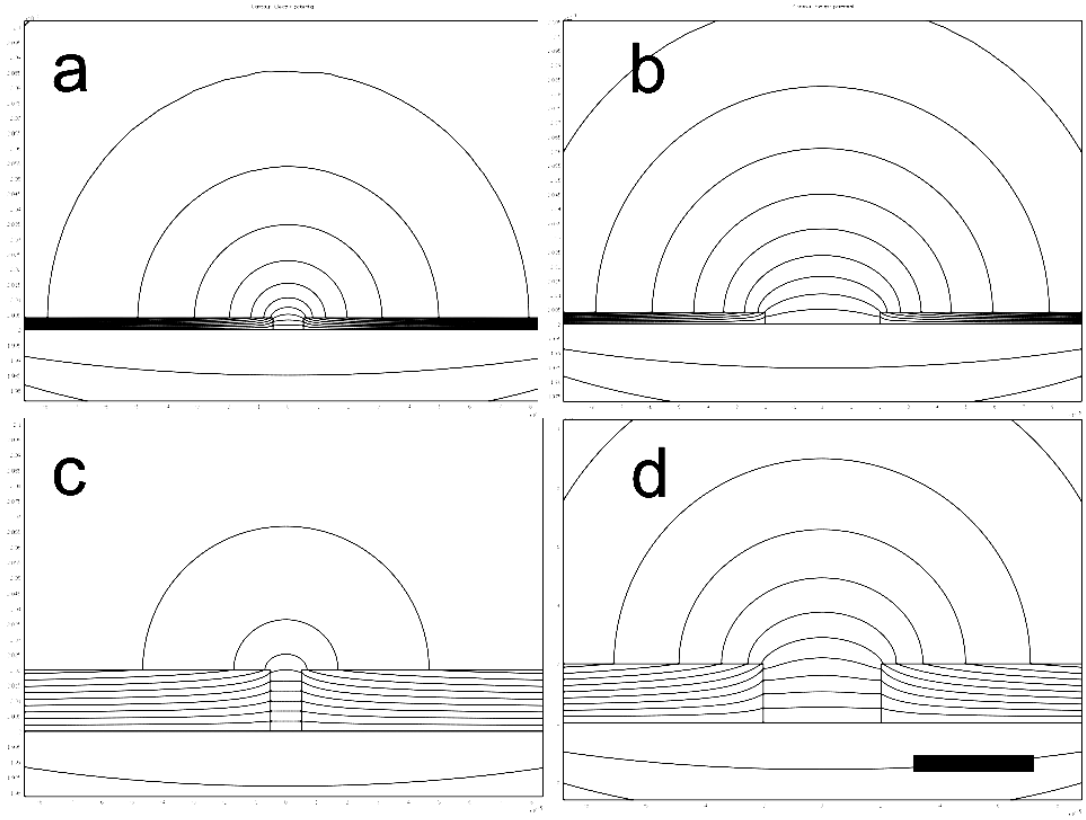

Fig. 55 2D Scalar potential for various pit dimensions.

Cross section of central micropit is shown. Interval between equipotential lines is 0.05 of the electrode voltage. Scale bar 40 μm.

[55] $2E\nabla E = \nabla(E)^2$ cf. Equation 35.

Variation in equipotential line curvature is observed with pit diameter. However, for the region r > w no curvature change occurs due to variations in pit diameter. In this region, the reduction in DEP force due to decreased pit diameter (statement (b) above) could be compensated for by increasing the electrode voltage.

The significance of the DEP force to cell handling depends upon the diameter of the cell (d) relative to the pit dimensions. While the forgoing qualitative statements on trapping force are valid when d $\simeq$ w, if d > w , the approximation of a uniform field throughout the volume of the cell is invalid[56] and larger pit diameters might[57] exert a greater trapping force than smaller diameter pits. If d<w, it is possible for the cell to move within the pit. In this case there is a DEP force that acts towards the convex corner at the top edge of the pit[58]. Within the pit the field is relatively uniform (equidistant equipotential lines, Fig. 55) so for example at the bottom of a pit, with sufficient depth, the DEP force is expected to be zero.

The following equation was proposed as an approximation for $\boldsymbol{E}$ within the given limits.

$$\boldsymbol{E} = \frac{kV}{r^2}\boldsymbol{r}^{\mathbf{0}} \quad (\mathrm{w} < \mathrm{r} < \mathrm{g}/3) \tag{44}$$

Where 'V' is the inter-electrode voltage and k is a proportionality constant dependent on g, w and the film thickness (h).

Experimental Results

Results of positioning tests are shown in Figures 56-59. In the negative DEP test (Fig. 56), cells were excluded from a circular region centred upon and encompassing the micropits. In one trial, exclusion radii were (on average) 55, 83, 110 and 139 μm (±10 μm) in order of increasing pit diameter (5,10 20 and 40 μm).

The positive DEP test (Fig. 57) showed trapping of cells at pits above the electrodes, and not at other pits. Cells did not trap at any pits when no AC voltage was applied. Adhesion

[56]see calculation of equivalent dipole moment pg. 174.

[57]This has not been evaluated by computer simulation or experiment

[58]This is due to a field local maxima (see Fig. 53b) that occurs at the top edge of the pit. See also the discussion section regarding a cell located at the centre of the pit.

was therefore not a cause of cell trapping. Cells were observed to trap next to the edge of the micropit by DEP as predicted for d<w (Fig. 58).Trapping also occurred at the edge of the electrodes, due to the current not being conduction dominated (i.e. the insulating layer was too thin to shield cells from the 1MHz field).

Yeast cells were often observed to be attracted towards micropits, held briefly and subsequently expelled from the micropit.

Discussion

The electric field simulation (Fig. 55 a,b) is consistent with simulations by Lian et al [213] and Gray et al [214] who worked on cell positioning with effectively zero-height micropits.

Equation (44) could be used in combination with Equation 35 to predict the direction of cell movement. This is supported by the observed (Fig. 56) circular distribution of cells surrounding the micropits, as cells would tend to form a circular pattern if a hemispherical negative DEP field were to exist. The measured increase in exclusion radii with pit diameter is consistent with simulation predictions that indicated, at intermediate distances ($w < r < g/3$), the electric field magnitude increased with pit diameter (Fig. 56). In other experiments using bovine oocytes (chapter 6.6), shallow pits were observed to attract cells (at intermediate distances) more than deep pits, which is also consistent with computer simulations.

In contrast to the yeast cell experimental results (Fig. 58) where yeast cells were observed to position near the pit edge, in cell positioning experiments with bovine donor cells, cells were not observed (personal communication P. Gaynor) to drift to the top edge of micropits when the cell diameter was half the pit diameter (Table 3, trial 2). This might be explained by obstruction of the pit increasing the field intensity on the unobstructed side of the cell causing the cell to centre.

The trapping and expulsion of yeast cells from the micropit is in the authors opinion due to membrane poration as it is difficult to see how an electrophoretic or thermal effect could explain the cell trajectory. Cell acceleration and deceleration (supplementary video[59]) is also observed on approach and exit from the pit commensurate with the radial dielectric

[59]yeast trapB.avi

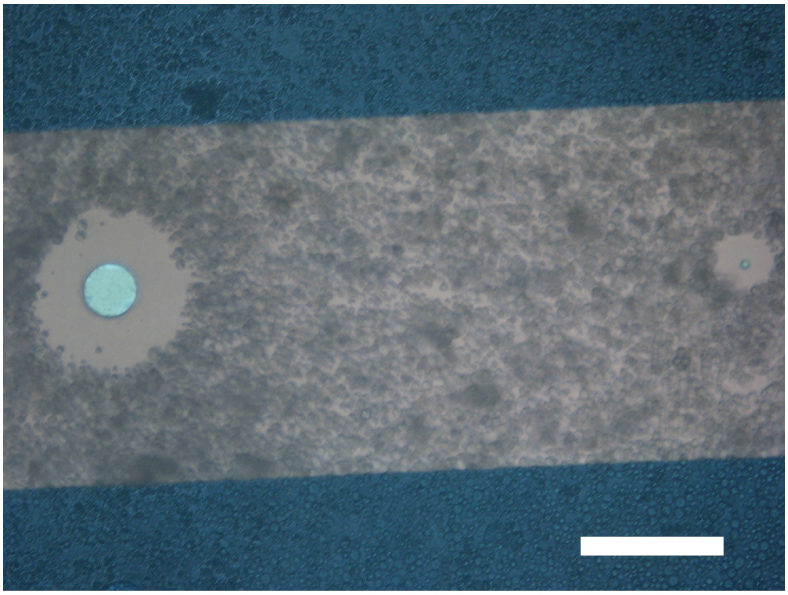

Fig. 56 Yeast cells repelled from two pits in the micropit array.

Pit diameters are 40 µm and 5 µm. Microscope coverslip not used. Scale bar 100 µm.

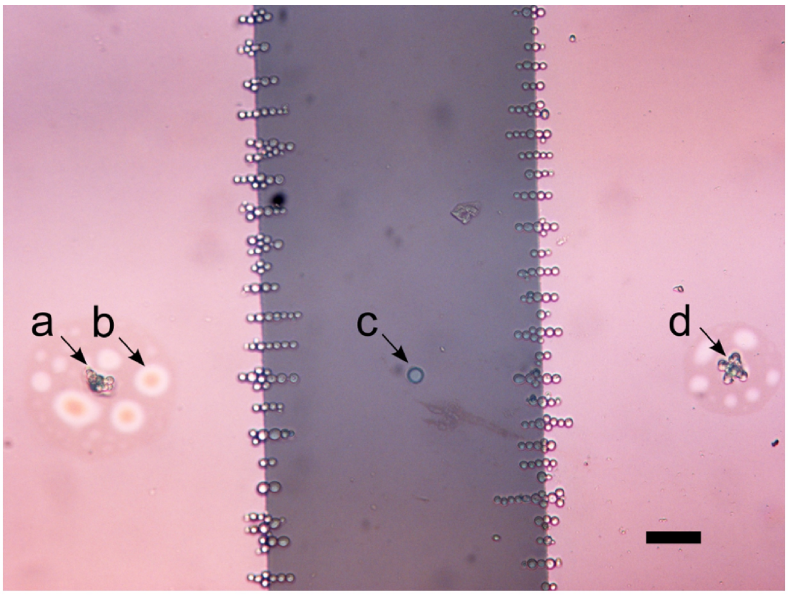

Fig. 57 Location of yeast cells after DEP trapping.

Cells are clustered around pits situated on top of electrodes (‘a’ and ‘d’). No cells are at pit ‘c’ which is above glass. Pearl chains are visible above the electrode extending either side of the electrode edge. Pits at 'a', 'c' & 'd' are 10 µm in diameter. Prolonged immersion caused hydration of the photoresist 'b'. Scale bar 50 µm.

force that would be associated with a field distribution described by Equation 44. In similar experiments with bovine cells this was not observed, probably due to the low voltages (~3 Vrms) employed.

Additional Experiments regarding cell registration to a micropit array

Grey et al [214] have suggested quantifying the quality of cell registration to a micro-array. No published work with quantitative single cell registration rates was found. However, high single cell positioning rates are evident from Skelley et al [165].

During the course of PhD experiments single cell trapping using pits with diameter similar to the yeast cells was accomplished (Fig. 59). However, numbers varied from 0-4 cells per pit and it was difficult to distinguish an empty pit from those containing a single cell.

It remains to demonstrate high rates of single cell trapping at each pit. This could be assisted by use of Fluorescent dyes and a low cell concentration. Fluorescent dyes or use of larger (20 μm) bovine donor cells would assist determining cell count per pit. Utilising a low cell concentration, reduces the likelihood of multiple cells being trapped at a single pit, but increases the probability of vacant pits.

Bovine Micropit Tests

Observations regarding the positioning of bovine cells using the micropit were made during cell fusion experiments. During testing donor cells that flowed across the surface of a micropit array were observed to alter trajectory and trap at unoccupied micropits. Less frequently two cells were trapped in fluid flow at a pit. Further tests with a fluid flow would be required to determine whether this method is superior to a static dispense of a droplet onto the micropit.

Cell registration using a micropit array and a wash rinse was not tested with bovine cells. Practical problems not encountered with yeast cells may be present. It is unknown for example whether bovine donor cell agglomeration would be significant. Improvements are probably required in the rinse stage, possibly by providing a controlled laminar flow across the surface of the pits during rinsing. A laminar flow could be achieved either by use of enclosed or open[60] microchannels.

[60]see section 7.3 Capillary transport. Open microchannels would provide access for oocyte retrieval by pipette at all stages of the procedure.

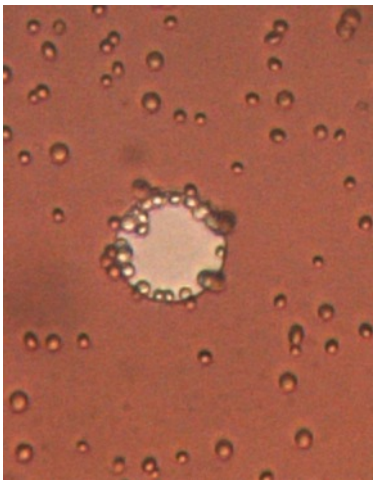

Fig. 58 Yeast trapped at the edge of a micropit.

No rinse applied. Note the absence of cells in a ring surrounding the pit. Cells were easily rinsed from the AZ1518. However, some small adhesive forces may have influenced the attraction radius surrounding the pit.

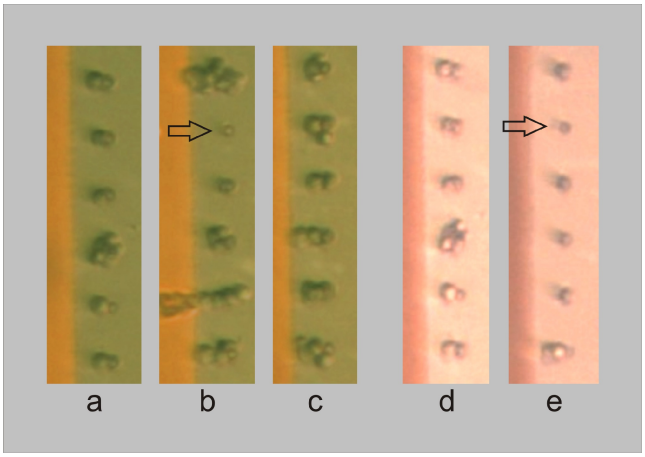

Fig. 59 Cell trapping using a wash bottle rinse.

In these photos (a-e), the micropit size was reduced to 4 μm and placed near the edge (the visible vertical line) of the electrode to reduce the influence of the field generated at the electrode edge. Arrows indicate pits that were estimated as unoccupied (see text). Photos (a-c) were from one trial and (d&e) from another.

7.2 Travelling wave dielectrophoresis.

Background

Dielectrophoresis occurs due to the interaction between a non-uniform electric field and the difference in polarisation between a particle and the fluid media. Non-uniform travelling fields were proposed as a means for cell transport by Masuda et al in 1988 [8] and a cell separation device was demonstrated using a travelling wave. An approximate travelling wave field can be generated by a n-phase (n>=3) power source connected in sequence to coplanar electrodes. Fuhr et al (cf. [215]) later demonstrated propulsion of cells at high frequency (10kHz-39MHz) and named the effect travelling wave DEP (twDEP). Wang et al [216] then extended Equation 35 concerning the field magnitude to include forces due to phase (Equation 45). Further refinements to twDEP theory are listed in the references (Green's theorem [217]; Fourier analysis [218]).

$$\boldsymbol{F}_{av} = 2\pi R^3 \epsilon_a \left[\Re[\underline{K}] \nabla (\boldsymbol{E}_{rms}{}^2) + \Im[\underline{K}] \left(E_x^2 \nabla \psi_x + E_y^2 \nabla \psi_y + E_y^2 \nabla \psi_y \right) \right] \tag{45}$$

where x, y and z represent the Cartesian axes; ψ_i represents the phase of the corresponding electric field vector E_i, $i \in x, y, z$; and the other symbols are defined in chapter 3.

Aim

The objective was to determine if twDEP could be used as a simple method for transporting bovine cells, eliminating moving mechanical parts (on-chip or off-chip) and fluid connections to macro-scale off-chip pumps.

Method

The first test was to determine if twDEP could be observed. The experimental apparatus is shown in Fig. 60. A four phase programmable power supply was constructed, with each phase separated by 90 degrees. A NiCr adhesion layer ~30nm, and then ~100nm of gold were deposited by thermal evaporation onto a standard (25 by 75mm) glass microscope slide. Patterned AZ1518 photoresist was used to protect the metal layer during etching. A standard printed circuit board edge connector with spring contacts was plugged onto the

narrow edge of the microscope slide to make contact with the thin film coplanar electrodes. A milled plastic ring was sealed to the microscope slide to form a small open reservoir above the microelectrodes (Fig. 60, inset; & Fig. 28).

As bovine cells were not readily available, yeast cells were used for preliminary tests[61]. Yeast cells were cultured, and dispensed into the reservoir, and diluted with water. A frequency of ~25 kHz was used to drive the electrodes. Deionized water and samples from the yeast culture were added until DEP could be observed. The supply was then switched from two phase to four phase to commence cell transportation.

Electro-osmotic flow due to the Debye charge layer and electrolysis were avoided by using low conductivity media and maintaining the frequency above 10 kHz so that a charge layer did not have time to form [219]. Thermal convection effects due to resistive heating were avoided by using low conductivity media and square wave voltages below 8 V_{rms}. Heating due to high frequency media polarisation was not significant.

Results & discussion

Travelling wave motion was observed (Fig. 61). The yeast are observed at t=6 s to split into two “waves”, which become more clearly visible at t=12 s. The group of cells appear to bridge the two waves, and then gradually thin at t=20 s separating the two groups of cells. The speed of the faster group from t=2 s to t=12 s is ~80 μm/s. Some yeast cells were observed to remain in DEP "eddies" at the edges of the electrodes (cf. simulation by Green et al [220]) and were not levitated into the translation layer above the electrodes.

The observed failure to consistently transport some cells (those located in 'eddies' at the electrode edge) is undesirable, especially if cells were to be retained on the chip for sometime before being used as donors in the NT process. To remove these cells the chip could require rinsing.

Bovine twDEP

The equipment was shipped to AgResearch in Hamilton, and travelling wave tests were repeated with bovine oocytes. Under twDEP operation, a negative DEP force levitates cells into a region of relatively uniform DEP force that is directed parallel to the surface of the

[61]see [15] regarding DEP of yeast cells. Polystyrene beads can be used for twDEP tests as they display negative DEP in deionized water [16]. See also [17, 18] for modelling of polystyrene beads in aqueous solutions.

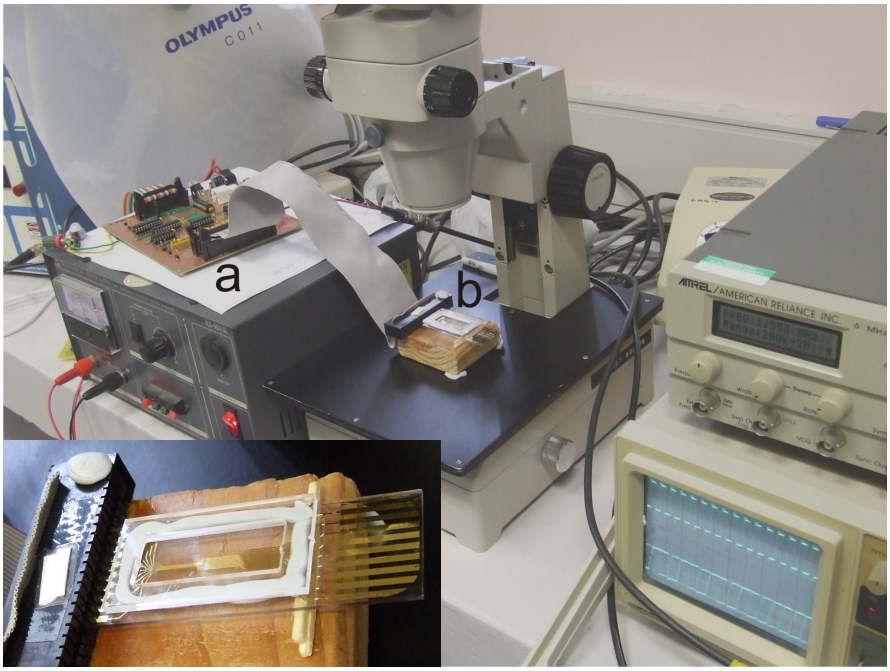

Fig. 60 Travelling wave apparatus for Cell Transport.

A four phase waveform generator circuit board ('a', main photo) was custom-built. The fluid chamber used in testing ('b', main photo; & inset) consisted of coplanar film electrodes on a glass microscope slide sealed to a plastic rectangular ring by putty (Blutak™). A ribbon cable connects the waveform generator with the microscope slide by swiping spring contacts (black PCB edge connector, inset photo).

substrate [218]. Oocytes were observed to be attracted to the electrodes due to positive DEP, but they were not observed to be repelled from the electrodes.

Oocytes in the baseline fusion buffer were tested from 10 kHz - 2 MHz for negative DEP but no negative DEP force was observed. In an attempt to achieve negative DEP, the electric permittivity ϵ (or 'polarizability') of the media was increased by adding HEPES[62] to the baseline process fusion buffer [221]. Initial tests indicated capacitive heating (even liquid boiling) and increased fluid viscosity which could be detrimental to the utility of the device for cell transportation. The liquid media conductivity did not contribute significantly to boiling, as heating was frequency dependent and the conductivity of HEPES buffer is also low (0.67M solution is 52µScm^{-1} [16]).

[62]HEPES is used in the baseline process as a pH buffer when handling cells outside a CO_2 incubator. It is a highly polar (zwitterionic) molecule to which the cell's plasma membrane is impermeable [19].

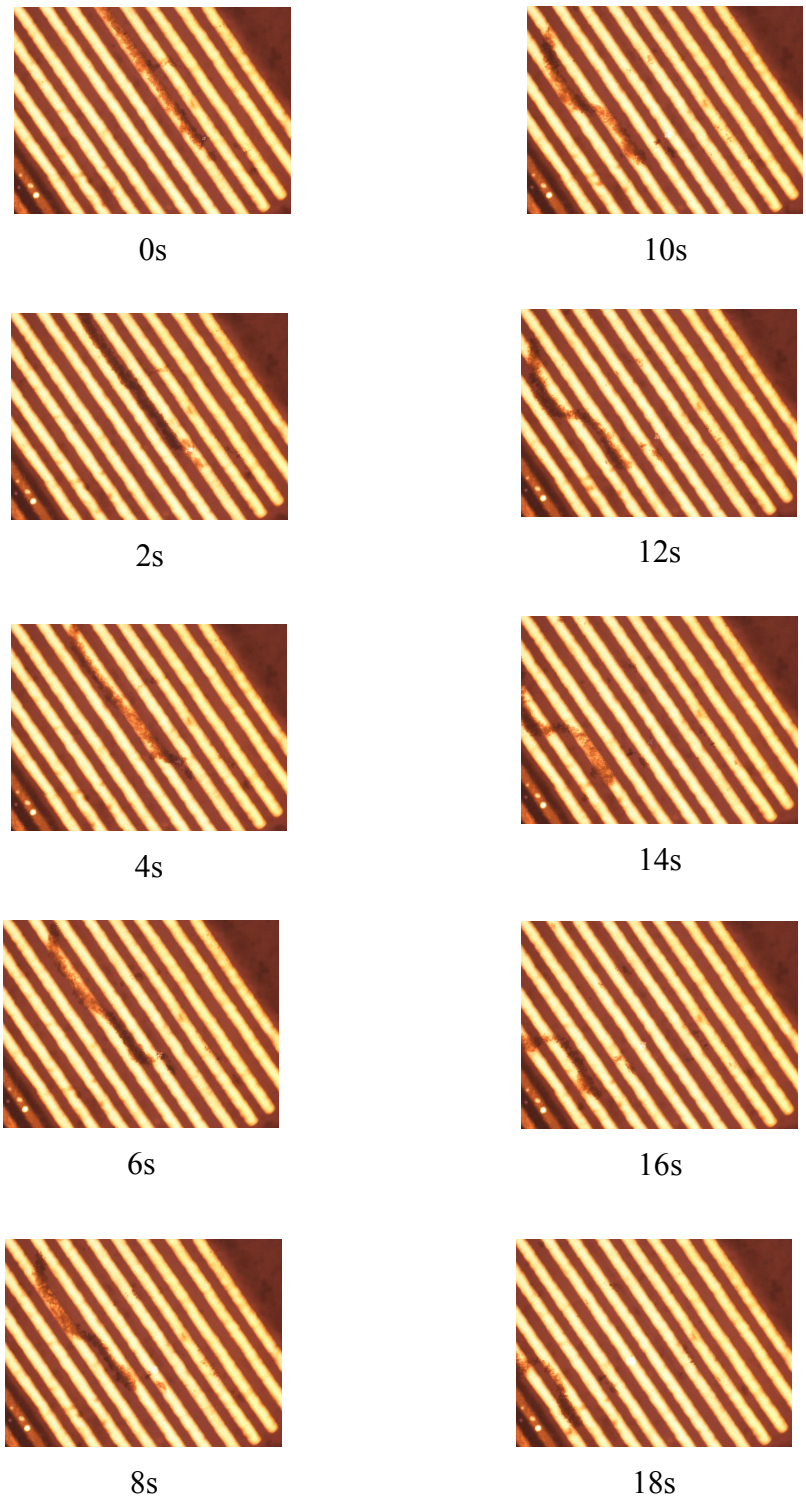

Fig. 61 Travelling wave transport of yeast cells.

Coplanar gold micro-electrodes that were fabricated on a standard glass microscope slide are visible. Electrodes were 100 μm wide, 100-200 nm thick. The inter electrode gap was 100 μm.

Changing the buffer media would require large scale trials to determine influence on embryo viability as uptake during electrofusion of organic buffer substances such as HEPES may lead to adverse side effects [89].

Other bovine cells, such as fibroblasts, and embryonic cells were not tested for negative DEP to determine if twDEP is a suitable means for their transportation.

Because negative DEP of the oocytes was not obtained, and that while the author was based in Christchurch travelling wave testing was prohibitively expensive, attention turned to other means of cell transportation.

7.3 Capillary transport

Cell motion may be induced indirectly by fluid flow. A number of effects can cause fluid movement in microchannels. These include DC and AC electro-osmosis, thermal convection [213], travelling wave induced fluid motion [222, 223] and surface wetting [224]. Capillary action relies on surface wetting [225] and therefore has similarities with droplet electrowetting used in some lab-on-chip systems [226].

An open channel filled with liquid has a free surface which is not defined a priori, and is difficult to model [227]. The modelling of these free surface flows continues to receive attention in the fields of applied physics and fluid mechanics.

Open channel capillary transport devices were tested because they are quicker and simpler to fabricate than closed channels. Rapid and inexpensive fabrication is due to a simple single layer construction. No additional metal layer or electrical connections are required as is necessary in twDEP, AC electro-osmosis, or electrowetting devices. No hazardous voltages are used. There are no moving parts, so actuation is more reliable than mechanical based methods and the fabrication of fluid connections (for external pumps) is unnecessary. Over pressure will not cause damage the device as can occur with microchips utilising closed channels.

Aim

The purpose of investigation was to test a simple method of transporting bovine cells that would be useful in the baseline NT system. One part of the NT system where capillary fluid flow could be used is for dispensing donor cells onto a micropit array to facilitate cell positioning or for rinsing donor cells from the array. Preliminary observations were made regarding fluid and particle transport in open capillary channels, particularly fluid velocity and achievable transport range.

Method

A single layer of SU8 photoresist was spun on a silicon substrate and photo-patterned to form microchannels. A droplet of deionized water was dispensed and the speed of the front of the front of the liquid was measured for both straight and winding microchannels (Table 4, Fig. 62 & 63, supplementary material video capil6 and capil3). Particles transported in the capillary flow were also observed.

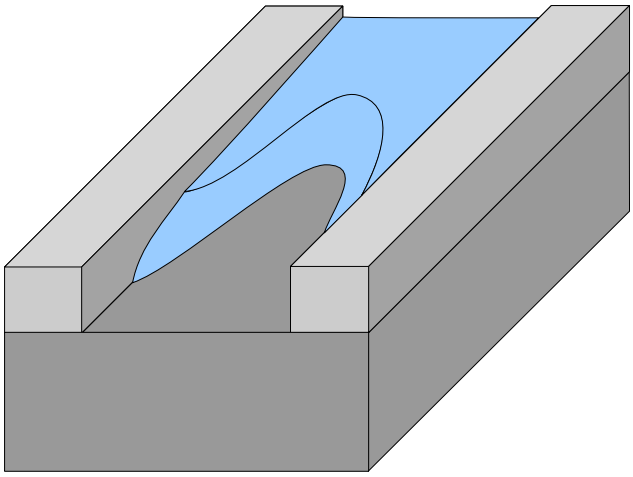

Fig. 62 Micro-channel created by a single layer of SU8 on silicon.

The base of the channel is silicon, the channel walls consist of SU8 epoxy. Fluid front (stylized) is shown in the open microchannel.

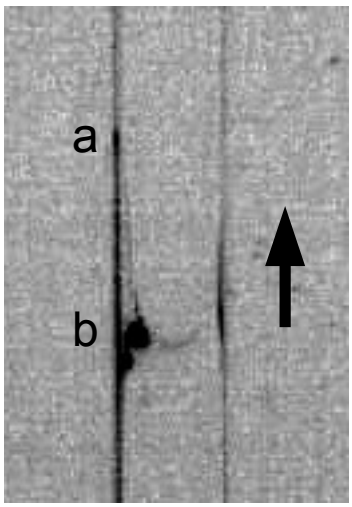

Fig. 63 Liquid flow in an open channel capillary.

Channel is 500 µm wide, ~110 µm deep. The two vertical lines visible in the photo are the edges of the SU8 channel walls. The fluid wicks along the edge of the channel forming two filaments. (a) leading 'front' of meniscus. (b) trailing 'front' of meniscus Image is false colour: the black near the trailing front is a reflection from the light source. Arrow shows direction of fluid flow.

A laser mask writer (μPG 101, Heidelberg Instruments) was used to create a photo-mask for channels of width 25, 50, 100, 200, 500 and 1000 μm. SU8 epoxy was spin-coated on a silicon wafer, exposed and then developed to form microchannels. Multiple channels connected to the same reservoir (supplementary video[63]).

To permit capillary flow, the device was plasma treated for ~30 s to create a hydrophilic surface. Deionized water and (in some tests) polystyrene microspheres (roughly 10 μm diameter, Polysciences™) were used for testing the capillaries. A single drop of liquid was dispensed onto the surface of the chip using a pipette. A high speed camera (up to 500 frames/sec) was used to film the fluid and particles within it. Due to the dark silicon substrate, small dimensions and rapid movement, video recording required a strong topside light source was used. After a few hours, the water contact angle increased, and the capillary device ceased to function. The device was then dried with N_2 and reactivated by ozone plasma treatment.

Results

The contact angle of deionised water on the bare silicon wafer (before SU8 coating and removing by development) was ~20º. The contact angles between deionised (DI) water and SU8 and between DI water and the silicon surface after SU8 development were measured. Before ozone treatment they were both approximately 80 - 90 degrees. After ozone treatment the contact angles were estimated as: SU8 - 15° and silicon - 5°.

Channel depth was between 103-123 μm (Dektak 150 surface profiler, Veeco Instruments Inc.). Channels 100 - 1000 μm wide were unobstructed, but the 25 and 50 μm channels did not develop cleanly.

The fluid flow was observed to initiate along the edges of the channel. Two pseudo triangular cross-section filaments on either side of the channel were formed (Fig. 62 & 63). These filaments extended along the channel walls were bridged as fluid continued to fill the microchannel. The fluid surface was seen to pin to the acute top edges of the microchannels. The location of the fluid front will be defined as the "leading front" for the front of the filament flow, and the "trailing front" as the location of the base of the meniscus curve where the fluid bridges the two filaments (Fig. 63).

The wider the channel, the further the distance between the leading and trailing 'front'. The distance between the leading and trailing fronts in the 100 μm and 200 μm channels

remained constant over the first 11 mm. This distance was in the order of two times the channel width. In both the 500 and 1000 µm channels, the distance between the leading front and the trailing front over the first 11 mm was not static: it appeared to increase as the fronts (leading and trailing) moved further from the reservoir. The width of the filament in the 1000 µm channel was not constant but decreased with distance from the reservoir, and increased with time (supplementary video[63]). The speed of fluid flows for the different channels are shown in Table 4.

Dispensing the exact quantity to fill the reservoir and obtaining a droplet pinned exactly to the outline of the reservoir was not achieved by manual pipetting. Capillary flow started before the droplet had reached a steady state free surface shape. Consequently fluid flow in capillaries that were connected to the same reservoir did not commence at the same time. Entrainment of air bubbles did not occur.

Forward movement of the trailing front in the 500 µm and 1000 µm channels was erratic and at times ceased (the trailing edge on occasion pinned temporarily) while the leading front continued to advance. This may have been due to microscopic defects on the surface of the capillary channel [228]. The speed of the leading front appeared to be related to the distance from the trailing front as it slowed when pinning of the trailing front occurred.

Microspheres were suspended in deionized water and dispensed onto the chip. This resulted in an initial transport of particles away from the source reservoir. When the source reservoir began to empty, the flow velocity reduced. Some particles were then observed (supplementary video[64]) to move in the direction opposing the original flow emanating from the source reservoir. Two laminar flows occurred concurrently within the microchannel. In the bottom flow layer particle movement was away from the source reservoir and in the top flow layer particles moved in the opposite direction towards the source reservoir.

On occasion some micro-sphere clusters became wedged in a channel. When particles suspended in the moving liquid were near the constricted area, they temporarily increased in velocity and passed around the obstruction. It is conjectured that in the obstructed region the fluid surface was raised above the hight of the fluid where no obstructions existed.

[63] videos Capil3 and Capil6

[64] video 'dispense short channel 10' (Channel width 200 µm)

Channel	Meniscus Edge	Distance[2]	Source file	Distance (10^3µm)	Frames	Velocity (10^3µm/s)
100µm	T	-	Capil3	8	70	57
200µm	T	-	Capil3	8	72	56
500µm	T	-	Capil3	2.2	38	29
1000µm	L	-	Capil3	3.6	51	35
100µm	T	-	Capil6	8	56	71
100µm	T	~1.5mm	Capil6	1.12	4	140
100µm	T	~9.5mm	Capil6	1.12	9	62
200µm	T	n	Capil6	8	58	69
200µm	T	~1.5mm	Capil6	1.12	5	112
200µm	T	~9.5mm	Capil6	1.12	9.5	59
500µm	T	n	Capil6	3.4	34	50
1000µm	L	-	Capil6	3.44	43	40
200µm (w)	T	-	Capil6	14.1	156	45
200µm (w)	T	n	Capil6	7.6	78	49

Table 4 Open channel capillary flow rates

Camera frame rate was 500 frames/s.(w) winding channel; [1] L = leading edge; T= trailing edge; [2] Distance from reservoir (n= near; '-' = data not recorded)

Discussion

The reason for the fluid advancing first along the channel walls is not due to the low contact angle of the SU8 as it is greater than the silicon base. The filament flow along the channel edges is appears to support a droplet morphology predicted by Herminghaus et al [229] for a case where both the base and walls of the channel are constructed from the same material.

The increase in contact angle of water on the silicon wafer from (~20º to ~80º) after spin coating and removal of unexposed resist by development suggests that some of the

polymer remained on the surface of the wafer. However, the residual polymer was not sufficient to provide the silicon base with a contact angle identical to that of the SU8 film as after ozone exposure the contact angles were ~5º (Silicon) and ~15º (SU8).

Capillary velocity is known to increase as the dimensions of the capillary reduce. The initial velocities (Table 4) in the 100 μm & 200 μm channels were approximately 140 and 112 × 10^3 μm/s and dropped after travelling 8mm to 62 and 59 × 10^3 μm/s respectively. In comparison, the fluid flow rate of electro-osmotic systems is often around 100 μm/s and the droplet electro-wetting speed can be up to 250× 10^3 μm/s [25]. The fluid flow is thus quite fast: it can cross an entire centimetre in a few tenths of a second, which is the equivalent of an entire micro-chip or the field of view of a microscope. Manual control of such flows to position cells within a few micrometers is therefore not possible. Information on fluid velocity is however relevant to automated control of cell positioning, and control over the rate and quantity of cells transported.

The exit reservoir was effectively unlimited in size and fluid flow continued until the inlet reservoir was depleted. Because the reservoir droplet volume and curvature were not altered significantly during the first 0.2 s it is assumed that the inlet pressure was constant during the tests shown in Table 4. In analysing the liquid velocity as a function of channel width, it is assumed that the input pressure for all channels connected to the inlet reservoir were the same.

Fluid flow velocity is normally reduced in closed channel systems driven by a fixed input pressure. The liquid velocity in the rectangular open capillary channel increased as the dimensions of the channel were decreased. Pumping of fluid beads was observed to occur concurrently in multiple directions once the initial flow had begun to slow. The return flow in the top layer is expected to be due to a micro-thermal effect (supplementary video[64]) caused by the light source.

Channel clogging in a device can be irreparable[65], particularly in closed microchannels. Clog tolerant operation is therefore an interesting feature of fluid flow in open microchannels. For example, slight bridges of SU8 in the 50 μm channel did not prevent fluid from flowing through it and channels containing a cluster of beads wedged across the channel were still capable of transporting micro-spheres.

[65]Composite Fuser testing and conclusion, page 97

Conclusion

A reliable fluid flow was achieved in the 100 and 200 μm wide, 100 μm deep channels. Therefore no further optimisation of process parameters was made to achieve the 2:1 and 4:1 aspect ratios of the 25 and 50 μm wide channel structures.

In terms of application to bovine cell transport, there are a number of practical considerations. Plasma treatment is effective only for a few hours. The need for an ozone generator is not prohibitively expensive as a hand-held portable plasma "wand" (e.g. Model BD-20V, Electro-technic Products Inc., USA) modified the contact angle. It is however desirable to actuate fluid without pretreatment of the device with ozone. Plasma modification could be eliminated with naturally hydrophilic materials or coatings (e.g. metals or silicon dioxide, cf. [230]).

Dust collected on the surface of the chip during operation on the lab bench. It is suspected that dust settling within an empty microchannel could cause erratic fluid flow due to pinning [228]. It would be desirable that the device operate without requiring a filtered-air cabinet. Dust and media residue due to evaporation may mean that devices require disposal after a few hours of use in uncontrolled environments.

The duration of the fluid flow required for dispensing and rinsing bovine cells is yet to be determined. Reservoir pressure is a function of the reservoir droplet curvature and hence volume of fluid in the reservoir [231]. Long duration flow would require adjustment of fluid volume in the source and destination reservoirs.

7.4 Automated Cell Detection

The baseline cloning procedure inherently involves a human operator and a microscope to identify the location and quantity of cells manipulated.

Automated cell detection is often essential to the operation of automated cell handling systems. In such systems automated detection is necessary for the system to provide repeatable cell manipulation and high throughput by parallel (concurrent) manipulation of cells. Automated cell detection can enable the use of high speed (<0.5 s) automated cell handling devices.

Many automatic detection methods can be grouped into two categories: electrical and optical. Electrical methods involve measurement of the conductivity or permittivity of regions between two electrodes and under controlled conditions provide reliable cell detection [232].

Selection of the detection system was permitted to be arbitrary. However, a list of cell detector characteristics was made and a number of prospective devices were evaluated against it. An optical detection system was chosen for detailed examination [233]. The relatively large list of advantages to using this detection system are detailed later and reflect device selection criteria. This system incorporated a low cost DVD optical pickup for cell detection.

The most comparable detection system is that developed by Kostner & Vellekoop who reported [234] the development of a detection system based on a DVD optical pickup while experiments were being conducted by the author[66]. The operation of the DVD detection system has some similarities with the scanning flow cytometer in that a reflector is used to direct forward scattered light to a photosensor [235-237]. In the operation of a scanning flow cytometer, movement of the cell causes a time sequence of light scattered at different angles to be received by a detector via a curved reflector (absorption appears not to be significant). This is used for cell characterisation [238].

[66]see also the more recent publication [20] by Kostner & Vellekoop

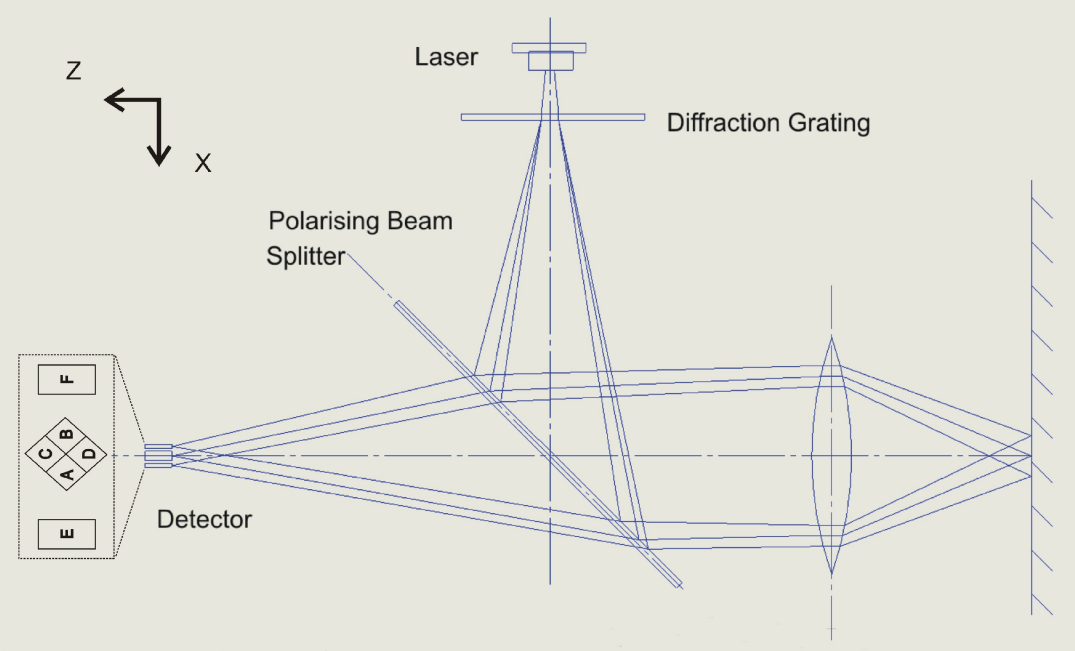

Fig. 64 Illustration of the main components of a DVD pickup.

Only the main and 1st order diffracted beams are shown

Materials and Methods.

The experimental set-up included an optical pickup removed from an inexpensive commercial DVD player (G1928, DickSmith Electronics, NZ). A simplified diagram of a pickup system is shown in Fig. 64. A 635-650nm diode laser in conjunction with a diffraction grating produces several beams which are focused via a beamsplitter and the main lens onto the target. Light reflected or scattered from the target is collected by the lens and is focused onto the detector array. The main lens is located within electromagnetic coil actuators. One is used to focus the lens by translating it in the z direction. Another one shifts (Fig. 64) the focal point in the y axis by tilting the lens about the x axis. In a DVD system the various elements of the detector array (Fig. 64) are necessary for autofocus, data retrieval, and tracking. The outer detectors E and F are designed to detect the ± 1st order diffracted beams, while the 0th order beam falls on the detectors A-D. In the experimental set-up only the outer detectors E and F are used.

The optical pickup was connected to custom made electronic circuits to provide current to the laser diode and to adjust the focus of the system. The signal was displayed on an oscilloscope and analysed.

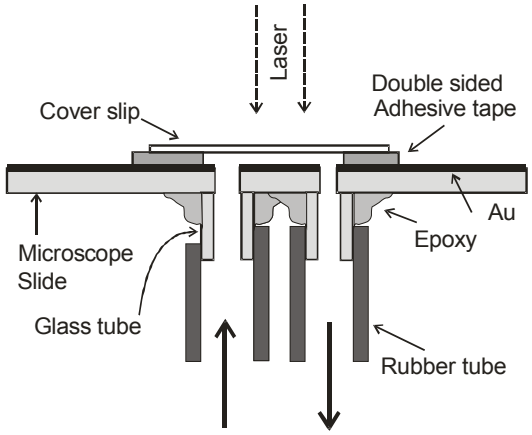

Fig. 65 Flow cell used for 3 µm bead detection

Initial tests were conducted with a a flow cell using 100 µm spheres. Subsequently a thinner flow cell was constructed as illustrated in Fig. 65 and was used for detection of 3 µm and 10 µm diameter micro-spheres. The flow cell was constructed using double sided tape as a 105±10 µm thick spacer between a microscope slide and a cover slip forming a channel 3 - 4 mm in width. The reflective surface was gold (100 nm thick) coated onto the top surface of the microscope slide. Two holes were diamond drilled through the gold coated slide to provide ports for fluid flow into the microchannel. The DVD pickup was attached to the flow cell by a custom aluminium frame which allowed coarse alignment using micrometer screw adjustment. The flow cells were connected to a syringe pump (PHD 2000, Havard Apparatus, Holliston, MA) via rubber tubes[67].

Results

Characterisation of the pickup proved that the main lens could be translated and the focal point shifted by ±500 µm with a linear coil current / distance response of 7.7 µm/mA. Using mechanical and the electronic adjustment of the main lens the laser beam was focused onto the gold reflector. The focus was adjusted so that maximum returned light was recorded by the detector. Fig. 66 shows the change in relative signal when the focus is

[67]The lag between pump activation and particle movement although not significant for this experiment, became evidently an important consideration if a particle positioning system using an external syringe pump were to be developed.

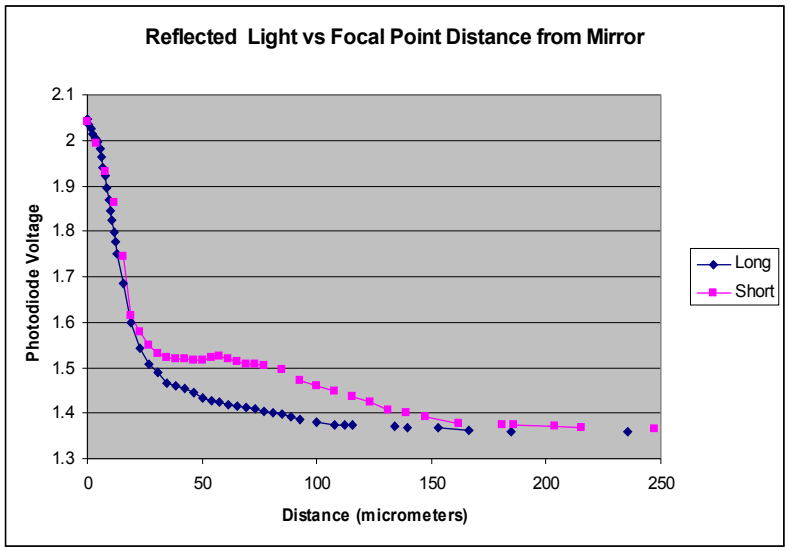

Fig. 66 Reflected light intensity as a function of distance.

'Short' indicates that the distance from the Laser to the focal point is less than the distance from the laser to the reflector.

shifted towards the pick-up (short) or behind the mirror (long). There is a rapid drop in intensity of about 25% over ±250 µm. The intensity then remains reasonably constant over ±2000 µm. For optimum signal level the pickup needs to be accurately kept in focus.

The detection region was estimated by measuring the beam angle and the beam width at the bottom of the flow channel using a scanning knife-edge technique. The beam width was measured to be 15-20 µm. This was larger than the expected diffraction limited spot size of less than 1µm, and could be due to inaccurate focussing. The full beam divergence angle was measured as 76º. The detection region is a conical volume with an approximately circular cross section (in the x-y plane) that for flow cell one increases from about 17 to 127 µm diameter (assuming a refractive index of 1.33) along the z axis.

Fig.68 shows the result for 10 µm beads at water flow rates of 0.2 and 10 ml/min. The two traces are the intensity change recorded by the two detectors used in the DVD pickup. The laser driver, modulated the light output at 210 kHz, causes the ripple on the photodiode detector voltage. To remove this effect from the photodiode voltage, the oscilloscope was set to detect the minimum and peak values as shown in Fig. 67 and Fig. 68. In these figures, the shaded area between the minimum and the peak trace is not a random noise signal. Fig. 68 illustrates the results for 3 µm beads at a water flow rate of 0.007-0.02 ml/min.

The detection pulse, as expected, deteriorates for smaller beads and is strongly dependant on particle trajectories. Particles that did not pass directly through the optical beam path caused lower amplitude pulses (Fig. 68 b). Some particle trajectories (Fig. 67 a,b and Fig. 68 c) produced an increase in the detected light, and sometimes particles passed at an angle to the two detectors so that one detector gave a signal but not the other (Fig. 68 b). A double pulse (Fig. 68 a) occurs when the flow direction was along the x axis of Fig. 64. This is caused by light received from two of the diffracted beams: if the 3 μm beads flow in the y direction, a double pulse is not observed. The fluid flow was generally chosen to be in the y direction to eliminate the second pulse.

As the particle passes through the detection volume, refraction may reduce or increase (Fig. 67 a bottom detector trace) light received by the photodiode.

The upper detection rate of the particle detector is limited. Two characteristics of the detector that influence this upper limit are the signal to noise ratio (SNR) and the inability to distinguish the simultaneous arrival of particles at the detector. Many factors influence the signal to noise ratio: the reflectors coefficient of reflection; vibration isolation of the flow cell; reflection losses on the flow cell viewing window; laser intensity; detection volume; particle size, speed and trajectory. An indication of the SNR at higher particle velocities (where SNR is reduced) is provided by the high flow rate test result shown in Fig. 67 b for which a peak to peak signal amplitude above 200 mV was detected, with the peak to peak noise level below 50 mV. Concerning simultaneous arrival of particles, the concentration of particles and the flow rate is adjusted so that, on average, the pulse width is often around 2.5% of the interval between pulses [239]. Thus for 10 μm beads and the SNR shown in Fig. 68 b, a 60 μs pulse equates to an upper detection rate of about 500 particles/s.

Discussion

The cell detector demonstrated a concept for reliable, low cost and high speed tracking of particles down to 3 μm. Later tests successfully detected yeast cells (~4 μm). In application to bovine cloning the detector would be used to track all cells on a microchip and remove operator dependent variations from experimental trials. A detector is, as discussed previously[68], necessary for high speed cell positioning and to reduce cost.

[68]Automated Cell Detection, page 126

The entire detection system developed, is small and lightweight and can be powered by a small 9V battery. Separate construction of the detection device from the LOC reduced the complexity of lab-on-chip fabrication and improved LOC yield. Detector operation did not require a transparent substrate permitting application to chips where transmitted optical detection is precluded. A reflector was required which may require an additional surface coating during fabrication. Although bare silicon could form an adequate reflective surface for oocytes and possibly donor cells due to their relatively large size.

Only a limited number of pickups can be interfaced with a small LOC due to their large area (~3 cm by 2 cm). This could be a problem where detection site density is important. It is however possible to move the pickup detection zone to different locations. This would however slow detection rates.

Optical systems (of which the detector discussed is a subset), are immune to interference from on-chip electrical actuation waveforms used AC electrokinetic transport systems, whereas electrical detection systems may not be. It is not uncommon for optical systems to require accurate positioning (<±25 μm for this system) for the system to operate. An optical pickup provided a rapid and cost effective method for focusing the detector optics by virtue of the inbuilt focussing coil, suiting the detection system for use with disposable/replaceable LOC devices and portable equipment.

On-chip detection would be beneficial for reducing operator workload, and enable the use of high speed cell handling devices. The DVD detection method could for example be used to track oocytes within capillary flow as they are transferred to a micropit fusion site. Assuming a cytoplast generates the same signal level as for a 10 μm bead[69], a 50 μs detection time would permits detection of an individual oocyte travelling at a velocity of 100 μm/50 μs = 2000 × 10^3 μm/s which is faster than the maximum capillary flow rate observed (140 × 10^3 μm/s). Detection is also non-contact and does not reduce transport speed.

[69]10 μm beads were detected at ~ 500 × 10^3 μm/s (10ml/s)

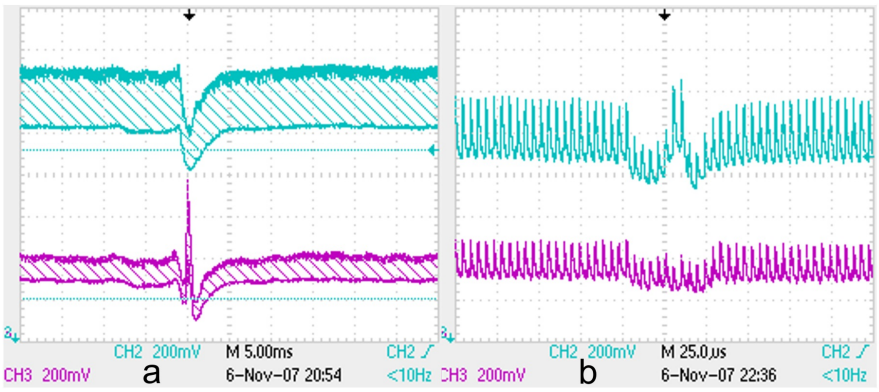

Fig. 67 Photo-diode pulse caused by 10 µm beads

(a) 0.2 ml/min (b) 10ml/min

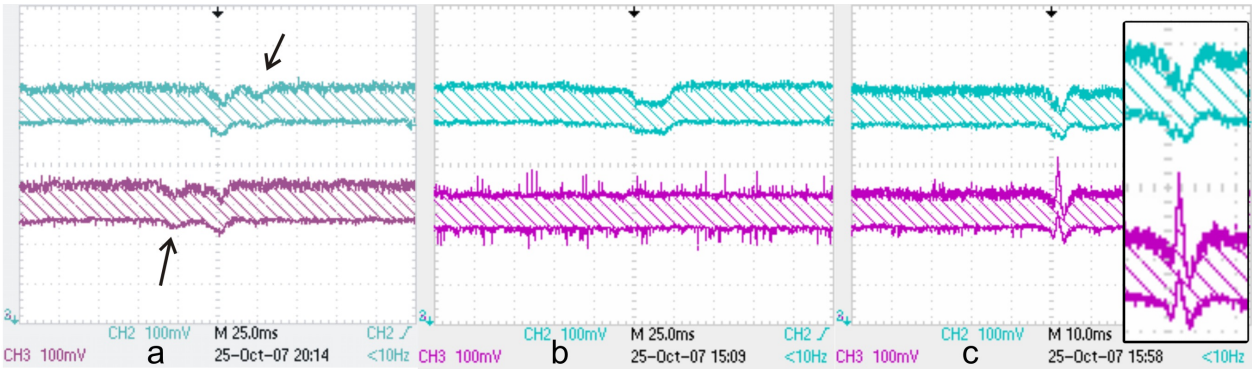

Fig. 68 Photo-diode pulse caused by 3µm beads

(a) Pulses from a single 3µm bead travelling in the x direction. Arrows show pulses for a single particle artificially generated by the 1st order diffraction beam (b & c) single pulses from 3µm beads with flow direction along the y-axis. An enlargement of figure (c) is shown inset.

8 Summary

Fabrication

A number of fabrication methods were used including: vacuum deposition (thermal evaporation and sputtering), photo-lithography, and elastomer casting. Fabrication of micro-scale structures of ~200 µm depth was near the maximum[70] usable thickness of SU8 film fabrication technology, and also at the border of advanced micro-scale mechanical machining (section 6.4.2 Rapid Fabrication).

Construction of the first device, the 'HourGlass Fuser', demonstrated that fabrication of thick (~200 µm) structures in SU8 [240-242] was slow. The speed of device fabrication was important as it influenced the rate at which process parameters could be optimised and therefore the delay before prototype construction commenced. It also influenced the period of the prototype development cycle. Various non-SU8 fabrication methods were tested to reduce the duration of fabrication.

A trade-off was observed between immediate commencement of a slow fabrication process (e.g. structures of 200 µm depth in SU8) and the setup delay in optimisation of any new rapid fabrication processes (e.g. mill rotational speed, depth & feed rate) before sufficient process quality could be achieved and device fabrication could begin.

Devices were designed to reduce device fabrication time and increase yield. This was often by simplification of the entire device or of stages within its construction. The capillary channel transport design was for example intentionally selected because its characteristics (a low aspect ratio, single polymer spin coating and absence of channel seals) reduced fabrication time and increased yield. The micropit was designed to shorten delays associated with solvent evolution and prevention of SU8 film cracking. The composite fuser was designed to facilitate fabrication of chip to capillary tubing connections and microchannel sealing. The magnetic clamp fuser and composite fusers increased device yield and simplified repair by separating construction into independent parts. The DVD design simplified fabrication by removing electrical contacts that were associated with particle detection.

[70]that is for rapid fabrication - manufacturer documents film process parameters up to 550 µm in a single spin coat.

Cell Fusion

The pre-existing coplanar fusion device was investigated due to its cost effectiveness, and the ease of integrating it with other micro-devices in a single lab-on-chip. The coplanar fusion device (which consisted of two film electrodes) was assessed for use within miniaturised bovine NT systems. Trials with coplanar electrodes were conducted to determine the fusion rate of various bovine cells. Coplanar electrodes were demonstrated to effect, within measurement uncertainties, similar fusion rates to existing parallel plate and wire electrodes [160]. A Petri-fuser design based on these test results was fabricated that facilitated cell handling (section 6.2).

Short range cell positioning for fusion was investigated to improve fusion throughput and repeatability. The micropit fusion system was the culmination of a number of fuser designs (HourGlass Fuser and 'T' junction Fuser) that integrated short range cell positioning and fusion. The micropit was shown to assist bovine cell pairing and fusion by increasing throughput and reducing operator involvement. The speed of operation was increased above the existing baseline process for small donor cells. Short range (<200 μm) automated cell pairing and fusion was achieved by dispensing a single oocyte near the micropit. The low-accuracy positioning requirement is an advantage for automated robotic systems that select and dispense single cells [243]. Early experimental work indicates cell fusion rates (60-80%) are commensurate with currently accepted levels [206] for NT. A wide variety of cell types and ratios of donor-oocyte diameters were demonstrated to fuse using the micropit. During device design, a high field intensity region was predicted near the top edge of the micropit. Testing showed that this did not preclude cell fusion. This work complements existing cell handling tools for cell pairing and fusion: the micro-orifice [207, 212] and adhesive and microfluidic devices [164, 165].

Cell Transport

Transport mechanisms that are suited to bovine cell handling were studied in the context of integrating them within a system of on-chip microfluidic devices. A number of transport mechanisms were studied for short (<1mm, DEP based devices) and long (>1mm, twDEP and capillary devices) range distances.

Short-range (~200μm) automatic, unaided, micro-positioning of a cell to the centre of a micropit was demonstrated. In the interest of increasing throughput, tests were conducted to achieve concurrent single cell positioning registered (aligned) to a micro-pit array.

While simultaneous positioning of single cells above pits was achieved, only a low percentage of pits were filled with a single cell. Characterisation of short range micro-positioning using a micropit was conducted. Modelling and experimental results demonstrated that increasing the pit diameter increases the micropit range of attraction, and that a small cell centres when the pit diameter is roughly 2 times the cell diameter[71]. An increase in the pit depth reduces the range of cell attraction.

Long range on-chip bovine cell transport was approached using two designs. A travelling wave transport system was demonstrated with yeast cells and tested with bovine cells in the NT baseline system. Attempts to use travelling waves to transport oocytes in the fusion buffer (conductivity 5.7×10^{-3} S/m, osmolarity 172 mOsm) were unsuccessful due to not attaining a negative Clausius-Mossotti coefficient.

A capillary channel transport system was shown to be effective for transporting cells over distances greater than 10 mm. Flow rates were evaluated ($\sim 50 \times 10^{3}$ μm/s) and open capillary channels were demonstrated to shift micro-beads. Elimination of channel seals, off-chip syringe pumps and inherent fluid connectors decreased chip fabrication complexity. This is expected to reduce device cost and increase reliability.

The speed of particle transport in fluid flow is often (as in the capillary transport device) faster than the reaction times of a human operator. Cell detection was investigated and a low cost method of high speed cell detection was demonstrated. The detection system was based on a DVD optical pickup component which is very low cost and is quick to optically align. The optical pickup was combined with a lab-on-chip flow cell that contained a reflective surface. Together this forms a platform for automated verification of cell location without the aid of a microscope or an operator. Rapid optical alignment and separation of the detector from the micro-chip indicate that the detection method could be suitable for designing a bovine NT system utilising inexpensive disposable lab-on-chip devices. Separation of the detector from the micro-chip reduces chip complexity and cost. Chip cost reduction may permit the time the device is in service to be reduced and thereby improve system reliability.

[71] perhaps the first report of this

8.1 Future work

Future research can proceed along a number of avenues and is not restricted to topics focused on in this thesis. Research topics which this thesis advances include: device analysis - micropit, open capillary channels; and improvement (Appendix C) of fabrication technology in use at the University of Canterbury. Evaluation of device cell handling performance within a bovine NT system can be continued by means of prototype testing and computer modelling.

Fabrication

Fabrication can be investigated separately to the development of cell handling tools. The following work could reduce tool development time by reducing device fabrication time.

SU8 is reported to bond to PDMS [14]. It would be beneficial to investigate the use of a composite base structure where the thin glass coverslip is replaced by a SU8 photo-patterned polymer coating. The layer thickness is very thin and can be quickly processed. Other fabrication stages would be similar to those described previously (Composite 'T' junction Fuser , section 6.5.5).

A rapid fabrication process for forming microchannels in the range of 100 - 1000 µm could be developed. This process could be, a two stage process where an aluminium mould is formed (micro-machining or microEDM) and PMMA is hot embossed. This may shorten the critical path from the start of device fabrication to device completion compared with that of processes using thick (>100µm) layers of SU8 polymer.

Fusion

Investigation of cell fusion using a micropit can be approached experimentally and theoretically. A large trial would improve the quality of the micropit fusion rate estimate, which could then be used as a benchmark for future research.

The influence of the following two quantities upon micropit fusion rates can be examined in trials: the ratio of cell size to pit diameter and the ratio of cell diameters in a couplet. This data could then be interpreted and used as design information when determining what kind of fusion device would be used in a bovine cloning system.

Micropit - cell models may be developed to quantify the field strength imposed on the membrane and predictions made regarding fusion rates. While the geometrical fusion arrangement differs significantly from existing electrorestriction fusers [181-183, 207] theoretical analysis of the micropit is similar to the micro-orifice [98, 212] and similar analysis techniques could be used.

A Cell positioning and Pairing system

Theoretically a low density cell suspension could be dispensed onto a micropit array. Individual cells would be attracted to the nearest micropits, so that isolated single cells would be located above many (but not all) pits. An operator (or robotic pipette) would then with low precision position an individual oocytes near a trapped donor cell, and release it. The oocyte would then, drift towards the donor cell and form a cell pair.

Elements of this cell pairing system such as cell micro-positioning and single cell trapping have been demonstrated. Rates of automated concurrent single small (20 μm) donor cell trapping are yet to be quantified. Authors have not currently quantified cell pairing rates in similar cell pairing and fusion systems, although Skelley et al [165] indirectly demonstrate by experimental photos (Fig. 26) good cell pairing in certain portions of the chip. Cell retrieval rates are also an important consideration as the cost of failing to recover a bovine NT fusion product is large.

Gamete Quality testing

The speed of oocyte movement in a non-uniform field can be used to select high quality oocytes and thereby increase the quality of reconstructed embryos [244]. The micropit was demonstrated to produce a non-linear electric field and some donor cells were repelled from the micropit. It is conjectured, because of differences in the cells electrical polarisation, that these donor cells were inferior to those attracted to the pit. Use of the micropit to discriminate (through the DEP induced cell velocity vector) between good and poor quality gamete cells has not yet been demonstrated.

Cell Transportation

An open channel valve would be useful for automated transportation of cells. An EWOD [245, 246] valve could be used to initiate flow from a reservoir and thereby control cell transportation. Controlled repeatable flow initiation could also be useful for experiments that concern modelling of free-surface fluid flows [229].

Chapter 8: Summary

9 Conclusion

Cell Handling Objectives

The design objective was to improve the handling of bovine cells. Improvements include increasing the throughput and repeatability of the NT procedure, and reducing operator workload. Devices for bovine cell handling were constructed and their performance was evaluated in reference to the baseline NT procedure.

Achievement of Fabrication objectives

Design simplification and rapid fabrication hastened prototype refinement and permitted adequate device numbers to be fabricated for cell-handling performance tests. Devices (capillary transport, micropit, DVD reflective flow cell) were suitable for integration as a part of a miniature lab-on-chip system. Devices (Petri Fuser, micropit) are suited for use as stand-alone components within the baseline cloning system and facilitate cell handling.

The micro-pit, capillary transport and DVD detection designs all had low construction complexity and rapid fabrication times: the micro-pit uses a thin quick curing layer of polymer; the capillary transport mechanism required no connection ports simplifying fabrication and eliminated sealing failure; and the DVD pick-up was independent of the lab-on-chip reducing chip complexity.

Achievement of Cell Handling objectives.

Coplanar device testing demonstrated that film electrodes were suitable for achieving high fusion rates with bovine cell lines. These electrodes were patterned onto the base of a Petri dish. The apparatus provides good micro-pipette access and is easier to clean than existing electrofusion chambers.

A low cost DVD detection system was demonstrated to detect cells and particles. It contributed toward microchip automation (and hence improved NT repeatability).

The micropit fuser and the Petri-fuser were demonstrated to assist cell handling at bovine NT laboratories. The micropit was shown to increase NT throughput when handling small donor cells. The operating mechanism repeatably positioned cells at the centre of the pit eliminating human dependent variation. Particle transportation was demonstrated to occur reliably and repeatably using the capillary transport device.

Contribution of tool designs to current research

Contributions were made in the area of testing and evaluating coplanar electrodes for miniaturised cell fusion systems. The DVD detection system was demonstrated to detect cells at high speed (section 7.4) at approximately the same time as Kostner & Vellekoop [234]. A new device, the micropit, was demonstrated to fuse biological cells. The device was also used to demonstrate for the first time bovine cell pairing and fusion without manual intervention. Theoretical predictions that were made concerning micropit cell positioning characteristics were experimentally confirmed by DEP positioning of cells [247].

Contribution of tool designs to future tool development.

Test results obtained concerning cell positioning and on-chip fusion are applicable to bovine NT and other applications where fusion of biological cells is required (monoclonal antibody production [177, 248], crop improvement [249] and cancer treatment [250]). Integrating the micropit field constriction device with other cell positioning methods (adhesives [214, 251] and fluid flow [164, 165]) is expected to further improve cell handling in terms of fusion throughput and cell positioning accuracy and repeatability.

Two of the tools developed, the capillary channels for cell transport and the DVD cell detection system are intended as components within a miniaturised lab-on-chip system. Proof of concept tests demonstrated that these lab-on-chip instruments should facilitate the future development of cell handling systems.

References

[1] E. A. Sinclair, J. B. Pramuk, R. L. Bezy, K. A. Crandall, and J. W. Sites Jr, "DNA Evidence for Nonhybrid Origins of Parthenogenesis in Natural Populations of Vertebrates," *Evolution,* Nov 17 2009.

[2] T. Tiba, S. Matsuzaki, and Y. Kojima, "Examination of spermatogonial multiplication of the bull using whole-mount seminiferous tubules," *Reproduction in Domestic Animals,* vol. 29, pp. 458-468, Nov 1994.

[3] S. P. Lorton and N. L. First, "Hyaluronidase does not disperse the cumulus oophorus surrounding bovine ova," *Biol Reprod,* vol. 21, pp. 301-8, Sep 1979.

[4] I. Turcu, "Electric-Field Induced Rotation of Spheres," *Journal of Physics a-Mathematical and General,* vol. 20, pp. 3301-3307, Aug 1 1987.

[5] P. T. Gaynor and P. S. Bodger, "Physical modelling of electroporation in close cell-to-cell proximity environments," *Physics in Medicine and Biology,* vol. 51, pp. 3175-3188, 2006.

[6] T. B. Jones, *Electromechanics of particles*. Cambridge ; New York: Cambridge University Press, 1995.

[7] A. Shadowitz, *The Electromagnetic Field*: Dover Publications, Inc., 1988.

[8] S. Masuda, M. Washizu, and I. Kawabata, "Movement of Blood-Cells in Liquid by Nonuniform Traveling Field," *IEEE Transactions on Industry Applications,* vol. 24, pp. 217-222, Mar-Apr 1988.

[9] E. B. Graper, "Charged Particle Flux Generated by an Electron-Beam Deposition Source," *Journal of Vacuum Science & Technology,* vol. 7, pp. 282-, 1970.

[10] A. R. Sapuri, M. M. Baksh, and J. T. Groves, "Electrostatically targeted intermembrane lipid exchange with micropatterned supported membranes," *Langmuir,* vol. 19, pp. 1606-1610, Mar 4 2003.

[11] F. Hamouda, G. Barbillon, S. Held, G. Agnus, P. Gogol, T. Maroutian, S. Scheuring, and B. Bartenlian, "Nanoholes by soft UV nanoimprint lithography applied to study of membrane proteins," *Microelectronic Engineering,* vol. 86, pp. 583-585, Apr-Jun 2009.

[12] L. Gitlin, P. Schulze, and D. Belder, "Rapid replication of master structures by double casting with PDMS," *Lab on a Chip,* vol. 9, pp. 3000-3002, 2009.

[13] B. H. Jo, L. M. Van Lerberghe, K. M. Motsegood, and D. J. Beebe, "Three-dimensional micro-channel fabrication in polydimethylsiloxane (PDMS) elastomer," *Journal of Microelectromechanical Systems,* vol. 9, pp. 76-81, Mar 2000.

[14] S. Jeon, J. Park, R. Cirelli, C. Heitzman, P. Braun, P. Kenis, and J. Rogers, "Fabricating complex three-dimensional nanostructures with high-resolution conformable phase masks," *Proceedings of the National Academy of Sciences of the United States of America,* vol. 101, p. 12428, 2004.

[15] I. Doh and Y.-H. Cho, "A continuous cell separation chip using hydrodynamic dielectrophoresis (DEP) process," *Sensors and Actuators A: Physical,* vol. 121, pp. 59-65, 2005.

[16] N. Flores-Rodriguez and G. H. Markx, "Improved levitation and trapping of particles by negative dielectrophoresis by the addition of amphoteric molecules," *Journal of Physics D-Applied Physics,* vol. 37, pp. 353-361, Feb 7 2004.

[17] M. Minor, H. P. van Leeuwen, and J. Lyklema, "Low-frequency dielectric response of polystyrene latex dispersions," *Journal of Colloid and Interface Science,* vol. 206, pp. 397-406, Oct 15 1998.

[18] H. Z. Zhang, K. Sekine, T. Hanai, and N. Koizumi, "Dielectric Observations on Polystyrene Microcapsules and the Theoretical-Analysis with Reference to Interfacial Polarization," *Colloid and Polymer Science,* vol. 261, pp. 381-389, 1983.

[19] N. E. Good, G. D. Winget, W. Winter, T. N. Connolly, S. Izawa, and R. M. M. Singh, "Hydrogen Ion Buffers for Biological Research," *Biochemistry,* vol. 5, pp. 467-&, 1966.

[20] S. Kostner and M. Vellekoop, "Cell analysis in a microfluidic cytorneter applying a DVD pickup head," *Sensors and Actuators B-Chemical,* vol. 132, pp. 512-517, Jun 16 2008.

[21] E. S. E. Hafez, *Reproduction in farm animals*, 5th ed. Philadelphia: Lea & Febiger, 1987.

[22] MesserWoland. Biological Cell [Online]. Available: http://upload.wikimedia.org/wikipedia/commons/1/1a/Biological_cell.svg

[23] M. R. Villarreal. Cell Membrane [Online]. Available: http://upload.wikimedia.org/wikipedia/commons/d/da/Cell_membrane_detailed_diagram_en.svg

[24] C. K. Haluska, K. A. Riske, V. Marchi-Artzner, J. M. Lehn, R. Lipowsky, and R. Dimova, "Time scales of membrane fusion revealed by direct imaging of vesicle fusion with high temporal resolution," *Proceedings of the National Academy of Sciences of the United States of America,* vol. 103, pp. 15841-15846, Oct 24 2006.

[25] J. Wu, "Interactions of electrical fields with fluids: laboratory-on-a-chip applications," *IET Nanobiotechnology,* vol. 2, pp. 14-27, Mar 2008.

[26] D. A. Glocker and S. I. Shah, *Handbook of thin film process technology*: Bristol : IOP Publishing, 1995-.

[27] R. J. Adamson and K. V. I. S. Kaler, "Multipole effects on the dielectrophoretic force in an 'isomotive' field," *Journal of Biological Physics,* vol. 13, pp. 95-98, 1985.

[28] B. Oback and D. N. Wells, "Cloning Cattle," *Cloning and Stem Cells,* vol. 5, pp. 243-256, 2003.

[29] C. Soanes and A. Stevenson, *Oxford dictionary of English*, 2nd ed. Oxford: Oxford University Press, 2005.

[30] C. Galli, I. Lagutina, and G. Lazzari, "Introduction to cloning by nuclear transplantation," *Cloning and Stem Cells,* vol. 5, pp. 223-232, Win 2003.

[31] G. Vajta and M. Gjerris, "Science and technology of farm animal cloning: State of the art," *Animal Reproduction Science,* vol. 92, pp. 211-230, May 2006.

[32] I. Wilmut, A. E. Schnieke, J. McWhir, A. J. Kind, and K. H. S. Campbell, "Viable offspring derived from fetal and adult mammalian cells," *Nature,* vol. 385, pp. 810-813, Feb 27 1997.

[33] T. Wakayama, A. C. F. Perry, M. Zuccotti, K. R. Johnson, and R. Yanagimachi, "Full-term development of mice from enucleated oocytes injected with cumulus cell nuclei," *Nature,* vol. 394, pp. 369-374, Jul 23 1998.

[34] A. Trounson, O. Lacham-Kaplan, M. Diamente, and T. Gougoulidis, "Reprogramming cattle somatic cells by isolated nuclear injection," *Reproduction Fertility and Development,* vol. 10, pp. 645-650, 1998.

[35] A. Onishi, M. Iwamoto, T. Akita, S. Mikawa, K. Takeda, T. Awata, H. Hanada, and A. C. F. Perry, "Pig cloning by microinjection of fetal fibroblast nuclei," *Science,* vol. 289, pp. 1188-1190, Aug 18 2000.

[36] C. Galli, I. Lagutina, I. Vassiliev, R. Duchi, and G. Lazzari, "Comparison of microinjection (piezo-electric) and cell fusion for nuclear transfer success with different cell types in cattle," *Cloning Stem Cells,* vol. 4, pp. 189-96, 2002.

[37] M. Samiec and M. Skrzyszowska, "Microsurgical nuclear transfer by intraooplasmic karyoplast injection as an alternative embryo reconstruction method in somatic cloning of pigs and other mammal species; application value of the method and its technical advantages - a review," *Czech Journal of Animal Science,* vol. 50, pp. 235-242, Jun 2005.

[38] G. Vajta, "Handmade cloning: the future way of nuclear transfer?," *Trends in Biotechnology,* vol. 25, pp. 250-253, Jun 2007.

[39] G. Vajta, P. Bartels, J. Joubert, M. de la Rey, R. Treadwell, and H. Callesen, "Production of a healthy calf by somatic cell nuclear transfer without micromanipulators and carbon dioxide incubators using the Handmade Cloning (HMC) and the Submarine Incubation System (SIS)," *Theriogenology,* vol. 62, pp. 1465-1472, Nov 2004.

[40] G. Vajta, I. M. Lewis, and R. T. Tecirlioglu, "Handmade somatic cell cloning in cattle," *Methods Mol Biol,* vol. 348, pp. 183-96, 2006.

[41] G. Vajta, P. M. Maddox-Hyttel, C. T. Skou, R. T. Tecirlioglu, T. T. Peura, L. X. Lai, C. N. Murphy, R. S. Prather, P. M. Kragh, and H. Callesen, "Highly efficient and reliable chemically assisted enucleation method for handmade cloning in cattle," *Reproduction Fertility and Development,* vol. 17, pp. 791-797, 2005.

[42] J. Watson, M. Gilman, and Z. M. Witkowski J, *Recombinant DNA*, 1992.

[43] H. Curtis and N. Barnes, *Biology*: Worth Publishers Inc., 1989.

[44] L. E. McDonald and M. H. Pineda, *Veterinary endocrinology and reproduction*, 4th ed. Philadelphia: Lea & Febiger, 1989.

[45] S. Tanghe, A. Van Soom, H. Nauwynck, M. Coryn, and A. De Kruif, "Minireview: Functions of the cumulus oophorus during oocyte maturation, ovulation, and fertilization," *Molecular Reproduction and Development,* vol. 61, pp. 414-424, Mar 2002.

[46] M. Alomar, H. Tasiaux, S. Remacle, F. George, D. Paul, and I. Donnay, "Kinetics of fertilization and development, and sex ratio of bovine embryos produced using the semen of different bulls," *Anim Reprod Sci,* vol. 107, pp. 48-61, Aug 2008.

[47] P. Sutovsky, C. S. Navara, and G. Schatten, "Fate of the sperm mitochondria, and the incorporation, conversion, and disassembly of the sperm tail structures during bovine fertilization," *Biology of Reproduction,* vol. 55, pp. 1195-1205, Dec 1996.

[48] A. J. Hackett, R. Durnford, R. J. Mapletoft, and G. J. Marcus, "Location and Status of Embryos in the Genital-Tract of Superovulated Cows 4 to 6 Days after Insemination," *Theriogenology,* vol. 40, pp. 1147-1153, Dec 1993.

[49] A. Van Soom and A. de Kruif, "Bovine embryonic development after in vivo and in vitro fertilization," *Reproduction in Domestic Animals,* vol. 33, pp. 261-265, Jun 1998.

[50] T. A. McGeady, P. J. Quinn, E. S. Fitzpatrick, and M. T. Ryan, *Veterinary Embryology*: Wiley-Blackwell, 2006.

[51] H. Spemann, *Embryonic development and induction*. New Haven, Conn. ; London: Yale University Press ; H. Milford, Oxford University Press, 1938.

[52] R. Briggs and T. J. King, "Transplantation of Living Nuclei from Blastula Cells into Enucleated Frogs Eggs," *Proceedings of the National Academy of Sciences of the United States of America,* vol. 38, pp. 455-463, 1952.

[53] J. Stewart-savage and R. D. Grey, "The Cell-Cycle Governs the Onset of Spherulation of Xenopus Eggs Fused by an Electric-Field," *Development Growth & Differentiation,* vol. 29, pp. 229-238, Jun 1987.

[54] J. D. Bromhall, "Nuclear Transplantation in Rabbit Egg," *Nature,* vol. 258, pp. 719-722, 1975.

[55] S. M. Willadsen, "Nuclear Transplantation in Sheep Embryos," *Nature,* vol. 320, pp. 63-65, Mar 6 1986.

[56] R. S. Prather, F. L. Barnes, M. M. Sims, J. M. Robl, W. H. Eyestone, and N. L. First, "Nuclear Transplantation in the Bovine Embryo - Assessment of Donor Nuclei and Recipient Oocyte," *Biology of Reproduction,* vol. 37, pp. 859-866, Nov 1987.

[57] K. R. Bondioli, M. E. Westhusin, and C. R. Looney, "Production of identical bovine offspring by nuclear transfer " in *1990 Annual Conf of the International Embryo Transfer Soc*, Denver, Co, 1990, pp. 165-174.

[58] K. H. S. Campbell, P. Fisher, W. C. Chen, I. Choi, R. D. W. Kelly, J. H. Lee, and J. Xhu, "Somatic cell nuclear transfer: Past, present and future perspectives," *Theriogenology,* vol. 68, pp. S214-S231, Sep 1 2007.

[59] K. H. Campbell, R. Alberio, I. Choi, P. Fisher, R. D. Kelly, J. H. Lee, and W. Maalouf, "Cloning: eight years after Dolly," *Reproduction in Domestic Animals,* vol. 40, pp. 256-68, Aug 2005.

[60] H. Tamada and N. Kikyo, "Nuclear reprogramming in mammalian somatic cell nuclear cloning," *Cytogenetic and Genome Research,* vol. 105, pp. 285-291, 2004.

[61] R. Blelloch, Z. D. Wang, A. Meissner, S. Pollard, A. Smith, and R. Jaenisch, "Reprogramming efficiency following somatic cell nuclear transfer is influenced by the differentiation and methylation state of the donor nucleus," *Stem Cells,* vol. 24, pp. 2007-2013, Sep 2006.

[62] K. H. S. Campbell, W. A. Ritchie, and I. Wilmut, "Nuclear-Cytoplasmic Interactions during the 1st Cell-Cycle of Nuclear Transfer Reconstructed Bovine Embryos - Implications for Deoxyribonucleic-Acid Replication and Development," *Biology of Reproduction,* vol. 49, pp. 933-942, Nov 1993.

[63] H. T. Cheong, Y. Takahashi, and H. Kanagawa, "Birth of Mice after Transplantation of Early Cell-Cycle-Stage Embryonic Nuclei into Enucleated Oocytes," *Biology of Reproduction,* vol. 48, pp. 958-963, May 1993.

[64] B. Oback, "Climbing mount efficiency - Small steps, not giant leaps towards higher cloning success in farm animals," *Reproduction in Domestic Animals,* vol. 43, pp. 407-416, Jul 2008.

[65] D. C. Smeaton, B. L. Harris, Z. Z. Xu, and W. H. Vivanco, "Factors affecting commercial application of embryo technologies in New Zealand: a modelling approach," *Theriogenology,* vol. 59, pp. 617-34, Jan 15 2003.

[66] F. Constant, M. Guillomot, Y. Heyman, X. Vignon, P. Laigre, J. L. Servely, J. P. Renard, and P. Chavatte-Palmer, "Large offspring or large placenta syndrome? Morphometric analysis of late gestation bovine placentomes from somatic nuclear transfer pregnancies complicated by hydrallantois," *Biol Reprod,* vol. 75, pp. 122-30, Jul 2006.

[67] K. Kasai, F. Sano, N. Miyashita, S. Watanabe, and T. Nagai, "Comparison of the growth performances of offspring produced by a pair of cloned cattle and their nuclear donor animals," *Journal of Reproduction and Development,* vol. 53, pp. 135-142, Feb 2007.

[68] Y. Heyman, C. Richard, H. Rodriguez-Martinez, G. Lazzari, P. Chavatte-Palmer, X. Vignon, and C. Galli, "Zootechnical performance of cloned cattle and offspring: preliminary results," *Cloning Stem Cells,* vol. 6, pp. 111-20, 2004.

[69] G. Vajta, P. M. Kragh, N. R. Mtango, and H. Callesen, "Hand-made cloning approach: potentials and limitations," *Reprod Fertil Dev,* vol. 17, pp. 97-112, 2005.

[70] J. C. Hay, "Calcium: a fundamental regulator of intracellular membrane fusion?," *Embo Reports,* vol. 8, pp. 236-240, Mar 2007.

[71] G. C. Lan, D. Han, Y. G. Wu, Z. B. Han, S. F. Ma, X. Y. Liu, C. L. Chang, and J. H. Tan, "Effects of duration, concentration, and timing of ionomycin and 6-dimethylaminopurine (6-DMAP) treatment on activation of goat oocytes," *Molecular Reproduction and Development,* vol. 71, pp. 380-8, Jul 2005.

[72] R. M. Moses and Y. Masui, "Enhancement of mouse egg activation by the kinase inhibitor, 6-dimethylaminopurine (6-DMAP)," *Journal of Experimental Zoology,* vol. 270, pp. 211-8, Oct 1 1994.

[73] S. C. Zhang and Y. Masui, "Activation of Xenopus laevis eggs in the absence of intracellular Ca activity by the protein phosphorylation inhibitor, 6-dimethylaminopurine (6-DMAP)," *Journal of Experimental Zoology,* vol. 262, pp. 317-29, Jun 1 1992.

[74] D. N. Wells, G. Laible, F. C. Tucker, A. L. Miller, J. E. Oliver, T. Xiang, J. T. Forsyth, M. C. Berg, K. Cockrem, P. J. L'Huillier, H. R. Tervit, and B. Oback, "Coordination between donor cell type and cell cycle stage improves nuclear cloning efficiency in cattle," *Theriogenology,* vol. 59, pp. 45-59, Jan 1 2003.

[75] D. K. Gardner, M. Lane, A. Spitzer, and P. A. Batt, "Enhanced rates of cleavage and development for sheep zygotes cultured to the blastocyst stage in vitro in the absence of serum and somatic cells: amino acids, vitamins, and culturing embryos in groups stimulate development," *Biol Reprod,* vol. 50, pp. 390-400, Feb 1994.

[76] J. Thompson, C. McNaughton, B. Gasparrini, L. McGowan, and H. Tervit, "Effect of inhibitors and uncouplers of oxidative phosphorylation during compaction and blastulation of bovine embryos cultured in vitro," *Journal of Reproduction and Fertility,* vol. 118, pp. 47-55, January 1, 2000 2000.

[77] D. A. Stringfellow, S. M. Seidel, and International Embryo Transfer Society., *Manual of the International Embryo Transfer Society : a procedural guide and general information for the use of embryo transfer technology, emphasizing sanitary precautions*, 3rd ed. Savory, Ill.: The Society, 1998.

[78] P. W. Farin, J. H. Britt, D. W. Shaw, and B. D. Slenning, "Agreement among evaluators of bovine embryos produced in vivo or in vitro," *Theriogenology,* vol. 44, pp. 339-349, 1995.

[79] T. Elston, H. Wang, and G. Oster, "Energy transduction in ATP synthase," *Nature,* vol. 391, pp. 510-3, Jan 29 1998.

[80] L. Ernster and G. Schatz, "Mitochondria: a historical review," *Journal of Cell Biology,* vol. 91, pp. 227s-255s, Dec 1981.

[81] K. Faxen, G. Gilderson, P. Adelroth, and P. Brzezinski, "A mechanistic principle for proton pumping by cytochrome c oxidase," *Nature,* vol. 437, pp. 286-9, Sep 8 2005.

[82] G. H. Patterson, K. Hirschberg, R. S. Polishchuk, D. Gerlich, R. D. Phair, and J. Lippincott-Schwartz, "Transport through the Golgi apparatus by rapid partitioning within a two-phase membrane system," *Cell,* vol. 133, pp. 1055-1067, Jun 13 2008.

[83] K. J. Palmer, P. Watson, and D. J. Stephens, "The role of microtubules in transport between the endoplasmic reticulum and Golgi apparatus in mammalian cells," *Cell Biology of Inositol Lipids and Phosphates,* pp. 1-13, 2005.

[84] K. Yoda and Y. Noda, "Vesicular transport and the Golgi apparatus in yeast," *Journal of Bioscience and Bioengineering,* vol. 91, pp. 1-11, Jan 2001.

[85] S. Mogelsvang and D. J. Simpson, "Protein folding and transport from the endoplasmic reticulum to the Golgi apparatus in plants," *Journal of Plant Physiology,* vol. 153, pp. 1-15, Aug 1998.

[86] C. Ramos and J. Teissie, "Electrofusion: A biophysical modification of cell membrane and a mechanism in exocytosis," *Biochimie,* vol. 82, pp. 511-518, May 2000.

[87] C. F. Graham, "Heterospecific Genome Interaction," in *Wistar Inst. Symp. Monogr.* vol. 9, ed Philadelphia: The Wistar Institute Press, 1969, pp. 19-35.

[88] N. M. Kane, S. McRae, C. Denning, and A. H. Baker, "Viral and non-viral gene delivery and its role in pluripotent stem cell engineering," *Drug Discovery Today: Technologies,* vol. In Press, Corrected Proof.

[89] U. Zimmermann and G. A. Neil, *Electromanipulation of cells*. Boca Raton, Fla.: CRC Press, 1996.

[90] K. Kinosita, I. Ashikawa, N. Saita, H. Yoshimura, H. Itoh, K. Nagayama, and A. Ikegami, "Electroporation of Cell-Membrane Visualized under a Pulsed-Laser Fluorescence Microscope," *Biophysical Journal,* vol. 53, pp. 1015-1019, Jun 1988.

[91] D. C. Chang and T. S. Reese, "Changes in Membrane-Structure Induced by Electroporation as Revealed by Rapid-Freezing Electron-Microscopy," *Biophysical Journal,* vol. 58, pp. 1-12, Jul 1990.

[92] K. Matsumoto, A. D. Vilarinhos, and S. Oka, "Somatic hybridization by electrofusion of banana protoplasts," *Euphytica,* vol. 125, pp. 317-324, 2002.

[93] J. T. Ling and M. Iwamasa, "Somatic Hybridization between Citrus-Reticulata and Citropsis-Gabunensis through Electrofusion," *Plant Cell Reports,* vol. 13, pp. 493-497, Jun 1994.

[94] I. Serraf, D. Sihachakr, G. Ducreux, S. C. Brown, M. Allot, N. Barghi, and L. Rossignol, "Interspecific Somatic Hybridization in Potato by Protoplast Electrofusion," *Plant Science,* vol. 76, pp. 115-126, 1991.

[95] M. H. Gallardo, C. A. Gonzalez, and I. Cebrian, "Molecular cytogenetics and allotetraploidy in the red vizcacha rat, Tympanoctomys barrerae (Rodentia, Octodontidae)," *Genomics,* vol. 88, pp. 214-221, Aug 2006.

[96] H. A. Pohl, *Dielectrophoresis : the behavior of neutral matter in nonuniform electric fields*. Cambridge ; New York: Cambridge University Press, 1978.

[97] I. V. Timoshkin, S. J. MacGregor, R. A. Fouracre, B. H. Crichton, and J. G. Anderson, "Transient electrical field across cellular membranes: pulsed electric field treatment of microbial cells," *Journal of Physics D-Applied Physics,* vol. 39, pp. 596-603, Feb 7 2006.

[98] M. Washizu and B. Techaumnat, "Cell membrane voltage during electrical cell fusion calculated by re-expansion method," *Journal of Electrostatics,* vol. 65, pp. 555-561, Aug 2007.

[99] H. Pauly and H. P. Schwan, "Dielectric Properties and Ion Mobility in Erythrocytes," *Biophysical Journal,* vol. 6, pp. 621-&, 1966.

[100] U. Zimmermann, W. M. Arnold, and W. Mehrle, "Biophysics of Electroinjection and Electrofusion," *Journal of Electrostatics,* vol. 21, pp. 309-345, Sep 1988.

[101] C. Grosse and H. P. Schwan, "Cellular membrane potentials induced by alternating fields," *Biophysical Journal,* vol. 63, p. 1632, 1992.

[102] B. Gabriel and J. Teissie, "Time courses of mammalian cell electropermeabilization observed by millisecond imaging of membrane property changes during the pulse," *Biophysical Journal,* vol. 76, pp. 2158-65, Apr 1999.

[103] A. R. Von Hippel, *Dielectrics and waves*. Boston: Artech House, 1995.

[104] T. B. Jones, "Basic theory of dielectrophoresis and electrorotation," *IEEE Engineering in Medicine and Biology Magazine,* vol. 22, pp. 33-42, Nov-Dec 2003.

[105] R. Pethig, *Dielectric and electronic properties of biological materials*. Chichester [England] ; New York: Wiley, 1979.

[106] L. H. Allen and Matijevi.E, "Stability of Colloidal Silica .2. Ion Exchange," *Journal of Colloid and Interface Science,* vol. 33, pp. 420-&, 1970.

[107] J. Gimsa, "A comprehensive approach to electro-orientation, electrodeformation, dielectrophoresis, and electrorotation of ellipsoidal particles and biological cells," *Bioelectrochemistry,* vol. 54, pp. 23-31, Aug 2001.

[108] J. Gimsa and D. Wachner, "A polarization model overcoming the geometric restrictions of the laplace solution for spheroidal cells: Obtaining new equations for field-induced forces and transmembrane potential," *Biophysical Journal,* vol. 77, pp. 1316-1326, Sep 1999.

[109] M. Washizu, T. Nanba, and S. Masuda, "Handling Biological Cells Using a Fluid Integrated Circuit," *IEEE Transactions on Industry Applications,* vol. 26, pp. 352-358, March/April 1990.

[110] J. Yang, Y. Huang, X. B. Wang, F. F. Becker, and P. R. C. Gascoyne, "Differential analysis of human leukocytes by dielectrophoretic field-flow-fractionation," *Biophysical Journal,* vol. 78, pp. 2680-2689, May 2000.

[111] G. H. Markx and R. Pethig, "Dielectrophoretic Separation of Cells - Continuous Separation," *Biotechnology and Bioengineering,* vol. 45, pp. 337-343, Feb 20 1995.

[112] W. M. Arnold and N. R. Franich, "Cell isolation and growth in electric-field defined micro-wells," *Current Applied Physics,* vol. 6, pp. 371-374, Jun 2006.

[113] R. Pethig, A. Menachery, E. Heart, R. H. Sanger, and P. J. Smith, "Dielectrophoretic assembly of insulinoma cells and fluorescent nanosensors into three-dimensional pseudo-islet constructs," *Iet Nanobiotechnology,* vol. 2, p. 31, Jun 2008.

[114] P. Moon, V. Chikarmane, K. Fischer, R. Grover, T. Ibrahim, D. Ingerly, K. Lee, C. Litteken, T. Mule, and S. Williams, "Process and Electrical Results for the On-die Interconnect Stack for Intel's 45nm Process Generation," *Intel Technology Journal,* vol. 12, pp. 87-92, 2008.

[115] S. Natarajan, M. Armstrong, M. Bost, R. Brain, M. Brazier, C. H. Chang, V. Chikarmane, M. Childs, H. Deshpande, K. Dev, G. Ding, T. Ghani, O. Golonzka, W. Han, J. He, R. Heussner, R. James, I. Jin, C. Kenyon, S. Klopcic, S. H. Lee, M. Liu, S. Lodha, B. McFadden, A. Murthy, L. Neiberg, J. Neirynck, P. Packan, S. Pae, C. Parker, C. Pelto, L. Pipes, J. Sebastian, J. Seiple, B. Sell, S. Sivakumar, B. Song, K. Tone, T. Troeger, C. Weber, M. Yang, A. Yeoh, and K. Zhang, "A 32nm Logic Technology Featuring 2(nd)-Generation High-k plus Metal-Gate Transistors, Enhanced Channel Strain and 0.171 mu m(2) SRAM Cell Size in a 291Mb Array," *IEEE International Electron Devices Meeting 2008, Technical Digest,* pp. 941-943,949, 2008.

[116] E. W. Becker, W. Ehrfeld, D. Munchmeyer, H. Betz, A. Heuberger, S. Pongratz, W. Glashauser, H. J. Michel, and R. Vonsiemens, "Production of Separation-Nozzle Systems for Uranium Enrichment by a Combination of X-Ray-Lithography and Galvanoplastics," *Naturwissenschaften,* vol. 69, pp. 520-523, 1982.

[117] C. K. Malek and V. Saile, "Applications of LIGA technology to precision manufacturing of high-aspect-ratio micro-components and -systems: a review," *Microelectronics Journal,* vol. 35, pp. 131-143, Feb 2004.

[118] T. Kawai, K. Sawada, and Y. Takeuchi, "Ultra-precision micro structuring by means of mechanical machining," *14th IEEE International Conference on Micro Electro Mechanical Systems, Technical Digest,* pp. 22-25, 610, 2001.

[119] Z. N. Lu and T. Yoneyama, "Micro cutting in the micro lathe turning system," *International Journal of Machine Tools & Manufacture,* vol. 39, pp. 1171-1183, Jul 1999.

[120] H. S. Liu, B. H. Yan, C. L. Chen, and F. Y. Huang, "Application of micro-EDM combined with high-frequency dither grinding to micro-hole machining," *International Journal of Machine Tools & Manufacture,* vol. 46, pp. 80-87, Jan 2006.

[121] M. Gower, "Laser microfabrication in industry - perspectives from the past, present and future - art. no. 687902," *Photon Processing in Microelectronics and Photonics Vii,* vol. 6879, pp. 87902-87902, 218, 2008.

[122] H. Exner, M. Horn, A. Streek, P. Regenfuss, F. Ullmann, and R. Ebert, "Laser Micro Sintering - A new method to generate metal and ceramic parts of high resolution with sub-micrometer powder," *Virtual and Rapid Manufacturing,* pp. 491-499, 849, 2008.

[123] L. Liu, N. H. Loh, B. Y. Tay, S. B. Tor, Y. Murakoshi, and R. Maeda, "Micro powder injection molding: Sintering kinetics of microstructured components," *Scripta Materialia,* vol. 55, pp. 1103-1106, Dec 2006.

[124] P. Regenfuss, A. Streek, L. Hartwig, S. Klotzer, T. Brabant, M. Horn, R. Ebert, and H. Exner, "Principles of laser micro sintering," *Rapid Prototyping Journal,* vol. 13, pp. 204-212, 2007.

[125] S. Franssila, *Introduction to microfabrication*. Chichester, West Sussex, England ; Hoboken, NJ: John Wiley & Sons, 2004.

[126] C. M. Chan, T. M. Ko, and H. Hiraoka, "Polymer surface modification by plasmas and photons," *Surface Science Reports,* vol. 24, pp. 3-54, 1996.

[127] A. Reiser, J. P. Huang, X. He, T. F. Yeh, S. Jha, H. Y. Shih, M. S. Kim, Y. K. Han, and K. Yan, "The molecular mechanism of novolak-diazonaphthoquinone resists," *European Polymer Journal,* vol. 38, pp. 619-629, 2002.

[128] L. J. Guerin. (2007, 2010). *The SU8 Homepage*. Available: http://www.geocities.com/guerinlj/

[129] G. M. Whitesides, E. Ostuni, S. Takayama, X. Jiang, and D. E. Ingber, "Soft lithography in biology and biochemistry," *Annu Rev Biomed Eng,* vol. 3, pp. 335-73, 2001.

[130] D. J. Laser and J. G. Santiago, "A review of micropumps," *Journal of Micromechanics and Microengineering,* vol. 14, pp. R35-R64, Jun 2004.

[131] M. Radisic, R. K. Iyer, and S. K. Murthy, "Micro- and nanotechnology in cell separation," *Int J Nanomedicine,* vol. 1, pp. 3-14, 2006.

[132] A. Thiel, A. Scheffold, and A. Radbruch, "Immunomagnetic cell sorting--pushing the limits," *Immunotechnology,* vol. 4, pp. 89-96, 1998.

[133] H. C. Zeringue, D. J. Beebe, and M. B. Wheeler, "Removal of Cumulus from Mammalian Zygotes using Microfluidic Techniques," *Biomedical Microdevices,* vol. 3, pp. 219-224, 2001.

[134] J. Edenfeld, B. Schopper, R. Sturm, K. Diedrich, and S. Al-Hasani, "Application of a 1.48-mu m diode laser for bisecting oocytes into two identical hemizonae for the hemizona assay," *International Journal of Andrology,* vol. 25, pp. 100-105, Apr 2002.

[135] T. Nakayama, H. Fujiwara, K. Tastumi, K. Fujita, T. Higuchi, and T. Mori, "A new assisted hatching technique using a piezo-micromanipulator," *Fertility and Sterility,* vol. 69, pp. 784-788, Apr 1998.

[136] K. Hiraoka, M. Fuchiwaki, K. Hiraoka, T. Horiuchi, T. Murakami, M. Kinutani, and K. Kinutani, "Effect of the size of zona pellucida opening by laser assisted hatching on clinical outcome of frozen cleaved embryos that were cultured to blastocyst after thawing in women with multiple implantation failures of embryo transfer: a retrospective study," *Journal of Assisted Reproduction and Genetics,* vol. 25, pp. 129-135, Apr 2008.

[137] K. Hiraoka, M. Fuchiwaki, T. Horiuchi, T. Murakami, M. Kinutani, and K. Kinutani, "Zona pellucida removal and vitrified blastocyst transfer outcome: a preliminary study," *Reprod Biomed Online,* vol. 15, pp. 68-75, Jul 2007.

[138] J. F. Li, R. Y. Fei, D. Z. Liu, G. Z. Wu, C. L. Guan, and X. Y. Yang, "Design and initial experiments of a micro vibration based micromanipulator," *IEEE ICMA 2006: Proceeding of the 2006 IEEE International Conference on Mechatronics and Automation, Vols 1-3, Proceedings,* pp. 130-135, 2006.

[139] G. P. Li, K. L. White, and T. D. Bunch, "Review of enucleation methods and procedures used in animal cloning: State of the art," *Cloning and Stem Cells,* vol. 6, pp. 5-13, Spr 2004.

[140] T. T. Peura and G. Vajta, "A comparison of established and new approaches in ovine and bovine nuclear transfer," *Cloning and Stem Cells,* vol. 5, pp. 257-277, Win 2003.

[141] V. Zakhartchenko, M. Stojkovic, G. Brem, and E. Wolf, "Karyoplast-cytoplast volume ratio in bovine nuclear transfer embryos: Effect on developmental potential," *Molecular Reproduction and Development,* vol. 48, pp. 332-338, Nov 1997.

[142] G. P. Malenko, O. I. Stepanov, A. V. Komissarov, T. A. Antipova, M. V. Pinyugina, and M. I. Prokofiev, "Efficiency of asynchronously in vitro-matured oocytes as recipients for nuclear transfer and of blind enucleation in zona-free bovine cloning," *Cloning Stem Cells,* vol. 11, pp. 287-92, Jun 2009.

[143] D. Y. Chen, M. X. Jiang, Z. J. Zhao, H. L. Wang, Q. Y. Sun, L. S. Zhang, R. C. Li, H. H. Cao, Q. J. Zhang, and D. L. Ma, "Cloning of Asian yellow goat (C-hircus) by somatic cell nuclear transfer: Telophase enucleation combined with whole cell intracytoplasmic injection," *Molecular Reproduction and Development,* vol. 74, pp. 28-34, Jan 2007.

[144] V. Bordignon and L. C. Smith, "Telophase enucleation: An improved method to prepare recipient cytoplasts for use in bovine nuclear transfer," *Molecular Reproduction and Development,* vol. 49, pp. 29-36, Jan 1998.

[145] J. L. Liu, M. K. Wang, Q. Y. Sun, Z. Xu, and D. Y. Chen, "Effect of telophase enucleation on bovine somatic nuclear transfer," *Theriogenology,* vol. 54, pp. 989-998, Oct 1 2000.

[146] B. G. Tatham, A. T. Dowsing, and A. O. Trounson, "Enucleation by centrifugation of in vitro-matured bovine oocytes for use in nuclear transfer," *Biol Reprod,* vol. 53, pp. 1088-94, Nov 1995.

[147] B. G. Tatham, A. H. Sathananthan, V. Dharmawardena, D. Y. Munesinghe, I. Lewis, and A. O. Trounson, "Centrifugation of bovine oocytes for nuclear micromanipulation and sperm microinjection," *Human Reproduction,* vol. 11, pp. 1499-503, Jul 1996.

[148] N. Z. Saraiva, F. Perecin, S. C. Meo, C. R. Ferreira, T. A. Tetzner, and J. M. Garcia, "Demecolcine effects on microtubule kinetics and on chemically assisted enucleation of bovine oocytes," *Cloning Stem Cells,* vol. 11, pp. 141-52, Mar 2009.

[149] J. Bradshaw, T. Jung, J. Fulka, and R. M. Moor, "Uv Irradiation of Chromosomal DNA and Its Effect Upon Mpf and Meiosis in Mammalian Oocytes," *Molecular Reproduction and Development,* vol. 41, pp. 503-512, Aug 1995.

[150] L. Liu, R. Oldenbourg, J. R. Trimarchi, and D. Keefe, "A reliable, noninvasive technique for spindle imaging and enucleation of mammalian oocytes," *Nat Biotechnol* vol. 18, pp. 223-225, 2000.

[151] N. Tomita, J. Higaki, T. Ogihara, T. Kondo, and Y. Kaneda, "A novel gene-transfer technique mediated by HVJ (Sendai virus), nuclear protein, and liposomes," *Cancer Detect Prev,* vol. 18, pp. 485-91, 1994.

[152] K. Chun, G. Hashiguchi, H. Toshiyoshi, and H. Fujita, "Fabrication of array of hollow microcapillaries used for injection of genetic materials into animal/plant cells," *Japanese Journal of Applied Physics Part 2-Letters,* vol. 38, pp. L279-L281, Mar 1 1999.

[153] Y. Kimura and R. Yanagimachi, "Intracytoplasmic Sperm Injection in the Mouse," *Biology of Reproduction,* vol. 52, pp. 709-720, Apr 1995.

[154] B. R. Lentz and J. K. Lee, "Poly(ethylene glycol) (PEG)-mediated fusion between pure lipid bilayers: a mechanism in common with viral fusion and secretory vesicle release? (Review)," *Molecular Membrane Biology,* vol. 16, pp. 279-296, Oct-Dec 1999.

[155] R. Golestani, A. A. Pourfathollah, and S. M. Moazzeni, "Cephalin as an efficient fusogen in hybridoma technology: can it replace poly ethylene glycol?," *Hybridoma (Larchmt),* vol. 26, pp. 296-301, Oct 2007.

[156] A. D. Irvin, E. R. Young, P. D. Luther, and A. P. Collins, "Interspecific fusion of bovine and other cells with parainfluenza viruses (Sendai and Pi-3)," *J Comp Pathol,* vol. 87, pp. 393-404, Jul 1977.

[157] P. Primakoff and D. G. Myles, "Cell-cell membrane fusion during mammalian fertilization," *Febs Letters,* vol. 581, pp. 2174-80, May 22 2007.

[158] M. A. Zhukovsky, E. Leikina, I. Markovic, A. L. Bailey, and L. V. Chernomordik, "Heterogeneity of early intermediates in cell-liposome fusion mediated by influenza hemagglutinin," *Biophysical Journal,* vol. 91, pp. 3349-3358, Nov 2006.

[159] R. Wiegand, G. Weber, K. Zimmermann, S. Monajembashi, J. Wolfrum, and K. O. Greulich, "Laser-induced fusion of mammalian cells and plant protoplasts," *Journal of Cell Science,* vol. 88 (Pt 2), pp. 145-9, Sep 1987.

[160] A. Clow, P. Gaynor, and B. Oback, "Coplanar film electrodes facilitate bovine nuclear transfer cloning," *Biomed Microdevices,* vol. 11, pp. 851-9, Aug 2009.

[161] D. N. Wells, P. M. Misica, and H. R. Tervit, "Production of cloned calves following nuclear transfer with cultured adult mural granulosa cells," *Biology of Reproduction,* vol. 60, pp. 996-1005, Apr 1999.

[162] P. Gaynor, D. N. Wells, and B. Oback, "Couplet alignment and improved electrofusion by dielectrophoresis for a zona-free high-throughput cloned embryo production system," *Medical & Biological Engineering & Computing,* vol. 43, pp. 150-154, Jan 2005.

[163] F. J. Liu, Y. Zhang, Y. M. Zheng, M. T. Zhao, Y. L. Zhang, Y. S. Wang, G. H. Wang, F. S. Quan, and Z. X. An, "Optimization of electrofusion protocols for somatic cell nuclear transfer," *Small Ruminant Research,* vol. 73, pp. 246-251, Nov 2007.

[164] J. Schaper, H. R. Bohnenkamp, and T. Noll, "New electrofusion devices for the improved generation of dendritic cell-tumour cell hybrids," *Cell Technology for Cell Products,* pp. 207-216, 821, 2007.

[165] A. M. Skelley, O. Kirak, H. Suh, R. Jaenisch, and J. Voldman, "Microfluidic control of cell pairing and fusion," *Nature Methods,* vol. 6, pp. 147-152, Feb 2009.

[166] M. P. Milazzotto, W. B. Feitosa, A. R. Coutinho, M. D. Goissis, V. P. Oliveira, M. E. Assumpcao, and J. A. Visintin, "Effect of chemical or electrical activation of bovine oocytes on blastocyst development and quality," *Reproduction in Domestic Animals,* vol. 43, pp. 319-22, Jun 2008.

[167] G. Vajta, T. T. Peura, P. Holm, K. Paldi, T. Greve, A. O. Trounson, and H. Callesen, "New method for culture of zona-included or zona-free embryos: The Well of the Well (WOW) system," *Molecular Reproduction and Development,* vol. 55, pp. 256-264, Mar 2000.

[168] W. M. Arnold, R. K. Schmutzler, A. G. Schmutzler, H. van der Ven, S. Al-Hasani, D. Krebs, and U. Zimmermann, "Electro-rotation of mouse oocytes: single-cell measurements of zona-intact and zona-free cells and of the isolated zona pellucida," *Biochim Biophys Acta,* vol. 905, pp. 454-64, Dec 11 1987.

[169] K. Chatzimeletiou, E. E. Morrison, N. Prapas, Y. Prapas, and A. H. Handyside, "Spindle abnormalities in normally developing and arrested human preimplantation embryos in vitro identified by confocal laser scanning microscopy (vol 20, pg 672, 2005)," *Human Reproduction,* vol. 20, pp. 1120-1120, Apr 2005.

[170] R. Zeggari, B. Wacogne, C. Pieralli, C. Roux, and T. Gharbi, "A full micro-fluidic system for single oocyte manipulation including an optical sensor for cell maturity estimation and fertilisation indication," *Sensors and Actuators B-Chemical,* vol. 125, pp. 664-671, Aug 8 2007.

[171] U. Zimmermann, P. Gessner, R. Schnettler, S. Perkins, and S. K. Foung, "Efficient hybridization of mouse-human cell lines by means of hypo-osmolar electrofusion," *J Immunol Methods,* vol. 134, pp. 43-50, Nov 6 1990.

[172] H. Q. He, D. C. Chang, and Y. K. Lee, "Using a micro electroporation chip to determine the optimal physical parameters in the uptake of biomolecules in HeLa cells," *Bioelectrochemistry,* vol. 70, pp. 363-368, May 2007.

[173] G. Tresset and S. Takeuchi, "A Microfluidic Device for Electrofusion of Biological Vesicles," *Biomedical Microdevices,* vol. 6, pp. 213-218, 2004.

[174] D. Marcuse, "Electrostatic-Field of Coplanar Lines Computed with the Point Matching Method," *IEEE Journal of Quantum Electronics,* vol. 25, pp. 939-947, May 1989.

[175] E. Neumann, A. E. Sowers, and C. A. Jordan, *Electroporation and electrofusion in cell biology*. New York: Plenum Press, 1989.

[176] M. Washizu and T. B. Jones, "Dielectrophoretic interaction of two spherical particles calculated by equivalent multipole-moment method," *IEEE Transactions on Industry Applications,* vol. 32, pp. 233-242, Mar-Apr 1996.

[177] M. A. van Dijk and J. G. J. van de Winkel, "Human antibodies as next generation therapeutics," *Current Opinion in Chemical Biology,* vol. 5, pp. 368-374, 2001.

[178] V. L. Sukhorukov, R. Reuss, J. M. Endter, S. Fehrmann, A. Katsen-Globa, P. Gessner, A. Steinbach, K. J. Muller, A. Karpas, U. Zimmermann, and H. Zimmermann, "A biophysical approach to the optimisation of dendritic-tumour cell electrofusion," *Biochem Biophys Res Commun,* vol. 346, pp. 829-39, Aug 4 2006.

[179] K. Kovacs, C. Catana, and D. Pamfil, "Somatic hybridization on potato," *Bulletin of the University of Agricultural Sciences and Veterinary Medicine, Vol 59,* vol. 59, pp. 279-283, 312, 2003.

[180] S. Masuda, M. Washizu, and T. Nanba, "Novel Method of Cell-Fusion in Field Constriction Area in Fluid Integrated-Circuit," *IEEE Transactions on Industry Applications,* vol. 25, pp. 732-737, Jul-Aug 1989.

[181] B. Techaumnat, K. Tsuda, O. Kurosawa, G. Murat, and M. Washizu, "High-yield electrofusion of cells using electric-field constriction," *2007 International Symposium on Micro-Nano Mechatronics and Human Science, Vols 1 and 2,* pp. 38-43, 619, 2007.

[182] B. Techaumnat, K. Tsuda, O. Kurosawa, G. Murat, H. Oana, and M. Washizu, "High-yield electrofusion of biological cells based on field tailoring by microfabricated structures," *Nanobiotechnology, IET,* vol. 2, pp. 93-99, 2008.

[183] T. Suzuki, H. Yamamoto, M. Ohoka, A. Okonogi, H. Kabata, I. Kanno, M. Washizu, and H. Kotera, "High throughput cell electroporation array fabricated by single-mask inclined UV lithography exposure and oxygen plasma etching," *Transducers '07 & Eurosensors Xxi, Digest of Technical Papers, Vols 1 and 2,* pp. U348-U349, 2616, 2007.

[184] M. Nordstrom, A. Johansson, E. S. Nogueron, B. Clausen, M. Calleja, and A. Boisen, "Investigation of the bond strength between the photo-sensitive polymer SU-8 and gold," *Microelectronic Engineering,* vol. 78-79, pp. 152-157, Mar 2005.

[185] X. G. Tang, X. Y. Yang, F. H. Gao, and Y. K. Guo, "Simulation and analysis for microstructure profile of optical lithography based on SU-8 thick resist," *Microelectronic Engineering,* vol. 84, pp. 1100-1103, May-Aug 2007.

[186] W. W. Flack, H. A. Nguyen, J. Buchanan, E. Capsuto, and A. Marks, "Contrast enhancement materials for thick photoresist applications," *Advances in Resist Technology and Processing Xxi, Pts 1 and 2,* vol. 5376, pp. 1190-1205, 1288, 2004.

[187] A. Bubendorfer, X. M. Liu, and A. V. Ellis, "Microfabrication of PDMS microchannels using SU-8/PMMA moldings and their sealing to polystyrene substrates," *Smart Materials & Structures,* vol. 16, pp. 367-371, Apr 2007.

[188] R. Dammel, *Diazonaphthoquinone-based resists*. Bellingham, Wash., USA: SPIE Optical Engineering Press, 1993.

[189] C. Molpeceres, S. Lauzurica, J. J. Garcia-Ballesteros, M. Morales, and J. L. Ocana, "Advanced 3D micromachining techniques using UV laser sources," *Microelectronic Engineering,* vol. 84, pp. 1337-1340, May-Aug 2007.

[190] D. Ilie, C. Mullan, G. M. O'Connor, T. Flaherty, and T. J. Glynn, "Controlled process for polymer micromachining using designed pulse trains of a UV solid state laser," *Applied Surface Science,* vol. 254, pp. 845-849, Dec 15 2007.

[191] M. J. Lopez-Martinez, E. M. Campo, D. Caballero, E. Fernandez, A. Errachid, J. Esteve, and J. A. Plaza, "Versatile micropipette technology based on deep reactive ion etching and anodic bonding for biological applications," *Journal of Micromechanics and Microengineering,* vol. 19, pp. -, Oct 2009.

[192] P. Waurzyniak, "Rapid manufacturing," *Manufacturing Engineering,* vol. 138, pp. 89-+, Feb 2007.

[193] M. J. Jensen, G. Goranovic, and H. Bruus, "The clogging pressure of bubbles in hydrophilic microchannel contractions," *Journal of Micromechanics and Microengineering,* vol. 14, pp. 876-883, Jul 2004.

[194] H. Okada, T. Kaneuchi, H. Takagi, and O. Ohashi, "Effect of Glass Materials on Joints in Anodic Bonding of Glass to Silicon," *Journal of the Japan Institute of Metals,* vol. 73, pp. 110-115, Feb 2009.

[195] U. Aljancic, D. Resnik, D. Vrtacnik, M. Mozek, and S. Amon, "Silicon-glass anodic bonding," *Informacije Midem-Journal of Microelectronics Electronic Components and Materials,* vol. 34, pp. 168-173, Sep 2004.

[196] W. W. Y. Chow, K. F. Lei, G. Y. Shi, W. J. Li, and Q. Huang, "Microfluidic channel fabrication by PDMS-interface bonding," *Smart Materials & Structures,* vol. 15, pp. S112-S116, Feb 2006.

[197] C. Gonzalez, S. D. Collins, and R. L. Smith, "Fluidic interconnects for modular assembly of chemical microsystems," *Sensors and Actuators B-Chemical,* vol. 49, pp. 40-45, Jun 25 1998.

[198] C. Gonzalez, S. D. Collins, and R. L. Smith, "Fluidic interconnects for modular assembly of chemical microsystems," *Transducers 97 - 1997 International Conference on Solid-State Sensors and Actuators, Digest of Technical Papers, Vols 1 and 2,* pp. 527-530, 1525, 1997.

[199] K. Haubert, T. Drier, and D. Beebe, "PDMS bonding by means of a portable, low-cost corona system," *Lab on a Chip,* vol. 6, pp. 1548-1549, Dec 2006.

[200] M. A. Eddings, M. A. Johnson, and B. K. Gale, "Determining the optimal PDMS-PDMS bonding technique for microfluidic devices," *Journal of Micromechanics and Microengineering,* vol. 18, pp. -, Jun 2008.

[201] L. Cui and H. Morgan, "Design and fabrication of travelling wave dielectrophoresis structures," *Journal of Micromechanics and Microengineering,* vol. 10, pp. 72-79, Mar 2000.

[202] J. Muys, M. M. Alkaisi, J. J. Evans, and J. Nagase, "Biochip: Cellular analysis by atomic force microscopy using dielectrophoretic manipulation," *Japanese Journal of Applied Physics Part 1-Regular Papers Brief Communications & Review Papers,* vol. 44, pp. 5717-5723, Jul 2005.

[203] M. M. Alkaisi, J. J. Muys, and J. J. Evans, "Bioimprint replication of single cells on a Biochip," *Biomems and Nanotechnology Iii,* vol. 6799, pp. U212-U221, 210, 2008.

[204] G. W. Bates, J. J. Gaynor, and N. S. Shekhawat, "Fusion of Plant Protoplasts by Electric Fields," *Plant Physiol,* vol. 72, pp. 1110-1113, Aug 1983.

[205] B. Oback, A. T. Wiersema, P. Gaynor, G. Laible, F. C. Tucker, J. E. Oliver, A. L. Miller, H. E. Troskie, K. L. Wilson, J. T. Forsyth, M. C. Berg, K. Cockrem, V. Mcmillan, H. R. Tervit, and D. N. Wells, "Cloned cattle derived from a novel zona-free embryo reconstruction system," *Cloning and Stem Cells,* vol. 5, pp. 3-12, 2003.

[206] G. Vajta, I. M. Lewis, A. O. Trounson, S. Purup, P. Maddox-Hyttel, M. Schmidt, H. G. Pedersen, T. Greve, and H. Callesen, "Handmade Somatic Cell Cloning in Cattle: Analysis of Factors Contributing to High Efficiency In Vitro," *Biology of Reproduction,* vol. 68, pp. 571-578, February 2003 2003.

[207] Y. Kimura, M. Gel, B. Techaumnut, K. Tsuda, H. Oana, H. Kotera, T. Tada, and M. Washizu, "High-yield parallel electro-fusion device based on field constriction at an orifice array," *Proc. 12th Int. Conf. on Miniat. Syst. for Chem. and Life Sci. (MicroTAS),* pp. 540-542, October 12 - 16, 2008, San Diego, California, USA 2008.

[208] B. Winsor and E. Schiebel, "Review: An overview of the Saccharomyces cerevisiae microtubule and microfilament cytoskeleton," *Yeast,* vol. 13, pp. 399-434, Apr 1997.

[209] W. Margolin, "Bacterial cytoskeleton: Not your run-of-the-mill tubulin," *Current Biology,* vol. 17, pp. R633-R636, Aug 21 2007.

[210] H. M. Shapiro, *Practical flow cytometry*, 3rd ed. New York: Wiley-Liss, 1995.

[211] I. K. Glasgow, H. C. Zeringue, D. J. Beebe, S. J. Choi, J. T. Lyman, N. G. Chan, and M. B. Wheeler, "Handling individual mammalian embryos using microfluidics," *IEEE Trans Biomed Eng,* vol. 48, pp. 570-8, May 2001.

[212] B. Techaumnat and M. Washizu, "Analysis of the effects of an orifice plate on the membrane potential in electroporation and electrofusion of cells," *Journal of Physics D-Applied Physics,* vol. 40, pp. 1831-1837, Mar 21 2007.

[213] M. Lian, N. Islam, and J. Wu, "AC electrothermal manipulation of conductive fluids and particles for lab-chip applications," *IET Nanobiotechnology,* vol. 1, pp. 36-43, Jun 2007.

[214] D. S. Gray, J. L. Tan, J. Voldman, and C. S. Chen, "Dielectrophoretic registration of living cells to a microelectrode array (vol 19, pg 1765, 2004)," *Biosensors & Bioelectronics,* vol. 19, pp. 1765-1774, Jul 15 2004.

[215] R. Hagedorn, G. Fuhr, T. Muller, and J. Gimsa, "Traveling-Wave Dielectrophoresis of Microparticles," *Electrophoresis,* vol. 13, pp. 49-54, Jan-Feb 1992.

[216] X. B. Wang, M. P. Hughes, Y. Huang, F. F. Becker, and P. R. Gascoyne, "Non-uniform spatial distributions of both the magnitude and phase of AC electric fields determine dielectrophoretic forces," *Biochim Biophys Acta,* vol. 1243, pp. 185-94, Feb 23 1995.

[217] X. J. Wang, X. B. Wang, F. F. Becker, and P. R. C. Gascoyne, "A theoretical method of electrical field analysis for dielectrophoretic electrode arrays using Green's theorem," *Journal of Physics D-Applied Physics,* vol. 29, pp. 1649-1660, Jun 14 1996.

[218] H. Morgan, A. G. Izquierdo, D. Bakewell, N. G. Green, and A. Ramos, "The dielectrophoretic and travelling wave forces generated by interdigitated electrode arrays: analytical solution using Fourier series (vol 34, pg 1553, 2001)," *Journal of Physics D-Applied Physics,* vol. 34, pp. 2708-2708, Sep 7 2001.

[219] A. Ramos, A. Gonzalez, P. Garcia-Sanchez, and A. Castellanos, "A linear analysis of the effect of Faradaic currents on traveling-wave electroosmosis," *Journal of Colloid and Interface Science,* vol. 309, pp. 323-331, May 15 2007.

[220] N. G. Green, A. Ramos, and H. Morgan, "Numerical solution of the dielectrophoretic and travelling wave forces for interdigitated electrode arrays using the finite element method," *Journal of Electrostatics,* vol. 56, pp. 235-254, Sep 26 2002.

[221] W. M. Arnold, "Positioning and levitation media for the separation of biological cells," *IEEE Transactions on Industry Applications,* vol. 37, pp. 1468-1475, Sep-Oct 2001.

[222] T. Muller, W. M. Arnold, T. Schnelle, R. Hagedorn, G. Fuhr, and U. Zimmermann, "A Traveling-Wave Micropump for Aqueous-Solutions - Comparison of 1-G and Mu-G Results," *Electrophoresis,* vol. 14, pp. 764-772, Aug 1993.

[223] J. Gimsa, P. Eppmann, and B. Pruger, "Introducing phase analysis light scattering for dielectric characterization: Measurement of traveling-wave pumping," *Biophysical Journal,* vol. 73, pp. 3309-3316, Dec 1997.

[224] M. G. Pollack, R. B. Fair, and A. D. Shenderov, "Electrowetting-based actuation of liquid droplets for microfluidic applications," *Applied Physics Letters,* vol. 77, pp. 1725-1726, Sep 11 2000.

[225] N. Ichikawa, K. Hosokawa, and R. Maeda, "Interface motion of capillary-driven flow in rectangular microchannel," *Journal of Colloid and Interface Science,* vol. 280, pp. 155-164, Dec 1 2004.

[226] S. W. Walker and B. Shapiro, "Modeling the fluid dynamics of electrowetting on dielectric (EWOD)," *Journal of Microelectromechanical Systems,* vol. 15, pp. 986-1000, Aug 2006.

[227] S. Z. Qian, S. W. Joo, Y. T. Jiang, and M. A. Cheney, "Free-surface problems in electrokinetic micro- and nanofluidics," *Mechanics Research Communications,* vol. 36, pp. 82-91, Jan 2009.

[228] T. Ondarcuhu and A. Piednoir, "Pinning of a contact line on nanometric steps during the dewetting of a terraced substrate," *Nano Letters,* vol. 5, pp. 1744-1750, Sep 2005.

[229] S. Herminghaus, M. Brinkmann, and R. Seemann, "Wetting and dewetting of complex surface geometries," *Annual Review of Materials Research,* vol. 38, pp. 101-121, 2008.

[230] C. Chung, Y. Chen, and T. Shih, "Fabrication and flow test of long-term hydrophilic fluidic chip without using any surface modification treatment," *Microfluidics and Nanofluidics,* vol. 6, pp. 853-857, 2009.

[231] J. Berthier and P. Silberzan, *Microfluidics for biotechnology*. Boston: Artech House, 2006.

[232] N. Bao, J. Wang, and C. Lu, "Recent advances in electric analysis of cells in microfluidic systems," *Anal Bioanal Chem,* vol. 391, pp. 933-42, Jun 2008.

[233] A. Clow, R. Künnemeyer, P. Gaynor, and J. C. Sharpe, "Low cost optical particle detection for Lab on Chip systems based on DVD technology," *Biomems and Nanotechnology III,* vol. 6799, pp. U189-U197, 210, 2008.

[234] S. Kostner and M. J. Vellekoop, "Detection of single biological cells using a DVD pickup read," *Transducers '07 & Eurosensors Xxi, Digest of Technical Papers, Vols 1 and 2,* pp. U1070-U1071, 2616, 2007.

[235] V. P. Maltsev, "Scanning flow cytometry for individual particle analysis," *Review of Scientific Instruments,* vol. 71, pp. 243-255, Jan 2000.

[236] G. V. Dyatlov, K. V. Gilev, K. A. Semyanov, and V. P. Maltsev, *The scanning flow cytometer modified for measurement of two-dimensional light-scattering pattern of individual particles*, 2008.

[237] V. P. Maltsev and K. A. Semyanov, *Characterisation of bio-particles from light scattering*. Utrecht ; Boston: VSP, 2004.

[238] A. N. Shvalov, I. V. Surovtsev, A. V. Chernyshev, J. T. Soini, and V. P. Maltsev, "Particle classification from light scattering with the scanning flow cytometer," *Cytometry,* vol. 37, pp. 215-20, Nov 1 1999.

[239] H. M. Shapiro and N. G. Perlmutter, "Personal cytometers: Slow flow or no flow?," *Cytometry Part A,* vol. 69A, pp. 620-630, Jul 2006.

[240] C. H. Lu, X. F. Yin, and M. Wang, "Fabrication of high aspect ratio metallic microstructures on ITO glass substrate using reverse-side exposure of SU-8," *Sensors and Actuators a-Physical,* vol. 136, pp. 412-416, May 1 2007.

[241] S. Bystrova, R. Luttge, and A. van den Berg, "Study of crack formation in high-aspect ratio SU-8 structures on silicon," *Microelectronic Engineering,* vol. 84, pp. 1113-1116, May-Aug 2007.

[242] S. Natarajan, D. A. Chang-Yen, and B. K. Gale, "Large-area, high-aspect-ratio SU-8 molds for the fabrication of PDMS microfluidic devices," *Journal of Micromechanics and Microengineering,* p. 045021, 2008.

[243] Y. H. Anis, M. R. Holl, and D. R. Meldrum, "Automated Vision-based Selection and Placement of Single Cells in Microwell Array Formats," *2008 IEEE International Conference on Automation Science and Engineering, Vols 1 and 2,* pp. 315-320, 1030, 2008.

[244] W. Choi, J. S. Kim, D. H. Lee, K. K. Lee, D. B. Koo, and J. K. Park, "Dielectrophoretic oocyte selection chip for in vitro fertilization," *Biomedical Microdevices,* vol. 10, pp. 337-345, Jun 2008.

[245] S. K. Cho and H. Moon, "Electrowetting on dielectric (EWOD): New tool for bio/micro fluids handling," *Biochip Journal,* vol. 2, pp. 79-96, Jun 20 2008.

[246] P. M. Young and K. Mohseni, "Calculation of DEP and EWOD forces for application in digital microfluidics," *Journal of Fluids Engineering-Transactions of the Asme,* vol. 130, pp. -, Aug 2008.

[247] A. Clow, P. Gaynor, and B. Oback, "A micropit for biological cell positioning," presented at the 7th IEEE International Conference on Control and Automation Christchurch, 2009 (In Press).

[248] G. Kohler and C. Milstein, "Continuous cultures of fused cells secreting antibody of predefined specificity," *Nature,* vol. 256, pp. 495-497, 1975.

[249] M. R. Davey, P. Anthony, J. B. Power, and K. C. Lowe, "Plant protoplasts: status and biotechnological perspectives," *Biotechnol. Adv.,* vol. 23, pp. 131-171, 2005.

[250] T. Hayashi, H. Tanaka, J. Tanaka, R. Wang, B. J. Averbook, P. A. Cohen, and S. Shu, "Immunogenicity and Therapeutic Efficacy of Dendritic-Tumor Hybrid Cells Generated by Electrofusion," *Clin. Immunol.,* vol. 104, pp. 14-20, 2002.

[251] R. S. Kane, S. Takayama, E. Ostuni, D. E. Ingber, and G. M. Whitesides, "Patterning proteins and cells using soft lithography," *Biomaterials,* vol. 20, pp. 2363-2376, Dec 1999.

[252] *Encyclopedia of life sciences*. London ; New York: Nature Publishing Group, 2002.

[253] G. I. Perez, X.-J. Tao, and J. L. Tilly, "Fragmentation and death (a.k.a. apoptosis) of ovulated oocytes," *Mol. Hum. Reprod.,* vol. 5, pp. 414-420, May 1, 1999 1999.

[254] W. Dai, K. Lian, and W. J. Wang, "A quantitative study on the adhesion property of cured SU-8 on various metallic surfaces," *Microsystem Technologies-Micro-and Nanosystems-Information Storage and Processing Systems,* vol. 11, pp. 526-534, Jul 2005.

Appendix A: Cell Growth and Division

The Cell Cycle

The process of cell replication consists of a number of stages (see Fig. 69). The G0 stage is a dormant phase. In stage G1 (Gap 1) the cell grows duplicating intracellular organelles. During the S (synthesis) stage the chromosomes are duplicated[72]. In stage G2 the chromosomes fold (condense) in preparation for cellular division.

In the final stage M (mitosis) of the cell cycle, where cellular division occurs, a number of events occur that are visible using dyes and light microscopy. The mitosis stage of the cell cycle was traditionally divided according to microscope observations. Eukaryotic animal cell mitosis is considered as a reference example as differences occur between different cells of multicellular organisms, between eukaryotes and prokaryotes, and between early division stages in embryonic development of various organisms. The mitosis stage of the cell cycle (Fig. 69) is often classified into four phases: prophase, metaphase, anaphase and telophase [43]. Cytokinesis may (and will here) be considered a phase of mitosis [252].

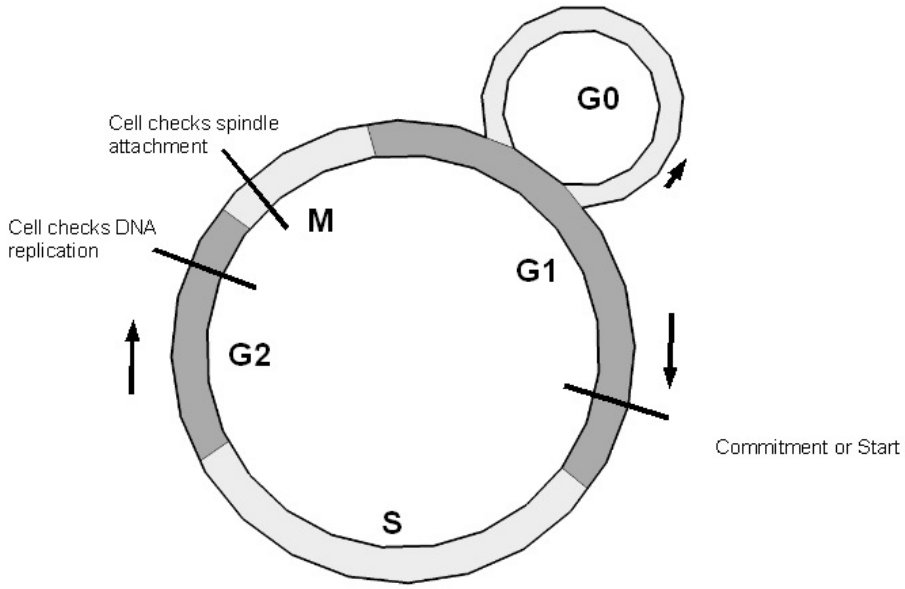

Fig. 69 Stages of the cell replication cycle.

Stages (G1,S,G2,M and G0) of the cell cycle are shown as shaded segments. Replication checks are made by the cell to ensure the process is effected correctly. Incomplete or incorrectly effected processes that fail certain checks (DNA replication, spindle attachment) trigger apoptosis.

[72] In animals, the centrosomes are also duplicated, but only separate at the onset of prophase

Phases of the mitosis stage of the cell cycle

The following phases of mitosis[252] are depicted in Fig. 69.

(0) Interphase

Interphase refers to the interval between successive mitosis stages (i.e. G1,S and G2). It is not a phase of the mitosis stage of the cell cycle.

(1) Prophase.

The chromatids become visible and are linked at the centromere. The chromatids fold by a factor of 10 times more than usual in mammals. Kinetochores develop in centromere region. The Centrosomes at the metaphase plate begin to separate (by microtubules) and move towards the poles. Segregation of daughter chromatids is critical upon correct folding and compaction of DNA.

(2) Prometaphase.

Beginning of prometaphase is indicated by the disappearance of the nuclear envelope. Microtubules extend from centrosomes. Kinetochore microtubules (MT) attach to the chromatid centromeres, polar MTs extend past the metaphase plate towards the opposite pole and astral MTs extend towards the cell cortex. There is dynamic addition and removal of tubulin monomers to both ends of the MTs. Sister chromatids move erratically in the direction towards the equatorial plane. Movement is induced by MT motor proteins (dynein and kinesin) which move along the surface of the MTs.

(3) Metaphase.

All chromatids are at the metaphase plate. One of the sister chromatids is attached to one pole, the other chromatid to the other pole. Chromosomes are maximally condensed. A protein cohesin at the centromere holds the sister chromatids together. A spindle checkpoint exists where if the kinetochore MTs are not attached, cell division is arrested. Until the check is passed, securin inhibits the protease separin from degrading the cohesin protein.

***(4a) Anaphase** A*

Separation of sister chromatids marks the beginning of anaphase. The start of anaphase appears to result from cohesion loss rather than increase in polar MT derived tension force.

The kinetochore MTs shorten and dynein molecular motor protein also shifts the daughter chromatids along the MT. The separated daughter chromosomes move (slowly) in opposite directions away from the metaphase plate.

***(4b) Anaphase** B*

The centrosomes begin to double the distance separating them. The molecular motors at the ends of the overlapping polar MTs cause them to slide past each other pushing the centrosomes further apart. Motors at the cell cortex (a structural network underlying the plasma membrane) may act upon astral MTs.

(5) Telophase

In telophase, the chromosomes begin to unfold, the spindle breaks down, the nuclear envelope coalesces, and the nucleoli reform.

(6) Cytokinesis

Actin and myosin filaments located in a ring just beneath the plasma membrane (and in the plane of the metaphase plate) contract pinching the cell in two. Most of the remaining organelles (mitochondria, endoplasmic reticulum, ribosomes) may not need to be equally divided so long as some of the organelles are received by both daughter cells [252].

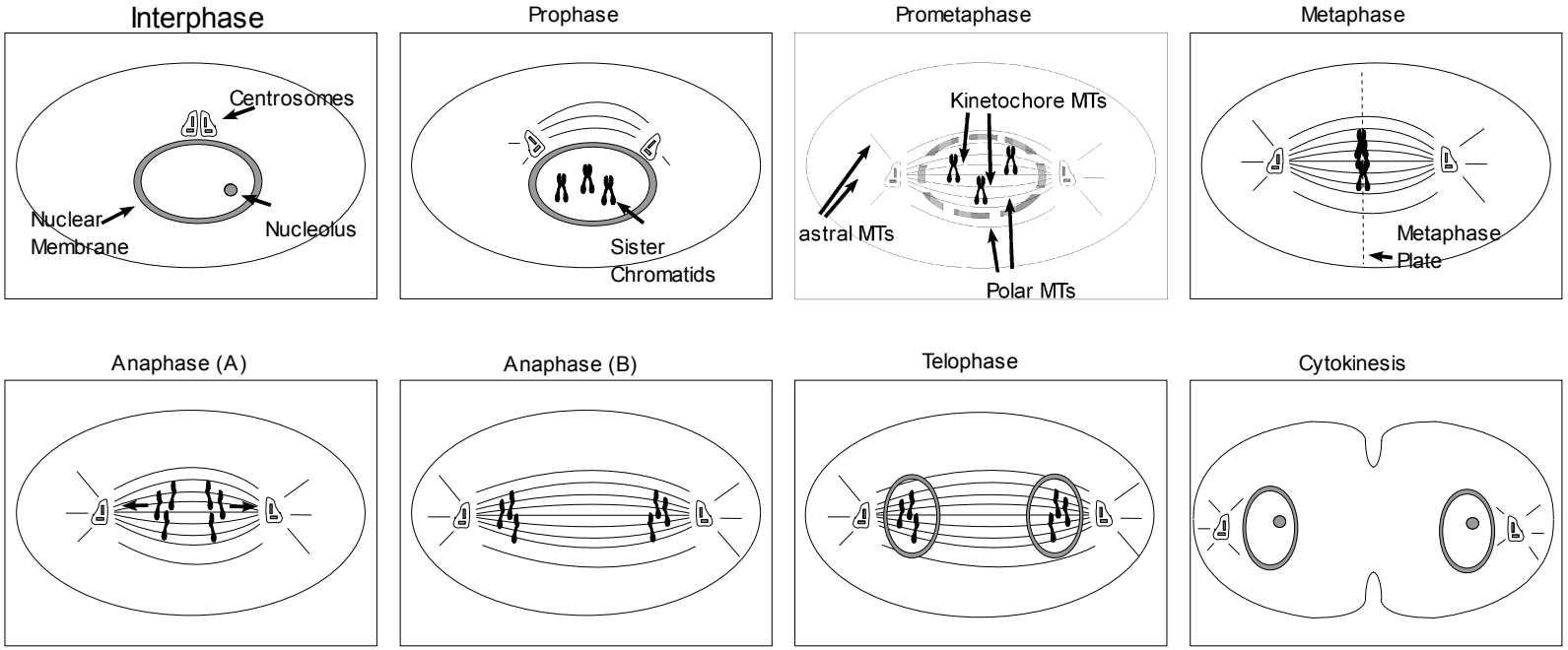

Fig. 70 Phases of mitosis

Meiosis

Gamete formation occurs through meiotic division (meiosis). The development of female germline cells over the final two generations are shown in Fig. 71.

The prophase of first generation cells (prophase I) is divided into five additional stages: leptotene, zygotene, pachytene, diplotene, and diakinesis. The majority of oocytes in the ovaries are arrested at the diplotene stage of prophase I.

In primary oocytes homologous recombination increases genetic diversity during anaphase I. Chromosomes are not copied in secondary oocytes (G1,S & G2 stages are absent). The secondary oocyte is arrested at metaphase II before ovulation (correspondence B. Oback). Fertilisation optimally occurs at around 24 hours post ovulation. If fertilisation does not occur the oocyte undergoes fragmentation (apoptosis) [253].

If the oocyte at metaphase II is fertilised, the cortical granules fuse with the oolemma modifying the membrane and vitrifying the zona pellucida blocking polyspermy. The genetic material of the sperm is released into the oocyte cytoplasm before extrusion of the second polar body (Fig. 71).

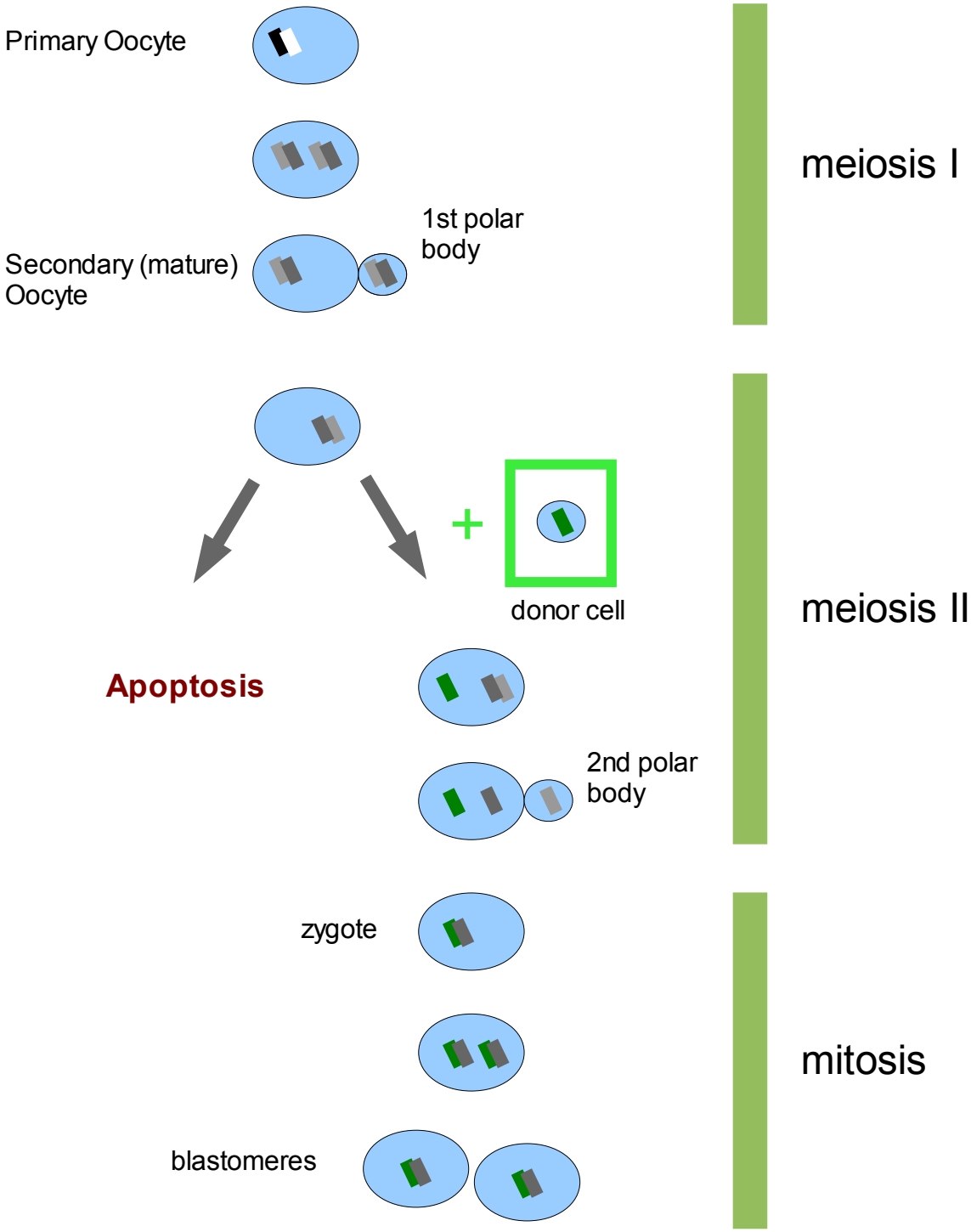

Fig. 71 In vivo maturation and fertilisation of an oocyte.

Appendix B: Dielectrophoresis

Force on an infinitesimally small dipole

A dipole is by definition two oppositely (but equally) charged particles attached separated by a fixed length. A vector $\boldsymbol{d}$ is defined, the direction being from the negative charge '-q' to the positive '+q' charge (Fig. 72) with a length equal to the distance between the charges. A vector quantity called the dipole moment is defined as $\boldsymbol{\mu} = q\,\boldsymbol{d}$.

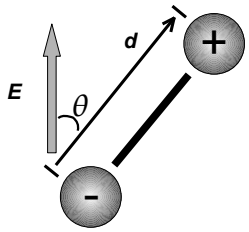

Fig. 72 An electric dipole.

The grey arrow indicates the direction of an external electric field.

The torque on the dipole is, considering a pivot point located at the negative charged particle

$$T = \left[q\,|\boldsymbol{E}|\sin\theta\right].\boldsymbol{d} = |\boldsymbol{\mu}||\boldsymbol{E}|\sin\theta \tag{46}$$

The potential energy (U)of a dipole in a conservative electric field can be found from the scalar potential W($\boldsymbol{r}$) due to an external applied electric field, where $\boldsymbol{r}$ is a position vector from the origin, and $\boldsymbol{r}_-$ is the position of the negative charge.

$$U = q[W(\boldsymbol{r}_-) - W(\boldsymbol{r}_- + \boldsymbol{d})] \tag{47}$$

omitting the '-' subscript on ***r***

$$U \simeq q\,\boldsymbol{d}.\nabla W(\boldsymbol{r}) = \boldsymbol{\mu}.\nabla W(\boldsymbol{r}) = |\boldsymbol{\mu}||\nabla W(\boldsymbol{r})|\cos\theta \tag{48}$$

where θ is the angle between ***d*** and ***E*** (Fig. 72).

Substituting $\boldsymbol{E}(\boldsymbol{r}) = -\nabla W(\boldsymbol{r})$

$$U(\boldsymbol{r},\theta) = |\boldsymbol{\mu}||\boldsymbol{E}(\boldsymbol{r})|\cos\theta \tag{49}$$

If theta (and hence ***d*** & $\boldsymbol{\mu}$) is maintained constant and the change in potential U is maximised, the force on the dipole is

$$\boldsymbol{F} = \nabla U(\boldsymbol{r}) = |\boldsymbol{\mu}|\cos\theta\,\nabla|\boldsymbol{E}(\boldsymbol{r})| \tag{50}$$

In practice of course, the dipole will rotate so that θ minimises $U(\boldsymbol{r},\theta)$ (in other words ***d*** aligns with ***E)***.

Equivalent dipole moment of a dielectric sphere in a dielectric medium

The effective dipole moment of a sphere in fluid is now calculated. The sphere and the fluid in which it is immersed are both assumed to be non-conducting (ideal) dielectrics; and the electric field is assumed not to change rapidly throughout the dimensions of the sphere.

The Poisson equation that describes this situation is

$$\nabla^2 W \equiv \nabla . \nabla W \equiv \frac{\partial^2 W}{\partial x^2} + \frac{\partial^2 W}{\partial y^2} + \frac{\partial^2 W}{\partial z^2} = 0 \tag{51}$$

Where W is the electric potential. In spherical co-ordinates [103]

$$\nabla^2 W = \frac{1}{r} \partial^2 \frac{r W}{\partial r^2} + \frac{1}{r^2 \sin^2 \theta} \frac{\partial^2 W}{\partial \phi^2} + \frac{1}{r^2 \sin \theta} | \sin \theta \frac{\partial W}{\partial \theta} | \tag{52}$$

Let the external field be homogeneous and in the positive z direction.

$$\nabla^2 W = \frac{\partial^2 W}{\partial r^2} + \frac{z}{r} \frac{\partial W}{\partial r} + \frac{\partial^2 W}{\partial \theta^2} + \frac{1}{r^2} \frac{\cos \theta}{\sin \theta} \frac{\partial w}{\partial \theta} = 0 \tag{53}$$

The solution of the scalar potential field W is different inside (*i)* and outside (*a*) the sphere.

$$W_a = \left(\frac{A}{r^2} + B r \right) \cos \theta \tag{54}$$

$$W_i = \left(\frac{C}{r^2} + D r \right) \cos \theta \tag{55}$$

The electric flux density $\boldsymbol{Đ}$ and potential W are continuous at the boundary ($r = R$) between the fluid and the sphere , thus

$$\epsilon_a \boldsymbol{E}_a = \epsilon_i \boldsymbol{E}_i \tag{56}$$

Constraints can be used to find the constants A,B,C and D.

(1) The potential at the centre of the sphere is not infinite (r= 0) so C = 0.

(2) Far from the sphere the field is uniform and

$$W_a = -E_0 r \cos\theta \tag{57}$$

so (comparing equation 54) $B = -E_0$

(3) The electric potential is continuous at the boundary (r=R) so

$$W_a = W_i \tag{58}$$

as C=0 and $B = -E_0$

$$\left(\frac{A}{r^2} - E_0 r\right)\cos\theta = D r \cos\theta \tag{59}$$

$$D = \frac{A}{r^3} - E_0 \tag{60}$$

(4) the electric field strength $\boldsymbol{E}$ is also continuous across the boundary because the electric field is defined excluding polarisation surface charges [103].

$$\epsilon_a \boldsymbol{E_a} = \epsilon_i \boldsymbol{E_i} \tag{61}$$

thus

$$\epsilon_a \frac{\partial W_a}{\partial r} = \epsilon_b \frac{\partial W_b}{\partial r} \tag{62}$$

$$\epsilon_a \frac{\partial}{\partial r}\left(\frac{A}{r^2} - E_0 r\cos\theta\right) = \epsilon_b \frac{\partial}{\partial r}(D r\cos\theta) \tag{63}$$

$$D = \frac{-\epsilon_a}{\epsilon_i}\left[\frac{2A}{r^3} + E_0\right] \tag{64}$$

Equating 60 with 64

$$A = \left[\frac{\epsilon_i - \epsilon_a}{\epsilon_i + 2\epsilon_a}\right] R^3 E_0 \tag{65}$$

and

$$D = -\left[\frac{3\epsilon_a}{\epsilon_i + 2\epsilon_a}\right] E_0 \tag{66}$$

thus as $r\cos\theta = z$

$$\phi_i = -\left[\frac{3\epsilon_a}{\epsilon_i + 2\epsilon_a}\right] E_0 z \tag{67}$$

thus the electric field strength $\boldsymbol{E_i}$ inside the sphere is (as the gradient is in the z direction)

$$\boldsymbol{E_i} = -\nabla\phi_i = -\left[\frac{\partial\phi_i}{\partial z}\right]\boldsymbol{k} = \frac{3\epsilon_a}{\epsilon_i + 2\epsilon_a} E_0 \boldsymbol{k} \tag{68}$$

The polarisation is normally defined as the polarisation with respect to free space. However, the sphere is not in free space, but immersed in a media which is also assumed to polarise. The difference in polarisation can be used to calculate the force on the sphere relative to the liquid.

$$\boldsymbol{P} = (\epsilon_i - \epsilon_a)\,\boldsymbol{E_i} = 3\,\epsilon_a \frac{(\epsilon_i - \epsilon_a)}{\epsilon_i + 2\,\epsilon_a}\,\boldsymbol{E_0} \tag{69}$$

If polarisation is defined as $\boldsymbol{P} = \chi\,\epsilon_0\,\boldsymbol{E}$ then as E is (in general) a function of position in space, so P is also a function of position.

The dipole moment is the volume integral of the polarisation. As P does not change within the volume considered

$$\boldsymbol{\mu} = volume \cdot \boldsymbol{P} \tag{70}$$

where $volume = \frac{4}{3}\pi R^3$

Substituting P from equation 69 gives

$$\boldsymbol{\mu} = 4\,\pi\,R^3\,\epsilon_a \frac{\epsilon_i - \epsilon_a}{\epsilon_i + 2\,\epsilon_a}\,\boldsymbol{E_0} \tag{71}$$

Dipole moment per unit volume

The polarisation ***P*** can be considered the dipole moment per unit volume. A parallel plate capacitor is considered where the plates are separated by a distance |d| (Fig. 73 a). Consider the field within a small cylinder of cross section area da that is perpendicular to and intersects the parallel plates. Consider the dipole made from polarisation charges Q and -Q located on the opposing capacitor plates contained within the cylinder.

$$\boldsymbol{\mu} = Q\,\boldsymbol{d} = (\sigma\, da)\,\boldsymbol{d} \tag{72}$$

By definition $P_n . da = \sigma\, da$ where σ is the polarisation charge density and the subscript n indicates the normal component to the surface (Fig. 73 b). Therefore

$$\boldsymbol{\mu} = (P_n .\, da)\,\boldsymbol{d} \tag{73}$$

$$P_n = \frac{|\boldsymbol{\mu}|}{da\,|\boldsymbol{d}|} = \frac{[\,dipole\ moment\,]}{[\,unit\ volume\,]} \tag{74}$$

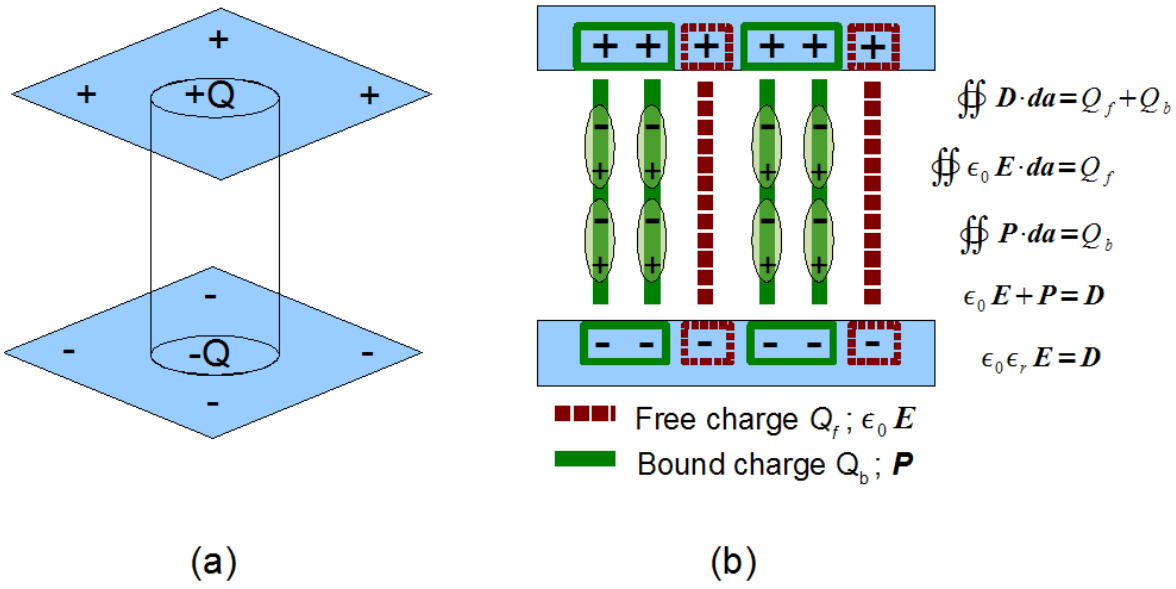

Fig. 73 Charges and Fields.

(a) A cylinder encloses two charges and forms a dipole (b) A pictorial representation of the field quantities using the illustration of a parallel plate capacitor filled with an ideal dielectric.

Appendix C: MicroPit Fabrication

A titanium film was used to form the electrode in the micropit devices. Greater adhesion was obtained with titanium to glass and SU8 than was obtained with the Ni-Au layers (cf. [254]). Titanium can be patterned by etching with hydrofluoric acid (HF). However, (HF) is fatal if small quantities come in contact with the skin are not treated rapidly. Two methods were used to pattern titanium without the use of HF: lift-off and a non-HF etch. The non-HF etch was found in a patent description and tested at Canterbury University. Micropit fabrication using the non-HF etching method is described below.

Thin film inter-digitated coplanar titanium electrodes (250 μm wide with an inter-electrode gap of 250 μm) were deposited on a borosilicate glass substrate (Fig. 51). The glass substrate wafer was dried at 185 ºC to enhance titanium adhesion, and coated with 200-300 nm of titanium by DC sputtering. AZ1518 photoresist (Clariant) was spin-coated over the wafer and exposed using a chrome mask made with a laser mask-writer (μPG 101, Heidelberg Instruments). The resist was hard-baked on a hotplate for 4 minutes at 150 °C to improve its adhesion to the substrate[73]. The wafer was etched for 5 minutes at room temperature using a non-hydrofluoric acid based etching solution (3.125% Ammonium hydroxide and 12.5% hydrogen peroxide in H_20) to remove the exposed titanium. The wafer was then etched again at room temperature in oxygen (50 sccm, 0.1 Torr) using a reactive ion etcher(PlasmaLab 80 plus, Oxford Instruments) at 200 W for 5 minutes to enhance surface adhesion. After etching, the electrodes were spin-coated with a thin film of SU-8 photoresist (MicroChem Corp.) in which circular pits were developed by photo patterning using an MA-6 mask aligner (Karl Süss GmbH). Areas of bare titanium were left for electrical contacts and scoring. SU-8 was hard-baked to reduce water absorption, cell adhesion, and surface delamination. SU-8 Spin coating, UV exposure, and hard-baking were conducted according to the manufacturer's datasheet (see section 4.2.1). The wafers were subsequently scored by a diamond cutter and cleaved to form 20 mm by 15 mm chips and placed in a chip holder for testing.

[73]An acrylic substrate was also used, but the bake temperature was reduced to 95°C